Morphological modelling of Longitudinal Training Walls

Exploring schematisation methods in Delft3D-4 for the development of auxiliary bank channels

I.G.A. Hille



Morphological modelling of Longitudinal Training Walls

Exploring schematisation methods in Delft3D-4 for the development of auxiliary bank channels

by

I.G.A. Hille

to obtain the degree of Master of Science in Civil
Engineering at the Delft University of Technology,
to be publicly defended on the 25th of September at 15:00.

Student number: 5173167
Project duration: March, 2026 – September, 2026
Thesis committee:

dr. J. A. Arriaga Garcia,	TU Delft
dr. ir. K. Sloff,	Deltares, TU Delft
dr. ir. R. J. Labeur,	TU Delft

An electronic version of this thesis is available at http://repository.tudelft.nl/.

Cover: Aerial photo of the Waal with longitudinal training walls, by Swart (2020).

TU Delft Delft University of Technology

Deltares

Preface

In front of you lies the thesis report that marks the final part of my MSc Civil Engineering studies, specialising in Hydraulic Engineering, at the Delft University of Technology. It is the result of six months at Deltares, where I was given the opportunity to learn about the practice of morphological modelling and the Dutch river systems.

I thoroughly enjoyed the MSc course, in which my interest in physics and mathematics came together with earth sciences and hydraulic systems in a practical way. I am grateful for the genuine interest and effort of the professors in sharing and conveying their knowledge, enriching my experience at TU Delft.

During my thesis research at the Rivers Department of Deltares, I was surrounded daily by knowledge and given the support to learn so much, not just about my own research, but also about underlying model workings and practices in the field. I am grateful to the whole department for the openness with which I was received, and for the many people who took the time to answer a question or share their experience. I would especially like to thank Kees Sloff, Anke Becker and Amgad Omer for always being willing to answer my questions, showing genuine interest in my research, and giving me confidence in my work.

From the TU Delft, I want to thank Robert Jan Labeur for his expertise and support in writing this report. I also want to thank Jaime Arriaga Garcia for his guidance, not only during my thesis, but throughout my entire master's. Thank you for being the kind of professor who is always willing to help students and who strives to improve the quality of their education

I would also like to thank my friends and family for their support and enthusiasm throughout this thesis. Especially my friend Denise Pierce, who, besides being an incredible study buddy, helped enhance and push my academic pursuit and became a true friend.

The whole thesis experience felt like everyone involved made my learning the priority, for which I am very grateful.

I wish you much pleasure in reading about what I have been working on over the past year. In case you have any questions regarding my work, feel free to reach out to me.

I.G.A. Hille
Delft, September 2026

Summary

As ongoing erosion in the Waal is causing multiple challenges for the Netherlands, the Room for the River 2.0 programme is looking at solutions to halt this erosion. One of the proposed solutions uses Longitudinal Training Walls (LTWs) to create a multi-channel system that reduces flow velocities while maintaining sufficient water levels in the main navigation channel. An LTW can narrow the main channel during low flow, but widen the total system during high flow. In 2015, three LTWs were constructed in the Waal as part of a pilot for potential application along the rest of the river. This research focuses on the one near Wamel.

The auxiliary bank channel near Wamel showed rapid sedimentation in its deeper sections during the first years. This appears to be linked to an initial response and bank erosion, rather than indicating an unstable system progressively filling up. After the inlet sill was heightened, the channel shifted to erosion over large parts of its reach. The remaining deposition along the stretch where the bank retreated seems to be slowing down as the bank stabilises.

Against the steep slope of the inlet sill and wall, gravity redirects near-bed flow and sediment back downslope towards the deeper main channel, forming a vortex with flow spiralling against the slope, reducing sediment transport into the auxiliary channel. Large-scale two-dimensional models are not able to explicitly resolve this local vertical vortex that plays a key part in the sediment distribution between the main and auxiliary channel and therefore in the stability of the LTW system.

Research into LTWs has grown considerably, but questions remain regarding the morphological stability of the auxiliary bank channel and how to schematise LTWs reliably in the large-scale coarse grids typically used for long-term river morphodynamic modelling. This research investigated different schematisation methods for LTWs in the coarse grid of the DVR model using ten-year simulations of the Waal from 2016 to 2025. A refined model, based on the same formulations and parameters as the DVR model, was developed and used as a benchmark to evaluate the coarse-grid schematisation variants. Representing the wall and inlet sill solely as a 2D weir with a small increase in bed level, as currently done in the DVR model's Baseline schematisation, proved insufficient, since this does not form a physical barrier able to block and redirect sediment once overtopped. Incorporating the structure directly into the bathymetry instead allows the model's transverse bed slope adjustment to act on the slope of the structure, activating the deflection needed to redirect sediment back into the main channel.

Even with the structure incorporated into the bathymetry, the coarse model struggled to reproduce the lower transport rates into the auxiliary bank channel seen in the refined model, for two reasons. First, the wide grid cells fail to represent the steep slope of the wall and inlet sill, weakening the gravitational deflection. Second, the structure was placed too far into the main channel, misaligning with the upstream bank, allowing longitudinal inflow that degraded the side-weir entrance geometry, and further increased the sediment transport into the auxiliary bank channel.

Two ways of compensating for the missing slope were tested: increasing the strength of the transverse bed slope deflection based on the Koch & Flokstra formulation, and locally reducing the transport magnitude through a calibration factor in the Meyer-Peter–Müller transport formula. However, both resulted in further problems in the main channel. The increased Koch & Flokstra deflection required to match the transport rates observed in the refined model or to correct the missing factor of local steep slopes unrealistically flattened the point bars in the main channel bends. Reducing the transport magnitude instead of the direction resulted in deposition in front of the inlet and an increase in transport rates again over time.

This research recommends incorporating LTW structures directly into the bathymetry, with careful attention to grid alignment relative to the crest and the effect of misrepresenting steep slopes. Local grid refinement, or a sub-grid formulation for the sediment deflection along a steep-sloped longitudinal structure, offers a future solution for representing the local geometry and the sediment distribution between the two channels.

Contents

1 Introduction **1**
- 1.1 Context . . . 1
- 1.2 Problem statement . . . 2
- 1.3 Aim and objective . . . 2
- 1.4 Research questions . . . 2
- 1.5 Research method and scope . . . 3
- 1.6 Reading guide . . . 3

2 Background information **4**
- 2.1 Dutch Rhine branches and Room for the River 2.0 . . . 4
- 2.2 Relevant sediment transport fundamentals . . . 6
- 2.3 Working principles of LTWs . . . 7
  - 2.3.1 Design concept . . . 7
  - 2.3.2 Hydrodynamic and morphodynamic response . . . 7
- 2.4 Background on existing LTW in the Waal . . . 11
  - 2.4.1 Design and dimensions . . . 11
  - 2.4.2 Monitoring and data-analysis performed . . . 12
- 2.5 Modelling of LTWs in the Waal with Delft3D-4 . . . 14
  - 2.5.1 Schematisation of the wall geometry . . . 14
  - 2.5.2 Schematisation of the inlet sill at the entrances . . . 15
  - 2.5.3 Sediment transport model . . . 15
  - 2.5.4 Morphologically inactive auxiliary bank channels . . . 16
- 2.6 Reflection on remaining uncertainties . . . 17

3 Methodology **18**
- 3.1 Field data analyses . . . 18
- 3.2 Numerical modelling . . . 19
  - 3.2.1 Model set-up . . . 19
  - 3.2.2 Modelling workflow . . . 22

4 Field observations of the LTW near Wamel **24**
- 4.1 Bed level observations in the auxiliary bank channel . . . 24
- 4.2 Cumulative sedimentation/erosion observations in the auxiliary bank channel . . . 24
- 4.3 Synthesis of the field observations . . . 26

5 Modelling results and analysis **27**
- 5.1 Hydrodynamic performance . . . 28
- 5.2 Varying schematisation approaches for the LTWs . . . 31
  - 5.2.1 Sediment balance and spatial patterns in the auxiliary bank channel . . . 31
  - 5.2.2 Influence of wall schematisation . . . 34
  - 5.2.3 Influence of inlet schematisation . . . 35
  - 5.2.4 Trends before and after the 2018 inlet adjustment . . . 38
  - 5.2.5 Testing a mild slope in refined model . . . 40
  - 5.2.6 Alluvial auxiliary bank channel . . . 41
  - 5.2.7 Summary of findings of the subchapter . . . 42
- 5.3 Sensitivity to transverse bed slope parameter (W3a-W3c) . . . 43
- 5.4 Parameter adjustments for local transport over the inlet sill . . . 46
  - 5.4.1 Quantifying the missing slope and corresponding A_{sh} . . . 46
  - 5.4.2 Short stationary test runs . . . 46
- 5.5 Summary of the modelling result analysis . . . 49

6 Discussion **50**

7 Conclusion **55**

8 Recommendations **58**

A Appendix **62**
A Additional field observations . . . 62
A.1 Bank erosion Wamel tranche 1 . . . 62
A.2 Sedimentation against the inlet sill. . . . 63
B Adjustments to inlet sills . . . 65
C Hydrograph . . . 66
C.1 Stepwise schematisation of discharge at Lobith . . . 66
C.2 Fit of the schematised stepwise hydrograph . . . 67
C.3 Discharge distribution to Waal and applied Morfac . . . 68
C.4 Days a year discharge high enough for the wall to be submerged . . . 68
D Model grids . . . 69
D.1 Schematization of inlets and walls . . . 69
D.2 Schematization of inlets and walls . . . 69
D.3 Cross sections and observation points locations . . . 71
D.4 Nourishment on inlets for run W5 and R5) . . . 71
D.5 Coarse model schematisation wall and inlet slope . . . 72
D.6 Refined model schematisation wall and inlet slope . . . 73
D.7 Local adjusted A_{cal} in S2 test run . . . 73
E Setting up the new refined model . . . 74
F CFD project of inlet sill at Wamel results . . . 76
G Additional model results . . . 78
G.1 Comparing W5, R5 and field data . . . 78
G.2 Influence of wall schematisation method . . . 80
G.3 Bedload transport through the inlet for W3a . . . 80
G.4 Total sedimentation/erosion of the auxiliary bank channel over time. . . . 81
G.5 Bed level change around outlet . . . 82
G.6 Sediment availability and outlet transport for W5 and R5 . . . 83
G.7 Alluvial auxiliary bank channel in the refined model . . . 86
H Discharge distribution short stationary model runs . . . 88

1 Introduction

1.1. Context

Over the past centuries, large rivers in the Netherlands have been heavily engineered to reduce flood risk and to facilitate inland navigation. River channels were straightened, meanders were removed, and structures such as groynes, dikes, weirs, and sluices were constructed. While these interventions have significantly improved flood protection and navigability, they have also fundamentally altered river hydraulics. Channel straightening and flow confinement have increased flow velocities in the main navigation channels, while decades of sand and gravel extraction have removed sediment from the system. Together with longitudinal variations in grain size that increase the sediment transport capacity in the downstream direction, this has triggered long-term riverbed degradation (Sloff et al., 2024; Ylla Arbós et al., 2021; Zanting & Van Rijn, 2024).

Riverbed erosion has been observed in several Dutch river branches for decades and continues to pose challenges for freshwater supply, navigation, ecology, and infrastructure stability (Chavarrías et al., 2021; Sloff et al., 2024). Projected changes in river discharge due to climate change further complicate this issue, as both higher peak discharges and longer periods of low flow are expected to occur more frequently. In response, a new programme called *Room for the River 2.0* (RFR2.0) was started to tackle these challenges (Asselman, 2025; Barneveld et al., 2025). For this programme, large-scale river interventions are being explored to counteract ongoing bed degradation while maintaining or improving river functions such as flood safety, water supply, navigation, and ecology. One of the proposed strategies is the use of side channels. By diverting part of the discharge away from the main channel, the flow velocity and bed shear stress can be lowered, reducing erosion in the main channel. The programme has been looking at creating a multi-channel system with two types of possible side channels: secondary channels in floodplains and auxiliary bank channels behind longitudinal training walls (Barneveld et al., 2025; Sloff et al., 2024).

Longitudinal training walls (LTWs) are hard dams placed in the river parallel to the bank, creating a sheltered side channel between the bank and the dam with an entrance spillway at the upstream end (Czapiga et al., 2022). In 2015, Rijkswaterstaat constructed the first three LTWs in the Netherlands inside the Waal as a pilot study (Chavarrías et al., 2021). Over the past decade, Rijkswaterstaat has been monitoring the effects of this new intervention in the Waal.

To assess long-term river dynamics and the effects of possible interventions, numerical modelling is used. Deltares developed a two-dimensional Delft3D-4 model, called the DVR model, of the entire Dutch Rhine branches, which has been used for numerous studies on morphological development. Numerical modelling has shown that widening the river system with an LTW can be effective in halting erosion while maintaining desired water levels (Barneveld et al., 2025; Sloff et al., 2024). However, uncertainties remain regarding the representation of sediment transport processes. In 2026, Rijkswaterstaat needs to choose a preferred strategy for the RFR2.0 programme, either LTWs, secondary channels or supplementation. Deltares and Rijkswaterstaat are concurrently developing the next-generation morphological model of the Dutch Rhine branches. To support informed decision-making and this model development, it is crucial to better understand large-scale morphological modelling with LTW. This concerns realistic sediment distribution for main channel development, and the stability of the auxiliary bank channel: whether it keeps its conveyance capacity over time, without excessive sedimentation or erosion, and at what maintenance cost.

1.2. Problem statement

To ensure that the long-term morphological development of the Dutch Rhine branches is accurately represented by numerical models, it is necessary to define a large spatial domain that captures reach-scale interactions and long-term trends (Mosselman & Sloff, 2026). Due to the extensive computation time, this requires 2D depth-averaged models with a relatively coarse resolution. This coarse-grid, 2D approach, however, does not explicitly resolve the local processes against the steep-sloped structure that play a key role in the sediment distribution in LTW systems.

Recent Delft3D simulations of possible LTWs along the Waal predict high sedimentation in the auxiliary bank channel, requiring yearly dredging and leading to high maintenance costs (Barneveld et al., 2025); however, the authors themselves note that this modelled sedimentation is expected to be significantly overestimated. This is consistent with a broader inconsistency across the literature: studies applying different model settings show strongly deviating morphological behaviour in auxiliary bank channels, with simulations producing opposing trends of sedimentation or erosion depending on whether the channel is schematised as non-erodible or as an active, erodible bed layer (Barneveld et al., 2025; Chavarrías et al., 2021; Sloff et al., 2024; Van der Niet, 2026). This sensitivity to model settings, combined with known unresolved local sediment distribution processes, shows that current predictions cannot yet be trusted to reflect the actual morphological response of the auxiliary bank channel. There is not yet a standardised, agreed-upon method of schematising LTWs for morphological modelling in Delft3D. The schematisation choice influences to what extent the morphological processes that determine sediment distribution and stability of the auxiliary bank channel are incorporated in the model simulation. Without a better understanding of how schematisation choices and calibration parameters affect sediment distribution in and around LTWs, model-based estimates of their morphological effectiveness and long-term maintenance needs remain unreliable.

1.3. Aim and objective

This research aims to improve the sediment transport modelling of LTWs in large-scale river models, to ensure realistic sediment distribution and exchange, contributing a more reliable modelling basis for future morphological research. In doing so, it supports the development of the next-generation morphological model of the Dutch Rhine branches and decision-making within the Room for the River 2.0 programme.

The objectives are to (1) identify and characterise relevant processes, (2) determine schematisation adjustments and model parameters to improve the simulations by evaluating sediment distribution and exchange over the LTW.

The focus is directed toward increasing insights into model configurations regarding the LTW schematisation to incorporate key morphological processes and improve predictions.

1.4. Research questions

The main research question is stated as follows:

How can the schematisation of longitudinal training walls in 2D morphological models be improved to better assess the stability of auxiliary bank channels?

To answer this question, four sub-questions are identified to guide the study:

1. *What processes play a key role in the morphological development of the auxiliary bank channels of LTWs?*
2. *How reliable is the current DVR (revised 2024) schematisation of LTWs for representing morphodynamic development?*
3. *How can the geometry of LTWs best be schematised in the coarse grid model to improve the representation of key morphological processes and the resulting development of the auxiliary bank channel?*
4. *To what extent can existing DVR calibration parameters compensate for the loss of local processes at the wall and inlet sill in a coarse grid?*

These sub-questions build towards the main research question in sequence. Sub-question 1 forms the basic understanding needed to identify relevant processes depending on the schematisation choices and parameter variations tested later. Sub-question 2 establishes how well the current DVR model reproduces observed field data, providing a baseline for assessing improvements. Sub-question 3 then investigates which schematisation method in the coarse grid can best be used for LTWs by comparing with a refined model and field observations. Finally, sub-question 4 looks at possible parameters to directly alter sediment transport rates that remain too high due to coarse grid limitations, since the coarse DVR model remains the practical tool for large-scale river management within RfR2.0. Together, the sub-questions address both what drives morphological development around LTWs and how this can be better represented in coarse-grid modelling.

1.5. Research method and scope

This research focuses on the assessment of 2D morphological modelling uncertainties of LTWs in the Dutch Rhine system, using the DVR model in Delft3D-4 as the primary modelling tool. The DVR model was last revised by Sloff et al. (2024). In addition to this relatively coarse model, a refined model is developed with the use of an existing locally refined grid of the LTWs in the Waal from Omer et al. (2019a).

This research is limited to analysing the morphodynamic development of one of the three LTWs in the pilot programme from Rijkswaterstaat: the upstream LTW near Wamel. This LTW has a standard side-weir at the inlet, for which laboratory experiments have been conducted and ongoing high-resolution CFD modelling is being conducted at Deltares.

The focus of this research is on sediment entering and morphological development of the auxiliary bank channel of the LTW near Wamel. It combines monitoring data from 2016, 2018, 2020 and 2025 with and model simulations from 2016-2025. To represent the hydrological conditions of this decade, an annually varying stepwise hydrograph was used based on discharge observations at Lobith. The effect of using an annually varying hydrograph compared to an annually repeating hydrograph is outside the scope of this thesis.

The research combines lessons learned from literature, discussions with experts at Deltares, RWS and HKV, numerical modelling, field data, and an ongoing project at Deltares (CFD LTW) performing high-resolution 3D sediment particle calculations. No physical experiments are conducted in this thesis.

An attempt is made to improve the 2D morphological modelling of LTWs. The study does not aim to recalibrate the model or ”fix” the limitations; it aims to enlarge insights into modelling decisions and the corresponding morphological response.

1.6. Reading guide

Chapter 2 provides background information on the Waal, LTWs and morphological modelling of the Dutch Rhine branches, and elaborates the research problem introduced above. The methodology used, and an overview of performed model runs are found in Chapter 3. Chapter 4 shows the bed level measurements to asses the system in the field and compare with model simulations. The results for the various model simulations are presented in Chapter 5. In Chapter 6, the results are discussed. The research questions are answered in the conclusion in Chapter 7. Finally, Chapter 8 provides further recommendations.

2

Background information

This chapter provides background information on the functioning and modelling of LTWs in the Waal and elaborates the research problem already introduced in Chapter 1 based on a literature review. Section 2.1 describes the challenges the Dutch Rhine branches face, for which LTWs can form a potential solution. Section 2.2 introduces relevant sediment transport fundamentals. Section 2.3 explains the working principles of LTWs. Section 2.4 gives background on the pilot LTWs built in the Waal. Section 2.5 discusses the modelling of LTWs in the Waal with Delft3D-4, including the divergences between the real-life system and the schematisation and the resulting model constraints. Finally, the chapter ends with reframing the research gap based on the discussed literature review in the chapter.

2.1. Dutch Rhine branches and Room for the River 2.0

The Rhine branches in the Netherlands are mixed rivers, fed by both rainwater and Alpine meltwater coming from Germany, entering near Lobith. Extensive human intervention over the past century, including channel straightening, construction of groynes and weirs, and sand/gravel extraction, has created an imbalance between sediment supply and transport capacity (Zanting & Van Rijn, 2024). Ongoing erosion exposes non-erodible layers and alters flow distributions among the branches, affecting navigation, nature, and water distribution and security. The latter comes from higher erosion rates in the Upper Waal compared to the Pannerdense Channel, which gradually redirects more water towards the Waal at the expense of the IJssel, which feeds the IJsselmeer, an important freshwater reservoir (Barneveld et al., 2025).

The sediment supply from the German Lower Rhine is estimated at approximately 400,000 m³/year, but the sediment transport to downstream reaches is approximately 550,000 to 570,000 m³/year (volume of sand and gravel including porosity), indicating a strong sediment transport gradient with 150,000 to 170,000 m³/year of sediment eroding away along the Waal according to Zanting and Van Rijn (2024). The increase in sediment transport capacity that is causing the erosion along the Waal is likely primarily driven by longitudinal variations in grain size rather than flow velocities, which remain fairly consistent in the Dutch branch (Sloff et al., 2024). In addition to the historical pressures that altered the river's equilibrium, climate change is expected to affect future discharge scenarios that can further increase the river's transport capacity and intensify the existing sediment imbalance in the Dutch Rhine branches (Sloff et al., 2024).

These challenges form the focus of the Room for the River 2.0 (RFR2.0) programme. Whereas the initial RFR programme focused on increasing the discharge capacity to maintain safe water levels while increasing spatial quality through measures such as lowering groynes, creating secondary channels, and temporarily widening floodplains, RFR2.0 aims to stabilise riverbed levels and develop a future-proof, multifunctional river system that balances safety, ecology, and navigation (Huthoff et al., 2011; Zanting & Van Rijn, 2024; Zevenbergen et al., 2015). The programme categorises possible interventions into two primary strategies: treating the causes and treating the symptoms. Sediment nourishment is a symptom-oriented measure that artificially replenishes the sand and gravel lost to erosion. Cause-oriented measures aim to fundamentally reduce the erosive forces in the system by decreasing flow velocities in the summerbed; this can be done with a multichannel system where part of the water is diverted out of the main channel to an auxiliary channel. To create a counteracting flow velocity gradient for the grain-size gradient,

auxiliary channels need to be implemented along the eroding reach of the Waal, and gradually increase in size downstream, to progressively divert more discharge into the auxiliary channels and decelerate flow velocities in the main channel. This reach spans around 68 Rkm, from the Pannerdensche Kop to Zaltbommel.

A study from HKV published by Barneveld et al. (2025) looked into 4 possible measure packages: MP1: do nothing, MP2: nourishment, MP3: a multichannel system using longitudinal training walls (LTWs) and MP4: a greener version of a multichannel system with secondary channels in floodplains. The LTWs modelled in the study of Barneveld et al. (2025) are shown in Figure 2.2. As LTWs are typically placed in the inner bends because of lower construction costs in the naturally shallower banks, the MP3 design entails many separate alternating dams. The design consisted of 80-100 m wide auxiliary bank channels that widen the total system to reduce flow velocities and erosion during high discharges, and narrowed the main channel by 20-40 m to raise low-water levels and steer more discharge towards the IJssel (Barneveld et al., 2025; Sloff et al., 2024).

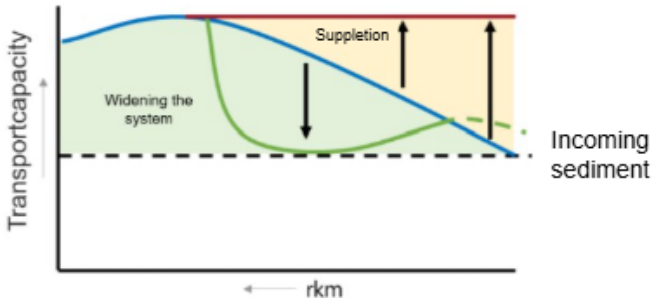


Figure 2.1: Conceptual effect of suppletion and river system widening with a multichannel system on sediment transport capacity compared to input (Barneveld et al., 2025)



Figure 2.2: Positioning of LTWs (black) with auxiliary bank channels (green) in MGS design for upstream section of the Waal (Barneveld et al., 2025)

The study analysed the four different scenarios using numerical simulations in Delft3D-4 with DVR instrumentation to test their effectiveness and predict potential maintenance needed. They found that all three tested interventions can be successful in halting erosion. However, the nourishment strategy shows low synergy with other river functions: it (1) does not provide a function separation between commercial shipping and nature, so does not provide protective habitats for nature to flourish, and (2) does not narrow the summer bed, so does not raise water levels for navigability. An advantage of sediment nourishment is that it is a highly adaptive measure; implementable when and where needed and adjustable to future changing needs or unexpected morphological responses (Barneveld et al., 2025). However, it does not transform the river into a more multifunctional or future-proof system in the way that a multi-channel concept can do.

Modelling of the MP3 design with LTWs showed unexpected morphological development in the auxiliary bank channels. To be able to keep the LTWs effective in reducing the flow in the main channel, channels were dredged in the model every year. If this is needed in reality, the yearly maintenance costs for MP3 are significantly high: about the same as the nourishment and navigation channel maintenance cost for MP2 (€10.3 to 12.2 million a year for MP3 and €12.1 million for MP2) (Barneveld et al., 2025).

Despite their high potential, several critical uncertainties remain regarding the long-term stability of these multichannel systems. A primary concern is the model's reliability: as models struggle to reproduce the complex three-dimensional flow effects on sediment partitioning at the inlets and bank erosion processes, confidence in predicted sedimentation and maintenance needs is lacking. Research with Delft3D-4 2D morphological models shows very different behaviour when certain model settings are altered: models with morphological inactive auxiliary channels (non-erodible) has shown significant sedimentation rates in bank channels (Barneveld et al., 2025; Chavarrías et al., 2021; Sloff et al., 2024), whereas Van der Niet (2026) who incorporated an active bed layer that can erode, got erosion in the bank channels.

2.2. Relevant sediment transport fundamentals

Morphological development of rivers is driven by gradients in sediment transport: where more sediment enters a reach than leaves it, the bed accretes; where less sediment enters, it erodes. This is expressed by the Exner equation:

$$(1-\lambda_p)\frac{\partial z_b}{\partial t} + \nabla \cdot \vec{q}_s = 0 \tag{2.1}$$

Where z_b is the level of the bed, λ_p is the porosity of the bed, and q_s the bedload transport.

No universal sediment transport formula exists; the appropriate formulation depends on flow conditions, sediment properties, and transport mode. Bedload is the dominant mode in sand and gravel-bed (coarse-grained) rivers such as the Rhine branches (Le et al., 2018). The general form of bedload transport formula:

$$\vec{q_s} = m\,|\vec{u}|^{\,b-1}\,\vec{u} \tag{2.2}$$

Where m and b are empirical coefficients, and u is the depth-averaged velocity. For bedload, b typically ranges between 3 and 5, depending on the transport formula and sediment characteristics. The strong nonlinearity means that transport rates are highly sensitive to flow velocity; small increases in discharge can disproportionately increase sediment flux.

Sediment is set in motion when the destabilising hydrodynamic drag and lift forces overcome the stabilising gravitational pull on a grain. Their ratio is characterised by the Shields (1936) parameter:

$$\theta = \frac{\tau_b}{(\rho_s - \rho)gD_{50}} \tag{2.3}$$

Where τ_b is the bed shear stress, ρ_s and ρ the sediment and fluid densities, g gravitational acceleration, and D_{50} grain diameter. Motion begins when θ exceeds the critical Shields parameter θ_{cr}. In graded sediment mixtures, hiding and exposure effects modify θ_{cr} for individual size fractions expressed as:

$$\theta_{cr,i} = \theta_{cr}\xi_i \tag{2.4}$$

Where, $\xi_i > 1$ indicates hiding (finer fractions) and $\xi_i < 1$ exposure (coarser fractions).

On a sloped bed, an additional gravity component works on the sediment transport particles, pulling sediment towards the deeper parts of the bed. Bed level gradients are commonly decomposed into a longitudinal and transverse slope. Effects from longitudinal bed level gradients are limited, as river slopes are typically small. Transverse bed gradients, for example in river bends, can be much larger and, since sediment transport is predominantly longitudinal, lead to a relatively larger deflection of the near-bed sediment transport vector.

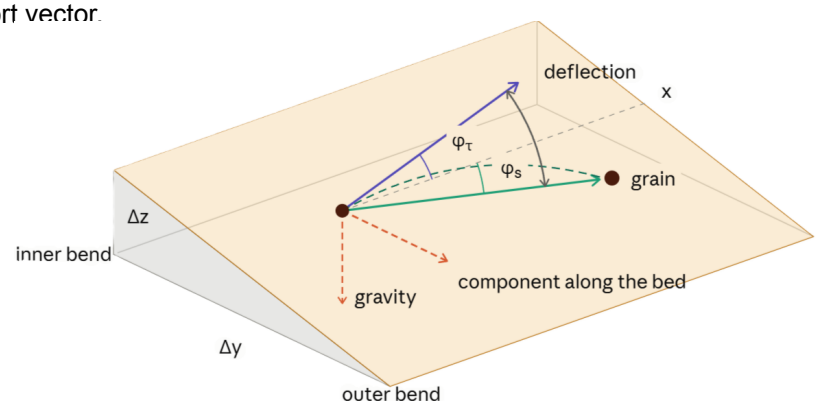


Figure 2.3: Gravitational deflection of sediment on traverse bed slopes.

The correction to the transport direction due to a transverse slope, formulated by Koch & Flokstra (1980) and extended by Talmon et al. (1995) is given by:

$$\tan(\phi_s) = \frac{\sin(\phi_\tau) + \frac{1}{f(\theta)}\frac{\partial z_b}{\partial y}}{\cos(\phi_\tau) + \frac{1}{f(\theta)}\frac{\partial z_b}{\partial x}} \qquad f(\theta) = 9\left(\frac{D_{50}}{h}\right)^{0.3}\sqrt{\theta} \tag{2.5}$$

Where ϕ_τ is the original transport direction, ϕ_s the corrected and $f(\theta)$ expresses the sensitivity of the transport direction to the transverse bed slope. A larger $f(\theta)$ reduces the deflection for a given transverse slope. This mechanism is revisited in the context of LTWs in Section 2.3.2. How these formulas are used in the model is explained in 2.5.3.

2.3. Working principles of LTWs

2.3.1. Design concept

Longitudinal training walls (LTWs) are river engineering structures consisting of a hard, long barrier placed inside the river parallel to the riverbank. LTWs separate the river into two channels, a (now narrower) main channel and an auxiliary bank channel that widens the total river system. Water and sediment can enter the auxiliary bank channel in three ways: (1) at the upstream inlet weir (2) through local lowered sections in the wall, called inter-wall notches, and (3) over the wall during high flow; see figure 2.4a (Czapiga et al., 2022). The height of the entrance weir, the inter-wall notches and the wall determine when these flow paths become active. The height of the inlet sill is seen as the main control valve for water distribution between the channels, providing robustness to the design with relatively easy realisable adjustment. The inlet sill is preferably low to keep the connectivity between the summer and winter for ecological purposes, but high to raise water levels for navigation.

2.3.2. Hydrodynamic and morphodynamic response

The wall affects the flow in the main channel in two ways: (1) the main channel is narrowed, which increases the water level and flow velocity, and (2) a fraction of the discharge is extracted, reducing water level and flow velocity. The dominant effect depends on the discharge and can be altered with the design dimensions. For the Waal, the structures and auxiliary channels are designed to maintain sufficiently high water levels during low flow due to the narrowing of the main channel, while simultaneously lowering the high flow water level by increasing the total conveyance capacity through widening the total system with the addition of the auxiliary bank channel (see Figure 2.4b).

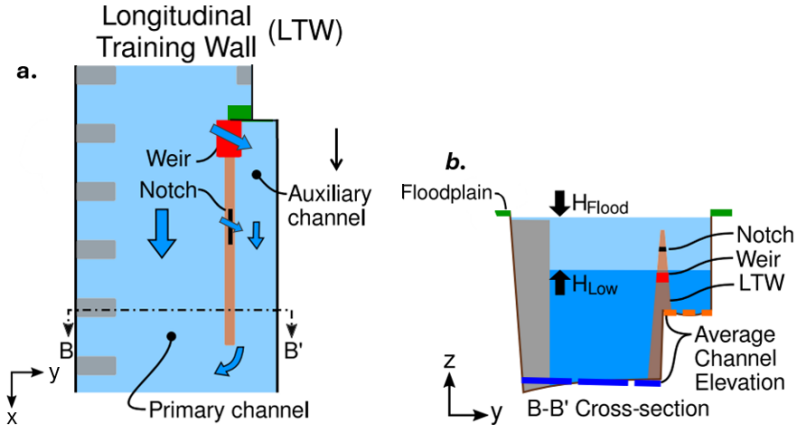


Figure 2.4: Longitudinal training wall: (a) plan view and (b) cross-section view. Flow enters the auxiliary channel at the upstream inlet, through inter-wall notches and by overtopping the wall during high flow. The LTW increases low-flow water depth and decreases high-flow water depth. (Adapted from Czapiga et al., 2022)

The LTWs trigger various hydro-morphological processes on different scales and during different discharges, resulting in distinct zones of sedimentation and erosion. Theoretically expected morphological responses over the total system and the separated main and bank channel under different flow regimes are discussed in the following paragraphs.

Total system widening

At the scale of the entire LTW reach, the structures increase the effective system width, promoting horizontal flow expansion across the two channels (Czapiga et al., 2022). As flow velocities reduce, so does the sediment transport capacity, resulting in sedimentation, as follows from the general transport formula (Eq.2.2) and sediment mass conservation, as described by the Exner Equation (Eq. 2.1). Neglecting transverse processes that influence the sediment distribution between the two parallel channels, this would give sedimentation just downstream of the LTW onset in both channels, which propagates downstream, or at least a reduction of pre-LTW erosion. However, the presence of a wall within the river, separating the two channels, introduces additional complexity to the system and the sediment distribution.

Flow regimes: emergent and submerged

A key distinction in LTW systems is whether the wall is emergent or submerged, as this determines possibilities of water and sediment exchange between the main and auxiliary bank channel. When the wall is emergent, the system resembles a zero-angle bifurcation with an inlet weir: water and sediment are exchanged between the main and bank channels exclusively through the upstream inlet (De Ruijsscher et al., 2020; Le et al., 2018). When water levels are sufficiently high, additional exchange becomes possible through the inter-wall notches. During high-flow conditions, when the wall becomes submerged, the distinction between the two channels diminishes. Water and sediment may then be exchanged directly over the wall crest along its entire length, introducing additional transverse transport processes. The dominant morphological processes in the main and auxiliary bank channel under emergent conditions are first discussed, followed by an examination of the mechanisms driving sediment transport over the wall under submerged conditions.

Emergent regime: main channel extraction

In the emerged system, the separated main channel is narrowed and water is diverted to the auxiliary bank channel. Long-term morphological changes are not primarily driven by extreme events, but by ”morphologically active” flows with medium discharges that occur around 40%-60% of the year (Zanting & Van Rijn, 2024). With these discharges in mind, the LTWs are designed such that the morphological effect of water extraction becomes dominant over the narrowing (Chavarrías et al., 2021). The extraction of discharge from the main channel lowers the sediment transport capacity and thereby mitigates erosion in the navigation channel. This response has been the main driver in the consideration of LTWs in the Waal. Figure 2.5 illustrates the hydrodynamic and morphodynamic response to discharge extraction.

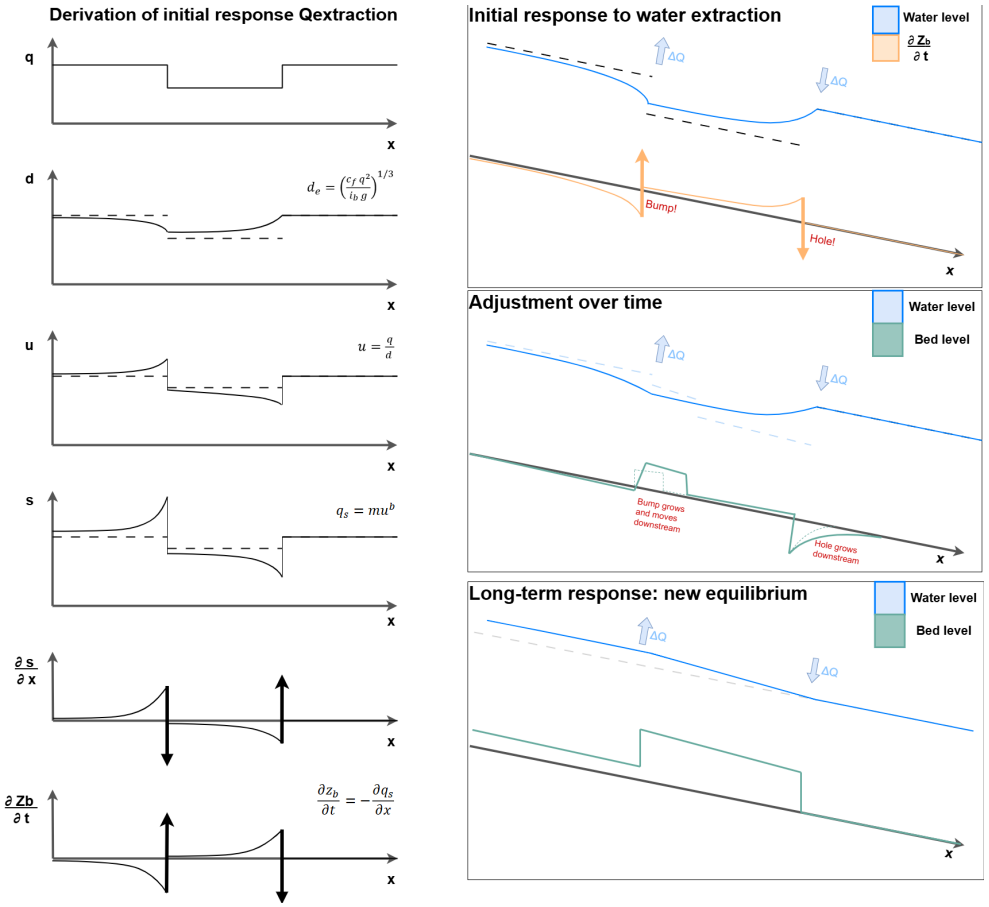


Figure 2.5: Longitudinal cross-section showing the hydrological and morphological response to discharge extraction, like in a LTW-system where water is diverted to the auxiliary channel. The derivation of the response is shown in the left graphs with the governing equations. A prismatic rectangular channel in initial equilibrium is assumed.

The water extraction shows similar behaviour as flow expansion: initially, a sedimentation bump develops in the main channel just downstream of the LTW onset, as the flow velocity (u) and sediment transport capacity (S) drop. At the downstream end of the LTW, the extracted water rejoins and the flow velocity and sediment

transport capacity increase again, causing a scour hole to develop. Over time, the bump and the hole will grow in the downstream direction. The initially mild erosion upstream of the LTW will turn into sedimentation as the water level along the LTW increases (Chavarrías et al., 2021). Under a constant discharge, the initial bump and hole propagate downstream, resulting in a evened out in a risen equilibrium bed level with a steeper slope after a prolonged time. However, in reality the discharge shows strong variability. The morphodynamic response is therefore not a smooth transition towards an equilibrium. Instead, the initial response mechanism is repeatedly reactivated during discharge peaks (flood waves). During such events, similar processes occur: a sedimentation bump forms just downstream of the LTW inlet, and a scour hole develops downstream of the LTW (Czapiga et al., 2022). Between flood events, the bed disturbances diffuse to a certain degree. Although high-water events do not set long-term morphodynamic trends, extreme disturbances can persist in the system for many years. For the Waal specifically, disturbances tend to travel downstream through the system at a speed of 1 km a year (Chavarrías et al., 2021; Sloff et al., 2024). The transition to a higher bed level with a new slope shown in the long-term response is therefore not smooth, but every year bumps and holes form during the winter months that tend to diffuse out during the low-flow summer months.

It is important to note that the Waal was not in equilibrium initially, but was subject to ongoing erosion. The LTWs in the Waal are not designed to cause sedimentation, but to hold the ongoing erosion.

Emergent regime: bank channel processes

The stability of bifurcation systems like the one created by LTWs is highly sensitive to the discharge distribution and relative location of the bifurcation with respect to steady river bars (Le et al., 2018; Wang et al., 1995). Laboratory experiments by Le et al. (2018) showed that a bifurcation positioned upstream of a bar crest tends to cause the auxiliary channel to silt up, while positioned at a pool location can cause the main channel to silt up. In the Waal pilot, the LTW inlets at Wamel and Dreumel were placed upstream of bar crests, expecting aggradation with this theory, while the Ophemert inlet, placed downstream of a crest, would be expected to erode (Chavarrías et al., 2021).

However, the entrance geometry distinguishes LTW systems from idealised bifurcations. In particular, the presence of a non-erodible inlet sill introduces an additional control on the partitioning of sediment. The sill exerts a blocking effect on bedload transport and induces complex three-dimensional flow structures, such as vortices and secondary currents, which influence sediment routing into the bank channel (Jammers, 2017; Van Os, 2020). As a result, the distribution of sediment does not directly follow the discharge distribution (Osorio et al., 2020). Laboratory studies have shown that the sediment partitioning is highly sensitive to inlet geometry, including sill height, slope, and orientation relative to the flow (Czapiga et al., 2021; De Ruijsscher et al., 2020; Jammers, 2017; Van Os, 2020). For example, Van Os (2020) showed in laboratory experiments for the Wamel inlet design that, at higher discharges towards the bank channel, the near-bed flow angle is reduced relative to the mid-depth flow angle, thereby limiting sediment transport over the sill.

The inlet sill height acts as a primary control parameter for sediment (and flow) distribution, providing robustness under varying future boundary conditions (Czapiga et al., 2022). Nevertheless, considerable uncertainty remains regarding the actual sediment entering the bank channel, as it is difficult to measure directly in the field or to scale reliably in laboratory conditions (Mosselman & Sloff, 2026; Osorio et al., 2020).

Additionally to sediment entering the bank channel from the upstream and or over the wall, local bank erosion can act as a significant internal sediment source. Contributing to the transverse redistribution of sediment and altering channel geometry in ways that locally affect flow velocities and sediment transport capacity, as seen with the pilot in the Waal (Chavarrías et al., 2021; Flores et al., 2022)

Flow separation

Looking from a top plane, the onset of the wall causes flow separation. This causes eddies and flow circulation at the entrance of the auxiliary bank channel against the wall and the upstream start, resulting in low-velocity shallow zones (see Figure 2.6) (Chavarrías et al., 2021). CFD high-resolution simulations of the heightened inlet sill near Wamel (see Appendix F) have shown that flow velocities are expected to be highest at the downstream end of the entrance. At the upstream end, velocities can become negative due to strong recirculation caused by the high inlet sill.

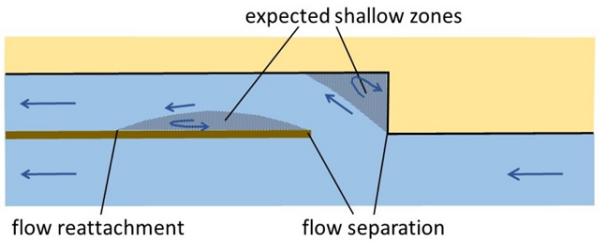


Figure 2.6: Expected shallow zones near the entrance of auxiliary bank channels due to flow separation (Chavarrías et al., 2021).

Submerged regime: wall overtopping

During high waters, the LTW submerges and flow and sediment exchange can happen along the entire wall, not just the inlet. Unlike the emergent regime where the inlet geometry is dominant, discharge partitioning during submergence is primarily controlled by the cross-sectional area (capacity) of the auxiliary bank channel, as a larger area draws in more water (Czapiga et al., 2022). In the case of a flood, higher water levels increase the possible flow paths for water exchange, leading to a larger portion of the discharge diverted to the auxiliary bank channel as the additional over-wall flow allows more utilisation of the channel's cross-section. The relative increase in discharge extraction, which locally lowers the sediment transport capacity, in combination with an increase in sediment in motion during floods, causes sediment deposition in the main channel; floods 'trap' sediment in the main channel (Czapiga et al., 2022).

Sediment transport over the submerged wall involves similar processes to those over the inlet sill. Over-wall flow primarily extracts water from the upper half of the water column, where suspended sediment concentrations are lower. The wall's blocking effect, which limits bedload transport into the auxiliary bank channel is expected to be greater than at the inlet sill due to its height.

The steep slope of the longitudinal inlet sill and the wall reduces the sediment transport passing over them. Just like at transverse bed level gradients that form naturally in rivers, discussed in 2.2, gravity deflects sediment in transport downslope, towards the deeper main channel, counteracting the transverse flow component carrying sediment towards the auxiliary bank channel. The steeper the rise towards the crest, the stronger this deflection and the more strongly sediment exchange is suppressed.

The longitudinal orientation distinguishes these structures from a frontal weir. In front of a frontal weir, sediment accumulates until a milder slope has formed over which sediment in transport can eventually pass. Along a longitudinal structure, sediment deflected back down-slope is taken along with the flow in the main channel instead. Laboratory work has shown that the flow along the longitudinal steep slope can organise into a vortex that prevents sediment from reaching the crest (De Ruijsscher et al., 2020; Van Os, 2020). A possible flow field is sketched in Figure

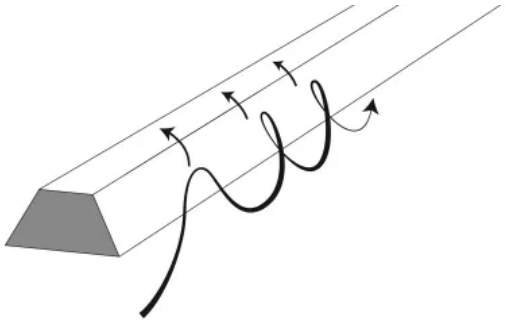


Figure 2.7: Sketch of vertical vortex developing along a longitudinal steep sloped structure (Van Os, 2020).

The gravitational deflection acts more strongly on bedload than on suspended sediment. Bedload moves in contact with the bed, so its direction responds directly to the bed slope, whereas suspended sediment travels within the fluid and passes over the structure more readily. The structure therefore blocks the two transport modes selectively.

Consequently, the transverse bed slope effect plays a critical role in sediment exchange between the main channel and the auxiliary bank channel, and therefore in the long-term morphological stability of LTWs.

2.4. Background on existing LTW in the Waal

2.4.1. Design and dimensions

In 2014, Rijkswaterstaat initiated a pilot project as part of the ”WaalSamen” programme, constructing three longitudinal training walls in the Waal River near Tiel between Rkm’s 911.5 and 922 (see Figure 2.8) (Chavarrías et al., 2021; Collas et al., 2020). The project served as a ”proof of concept” to test whether replacing traditional groyne fields with a two-channel system could simultaneously address flood safety, riverbed erosion, and ecological degradation (Chavarrías et al., 2021; Huthoff et al., 2011). The pilot consists of three wall segments in the inner bends at Wamel (3 km long), Dreumel (4 km long), and Ophemert (3 km long) (Collas et al., 2020). The walls were placed approximately 30 m further into the river than the original groyne heads, narrowing the main channel while creating auxiliary bank channels of 80 m wide behind them (Chavarrías et al., 2021; Collas et al., 2020). The height of the crest of the wall is designed to overflow at a discharge at Lobith of 2600 m^3/s, this means that the LTW is submerged at approximately 100 days per year (De Ruijsscher et al., 2018).

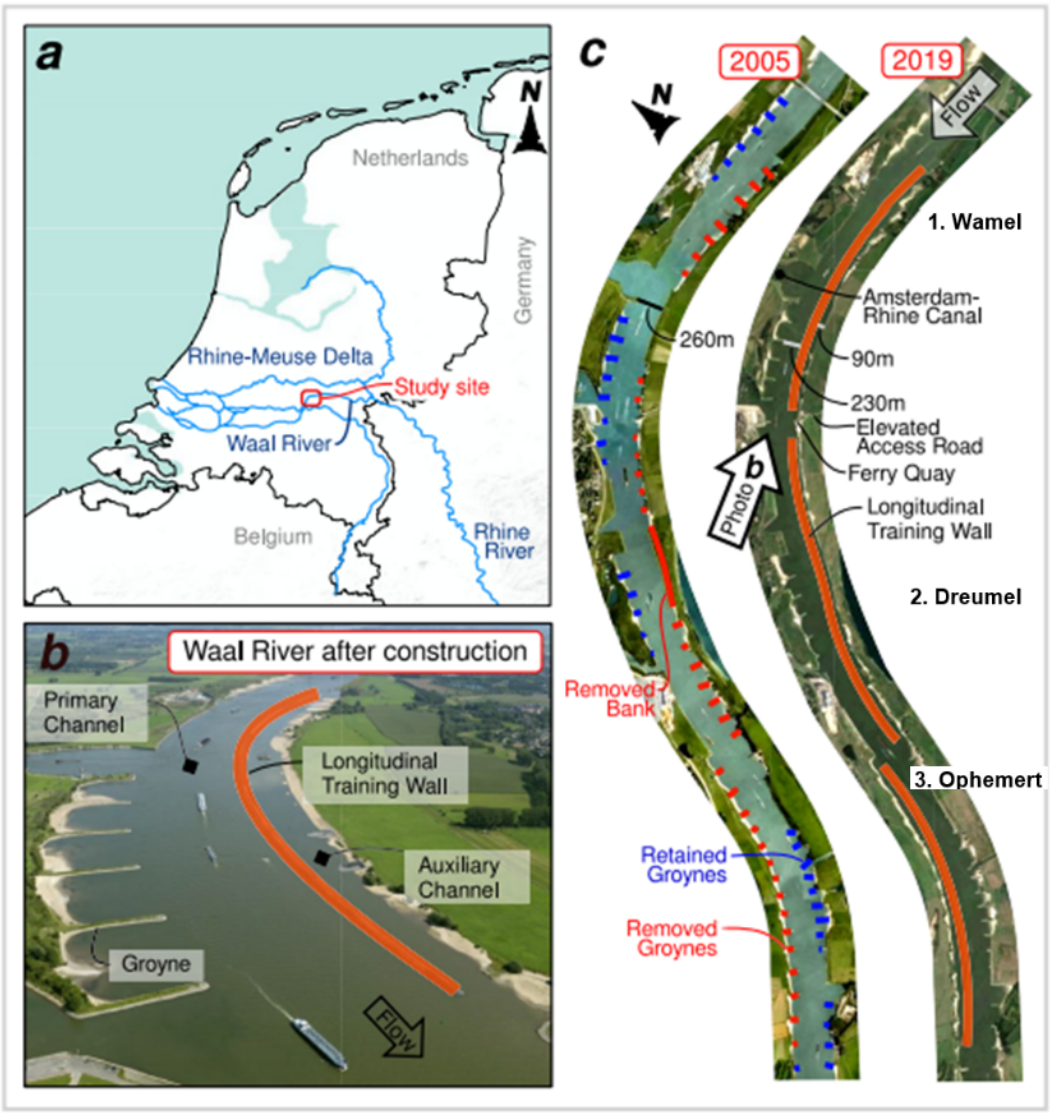


Figure 2.8: Pilot project of longitudinal training walls in the Waal river. (a) Study site LTW near Tiel, Netherlands. (b) Photo looking upstream at the first wall (Photo: Radboud University, 2017; orientation indicated in c). (c) Comparison of the channel controlled by groynes before 2014 (left) and the replacement LTW system with 3 sections after 2015 (right). (Adapted from Czapiga et al., 2022).

The orientation of the inlets of the three sections differs: the upstream (Wamel) and downstream section (Ophemert) both have a side-weir entrance and the middle section (Dreumel) has a curved weir attached to an adjacent bank, see Figure 2.9. The height of the wall is OLR + 2.78 m at the upstream start of Wamel, and goes down to OLR + 2.35 m at the downstream end of Ophemert. OLR (Overeengekomen

Lage Riverstand) is an agreed safe navigable low water level reference plane (Koedijk et al., 2017; Sieben, 2020).

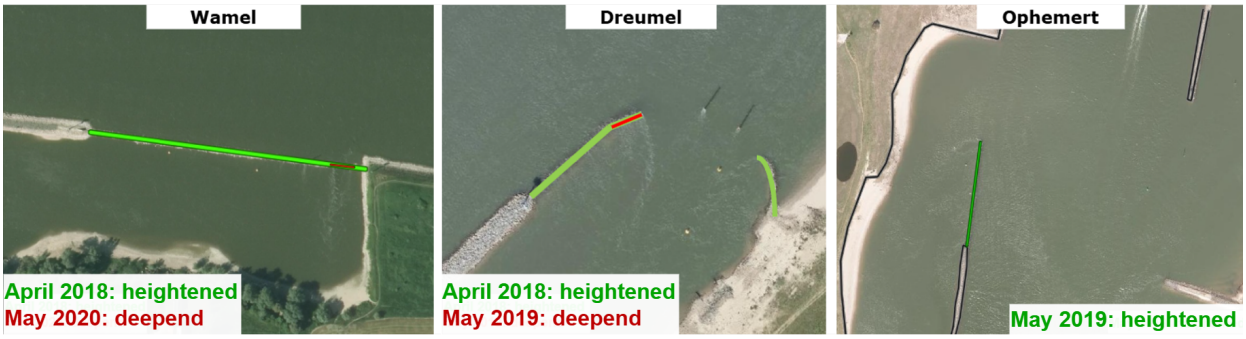


Figure 2.9: Plan view satellite pictures of LTW inlets in the Waal with adjustments done indicated in green (sill section heightened) and red (sill section lowered). See cross-section shown in Appendix B for specifics of the inlet alterations. (Rijkswaterstaat, nd.)

Originally in 2015 all the inlets sill crest heights were OLR -1.75 m, but in 2018, 2019 and 2020 adjustments were made to heighten the inlets, with the crests going up to +3 m at Wamel. In addition to Figure 2.9, Appendix B elaborates on the heights of the inlets over time with cross-sections.

Furthermore, on 23 January 2018 dredging took place in the downstream reach of the auxiliary bank channels of two of the pilot LTW sections: 15074 m^3 in the first channel near Wamel, with an average layer thickness of 0.35 m (locally up to 0.75 m) and 23400 m^3 in the second channel near Dreumel, with an average layer thickness of 0.08 m (locally up to 0.75 m) (M. Verbeek, Rijkswaterstaat, personal communication, April 2026).

2.4.2. Monitoring and data-analysis performed

Rijkswaterstaat has monitored the pilot LTWs in the Waal through two measurement campaigns; tranche 1 covered the first five years after construction (2016–2020), and tranche 2 started collecting measurements again in 2025. The measurement campaigns consist of multi-beam bed level measurements and ADCP discharge measurements. After tranche 1, extensive analysis of the LTWs was done in the project ”Final Evaluation Pilot Longitudinal Training Walls” commissioned by Rijkswaterstaat and executed by the ”WaalSamen” partnership. Under the ”RiverCare” research programme, academic research on the LTWs was conducted under the ’RiverCare’ research programme. This includes the work of Flores et al. (2022), who analysed the morphological development of mesohabitats in the auxiliary bank channels, and Czapiga et al. (2022), who used the multi-beam data to demonstrate how the walls mitigate erosion in the primary channel. Additionally, De Ruijsscher et al. (2020) combined laboratory experiments with field data to study flow and sediment diversion at the inlet sills. Some of the key findings relevant for this research regarding the bed level development of the main and auxiliary bank channels and sediment transport over the inlet sill are discussed.

Main channel

Data analysis from tranche 1 (2016-2020) confirmed that LTWs have effectively mitigated erosion in the main channel, changing an average pre-construction erosion rate of 1 cm/yr to an average sedimentation rate of 1.0 cm/yr (with inter-annual variations of +2 cm) in the main channel over the reach with the LTWs (Czapiga et al., 2022). The net effect of bed aggradation comes from a morphological response that follows a cyclic pattern (Czapiga et al., 2022). High-flow phases trap sediment in the system with aggregation bumps in the primary channel near the upstream end of each wall, while localised scour occurs at the downstream confluences. Between floods, the accumulated sediment disperses and scour pits tend to fill. The observations match the expectations described in section 2.3.2.

The heightening of the inlet sills showed to be of influences in the main channel: local sedimentation rates at the upstream end of the LTW decreased as less water was extracted (Chavarrías et al., 2021). This suggests that the morphological response of the main channel can be actively steered through the geometry of the inlet sills.

Large scour holes developed between the 1st (Wamel) and the 2nd (Dreumel) LTW, and behind the 3rd (Ophemert), but not between the 2nd and the 3rd wall, as these walls are placed along opposite banks

with the outlet and inlet overlapping. The downstream scour hole behind the last LTW section (Ophemert) spanned over 3 km (ending at the fixed layer at St. Andries) and reached depths over 1 m.

It is important to note that the contractor extracted sediment for the construction of the LTWs. Exact locations and volumes of extraction are unclear. Van Weerdenburg (2018) estimated a volume in the same order as the Waal's annual total sediment load, indicating a significant impact and possible reason for observed holes in the bed level when comparing pre- and post-construction measurements (Chavarrías et al., 2021).

Auxiliary bank channels

Analyses of morphological development in the bank channels from tranche 1 (2016-2020) showed a pattern of sedimentation in the deeper part of the auxiliary bank channels near the wall and erosion near the shoreline (Chavarrías et al., 2021; Collas et al., 2020; Flores et al., 2022). Both Chavarrías et al. (2021) and Flores et al. (2022) attributed this primarily to bank erosion processes redistributing sediment inside the auxiliary bank channel, rather than sediment transport from the main channel.

Chavarrías et al. (2021) found in the multi-beam data a bed level increase of 0.6 m to 1.0 m over the first year after the LTW construction in the deepest parts of the auxiliary bank channel. Collas et al. (2020) and Flores et al. (2022) combined the multi-beam measurement with LiDAR data to be able to include the shallower parts of the auxiliary bank channels in their analysis. With the help of a fill function in ArcGIS, they estimated total sediment volume change and found net erosion for all three of the auxiliary bank channels between 2015 and 2020. The erosion rates decelerated over time as the banks stabilised. Bank retreat is not observed everywhere. Erosion primarily occurred where hard bank protection had been removed and covered with sand during LTW construction (Collas et al., 2020). This was the case for two distinct stretches of roughly 1 km in the Wamel and Dreumel auxiliary bank channels. Along the 1 km stretch near Wamel (see Figure A.1), the bank line retreat rate decreased from 2.8 ± 1.0 m/yr (2015–2016) to 0.4 ± 1.7 m/yr (2018–2019) (Flores et al., 2022). Results of the volumetric analysis and the bank erosion from Flores et al. (2022) and Collas et al. (2020) are shown in Appendix A.1.

Sediment sorting

The Waal experiences a natural transverse sorting of with finer sediment concentrated on the left side of the river and coarser on the right. This may influence type of sediment entering the different auxiliary bank channels over the inlet sill. With the LTWs near Wamel and Dreumel on the left bank of the river, their inlets are exposed to a finer sediment load, while Ophemert is placed on the right bank where it is exposed to a coarser sediment mixture (De Ruijsscher et al., 2020; Mosselman & Sloff, 2026).

De Ruijsscher et al. (2020) discussed field measurements from 2017 that found coarser sediment (D_{50} of 2.48 mm) directly behind the inlet sill in the auxiliary channel of Ophemert. He concludes that the steep-sloped inlet sill limits, but does not prevent, bedload transport into the auxiliary channel. At the downstream end of this auxiliary bank channel, finer sand (D_{50} ≈0.59 mm) was found, suggesting a longitudinal sediment fining trend due to lower velocities in the channel. However, Chavarrías et al. (2021) points out that the spatial resolution of these samples is too limited to draw firm conclusions on transport modes or fining patterns.

Limitations of field measurement analysis

It is important to note that the construction of the pilot LTWs was paired with lowering of groynes and construction of the Passewaaij auxiliary channel, making it difficult to isolate the impacts of the LTWs in the data analysis. Also, no pronounced floods occurred during the five years, only a pronounced drought in 2018. Isolating the LTWs and testing more extreme discharges can be done with modelling.

Furthermore, it should be said that even though there have been volumetric analyses done with sediment balances accounting for bank erosion, it remains unclear how much sediment passes the inlet sill and the walls of the LTWs. Whilst quantifying discharge partitioning is feasible, the amount of sediment passing the structures remains a major knowledge gap.

2.5. Modelling of LTWs in the Waal with Delft3D-4

This section provides background information on modelling of the LTWs in the Waal in Delft3D-4 and the models used in this research, to help understand decisions made in the Methodology Chapter 3. Three Delft3D-4 models will be discussed:

1. The DVR model of the Dutch Rhine branches, originally developed between 2006 and 2015 and revised in 2024 by (Sloff et al., 2024).
2. The model used in the HKV study for RfR2.0 to investigate a multi-channel system for the Waal from Barneveld et al. (2025) discussed in paragraph 2.1. This model utilised the revised 2024 DVR model as its basis and added the MP3 design with LTWs along the Waal.
3. A refined model of only a 47 rkm reach of the Waal with the pilot LTWs from Omer et al., 2019a.

2.5.1. Schematisation of the wall geometry

Dutch river terrain information is stored in Baseline, a software tool developed by Deltares and Rijkswaterstaat that serves as the primary data repository for Dutch river schematisation, including bathymetry, hydraulic roughness, and geometry in the Netherlands (Paarlberg et al., 2021; Sloff et al., 2024). A standardised approach for the schematisation of LTWs in Delft3D has not yet been established. Rijkswaterstaat excludes bathymetry sample points at the place of the crest of the LTWs in Baseline and incorporates the walls (not the inlets) as 2D weir files. Individual modellers manually incorporate the structures using diverse techniques (Sloff et al., 2024; Van Linge, 2017).

LTWs are typically schematised by (i) incorporating the walls into the bathymetry as raised bed level in the depth file, (ii) as 2D weirs on the sub-grid, and (iii) as a combination of the two (Omer et al., 2019b; Sloff et al., 2024). 2D weirs are placed on grid-lines in the sub-grid and allow flow the wall crest to be represented without occupying horizontal space within the computational grid as they have a zero width. Since the weir is physically not in the model, it does not account for the blocking of sediment when they overflow. Incorporating LTWs in the bathymetry instead of (only) using a 2D weir introduces a physical barrier that the sediment has to overcome to be transported to the auxiliary bank channel. This approach strongly depends on the grid resolution, as the minimum width of the structure is constrained by the size of the grid cells. For coarse grid models, this can result in a reduction of true cross-sectional flow area. Although schematising with 2D weirs causes an overestimation of the cross-sectional flow area in the model, as the LTW have a significant width.

The Sloff et al. (2024) revision of the DVR model did not revise the schematisation of the LTWs in the model. The terrain information from Baseline was used without modification for the LTW schematisation, so the LTWs were schematised as 2D weirs with a small raised bed level in the bathymetry from interpolating samples close by the wall. Barneveld et al. (2025), who performed the HKV study with LTWs in the entire Waal, adjusted the bathymetry to incorporate the walls: the height of the grid cells adjacent to the 2D weirs on the main-channel side was increased to the crest height of the walls. These two different schematisations are shown in Figure 2.10. The difference in sediment blocking and cross-sectional flow area between the schematisation methods, may significantly influence the representation of sediment dynamics and morphological development around LTWs. Nevertheless, the optimal schematisation method or the extent to which these differences affect model outcomes remain uncertain.

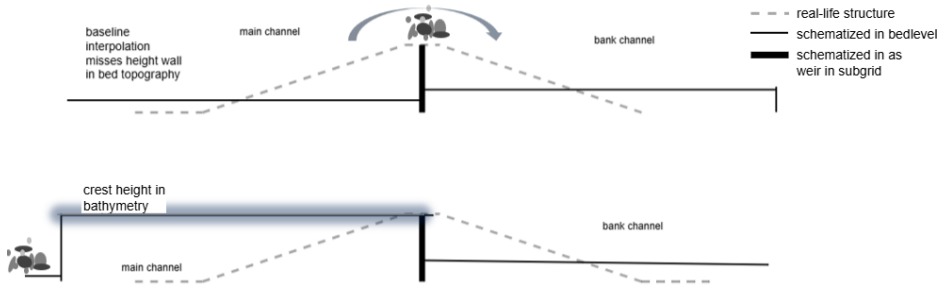


Figure 2.10: Sketch of schematisation's of the longitudinal walls in the DVR model of the Waal. The top shows the schematisation in the model of Sloff et al. (2024) and the bottom of Barneveld et al. (2025)

The refined model from Omer et al. (2019b) allowed a better representation of the steep slope of the structure. The grid-lines are not in line with the centre of the wall, but with the centre of the cell representing

the crest, see Figure 2.11.

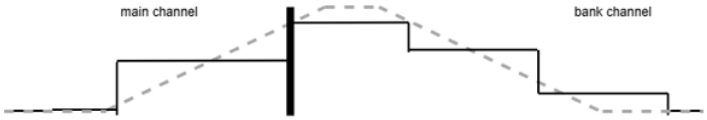


Figure 2.11: Sketch of schematisation of the LTWs in the refined model (Omer et al., 2019b).

2.5.2. Schematisation of the inlet sill at the entrances

The DVR model is based on the terrain in the beginning of 2018, which means that the inlets of the LTWs were not yet heightened (see Figure B.1). The DVR model did not use 2D Weirs to schematise the open inlets, but an increase in bed level can be seen in Baseline. Due to interpolation, the height of the inlet sill crest is not accurately incorporated in the model, see Figures D.2-D.4.

2.5.3. Sediment transport model

The updated DVR model utilises a multi-fraction Meyer-Peter and Müller (MPM) sediment transport formula, which has been calibrated per river branch to simulate large-scale transport gradients.

$$\theta_i = \left(\frac{u}{C}\right)^2 \frac{1}{\Delta D_i} \tag{2.6}$$

$$s_i = \alpha p_i D_i \sqrt{\Delta g D_i} \left(\mu\theta_i - \xi_i \theta_{cr,i}\right)^{1.5} \tag{2.7}$$

C = Chézy roughness value ($m^{1/2}/s$)
D_i = mean diameter of the sediment fraction ($D_i = \sqrt{D_{\text{upper sieve}} \cdot D_{\text{lower sieve}}}$) (m)
s_i = sediment transport per unit of width for size fraction i (excl. pores) (m^2/s)
p_i = availability of fraction i in the bed (-)
u = flow velocity (m/s)
α = calibration coefficient (-)
Δ = relative mass density of sediment in water (-)
μ = ripple factor (-)
θ_i = Shields parameter for grain size D_i (-)
$\theta_{cr,i}$ = Critical Shields parameter; 0.025 was used for all sediment types (-)
ξ_i = hiding-and-exposure coefficient for grain size D_i (-)

In the original MPM formula, an additional factor of 8 appears alongside α. This factor is absorbed into the calibration coefficient α in this case. For the Waal, α was calibrated to 2.4 to match summerbed observations.

Sediment transport is calculated per sediment fraction. The model currently simulates 11 sediment fractions ranging from fine sand (63 µm) to coarse gravel (125 mm), all with MPM with only bedload as possible transport mode. Fractions smaller than 63 µm (clay and silt) are considered 'washload' that does not contribute to bed-level changes in the summerbed, and are therefore intentionally excluded (Sloff et al., 2024). Recently, 1D modelling of the Rhine branches employed a combination of the Engelund-Hansen (EH) formula for sand (lower reaches only) and MPM for gravel. However, the 2D DVR model relies solely on MPM. This selection was made to avoid unrealistic large-scale sorting processes that can occur in 2D simulations when sand and gravel fractions are not perfectly aligned regarding their non-linearity and absolute transport magnitudes (Sloff et al., 2024).

The MPM implementation in the DVR model is combined with hiding-and-exposure effects using the Parker et al. (1982) formulation to account for the interactions between different grain sizes in a bimodal sand-gravel bed.

$$\xi_i = \left(\frac{D_m}{D_i}\right)^{A_{sklhe}} \tag{2.8}$$

The transverse bed slope effects are included with Koch & Flokstra (1980) extended by Talmon et al. (1995) (see Equation 2.5 and 2.5). Delft3D-4 represents equation 2.5 for the sensitivity of the transport direction to the transverse bed slope $f(\theta)$ as follows:

$$f(\theta) = A_{sh} \cdot \theta^{B_{sh}} \tag{2.9}$$

With A_{sh} and B_{sh} being adjustable parameters. $B_{sh} = 0.5$ is used across all modelled Rhine branches in the DVR model. A_{sh} was calibrated based on transverse bed slope observations in the summer bed to 1.1 for all modelled Rhine branches for all incoming discharges to maintain consistency across the hydrograph. The A_{sh} can be specified per incoming discharge step and domain in Delft3D-4. The parameter remains fixed spatially within a domain, meaning it does not vary locally between a standard river bend and a steep structure like an LTW inlet sill in Delft3D-4.

Van der Niet (2026) investigated the sensitivity of sediment inflow into the auxiliary bank channel to transverse bed slope by increasing the A_{sh}, from the originally calibrated 1.1 to 2.0, and 4.0. This increased the sediment entering the auxiliary bank channels; the yearly sediment inflow in all auxiliary channels together, increased by approximately 160% with the A_{sh} increased from 1.1 to 4.0. The higher A_{sh} reduces the relative contribution of gravitational downslope deflection, allowing a larger fraction of bedload to pass over the intake sills rather than being deflected back towards the main channel. The results demonstrated that the model's sediment partitioning is highly sensitive to this parameter. Altering the A_{sh} parameters also alters the main channel river bed; a higher A_{sh} value reduces the gravity working on the slope, allowing the spiral flow to increase the transverse bed slopes in the main channel over time. A lower value increases the gravitational pull and will flatten the bed.

HKV used in model 2 the DVR model settings for the transport. The refined used a different sediment transport formula and worked with only one uniform sediment fraction, more information can be found in the report of Omer et al. (2019a).

2.5.4. Morphologically inactive auxiliary bank channels

The sediment transport parameters in the DVR model are calibrated based on main channel observations. To prevent the model from producing unrealistic erosion results, auxiliary bank channels are considered morphologically inactive in the DVR model (Sloff et al., 2024; Van der Niet, 2026). With an initial sediment thickness layer of zero, the auxiliary channel can be seen as a fixed layer and sediment transport is only possible once sediment supplied from upstream enters a cell, making sediment available for transport.

In addition to the local sediment supply limitation, a reduction factor to the computed transport capacity based on the concept of Struiksma (1999). When the available sediment on top of a fixed layer becomes below a certain threshold thickness, a reduction factor is added to account for increasing exposure of local bedforms in the underlying non-erodible bed. The reduction factor is defined as the ratio between the available sediment thickness and the threshold value, limited to a maximum of 1.0 and reducing the transport to zero when there is no available sediment:

$$S_{\text{actual}} = \min\left(1.0, \frac{DPSED}{THRESH}\right) \cdot S_{\text{capacity}} \tag{2.10}$$

$DPSED$ = the depth of sediment available at the bed [m]
$THRESH$ = is the user-defined threshold (0.7 m in the DVR model)

As models are morphologically played in, some sediment is available at the start of the runs from the spin-up time on top of the fixed layer. This still allows some erosive behaviour in the auxiliary channel, although transport rates remain limited by the reduction factor and the supply limitation.

This research also adopts a zero initial sediment thickness in the auxiliary bank channels, since other research has shown strong instability when erodibility is increased. The influence of the assumed fixed layer on the sediment transport rates is revisited in the discussion in Chapter 6.

2.6. Reflection on remaining uncertainties

Large-scale morphological modelling of auxiliary bank channels remains limited in coarse Delft3D models calibrated to observations from the main channel. The schematisation of the walls and the inlet sills differs per modeller, altering morphological processes activated in the model. The gravitational transverse bed slope adjustment on the sediment transport vector has a strong relationship with the amount of sediment entering; a higher A_{sh} value weakens the transverse slope correction, reducing the deflection of bedload toward the deeper main channel and thereby allowing more sediment to pass over the inlet sill or submerged wall into the auxiliary bank channel. It remains unclear how much sediment actually enters over the side-weir at the inlet and the wall . This lack of field-validated benchmarks makes it difficult to assess whether current schematisation choices and calibration parameters adequately represent sediment distribution in models with LTWs. A better understanding of how schematisation choices affect the representation of sediment distribution and stability in LTW auxiliary bank channels, in the standard DVR model and under alternative schematisation methods, is therefore needed. Such insights are also relevant for the schematisation of LTWs in the next generation of morphological models of the Waal.

3

Methodology

To answer the research questions, this research combined two complementary approaches: field data analysis and numerical modelling. Numerical modelling primarily consisted of ten-year simulations for different schematisation variants, complemented by a small number of short stationary test runs to examine specific coarse-grid limitations in more detail.

Literature and field observations of the LTW near Wamel were used to identify key physical processes governing sediment exchange between two channels and the morphological development of the auxiliary bank channel, addressing sub-question 1. The ten-year numerical simulations then formed the core of this research: a refined model, in which the LTW geometry could be resolved in greater detail, was compared against several coarse-grid schematisation variants of the existing DVR model. This comparison served two purposes. First, it evaluated how reliably the standard DVR schematisation reproduces the morphological development of the auxiliary bank channel, addressing sub-question 2; this was assessed both against the refined model and, where available, against the field observations. Second, by systematically varying how the LTWs are represented across schematisation variants in the coarse-grid, model results were used to identify which schematisation choices improve the representation of key processes at the wall and inlet sill the most, addressing sub-question 3. Finally, short stationary test runs were used to examine, in more targeted detail, whether the DVR model's existing calibration parameters (A_{sh} and A_{cal}) can compensate for the weakened gravitational sediment transport deviation in the coarse grid, addressing sub-question 4. The remainder of this chapter elaborates on the approach taken.

3.1. Field data analyses

For this research, multi-beam echo sounder (MBES) bed level measurements of the auxiliary bank channel near Wamel from 2016–2020 and 2025, provided by Rijkswaterstaat, were used. MBES measures the bed level by mounting a transducer array beneath a survey vessel, which emits a fan of sonar beams and records the travel time of the reflected acoustic signals to reconstruct the bed surface.

Measurements through the years were selected from periods with low-flow conditions, when the river had sufficient time to dissipate bed disturbances caused by high-discharge events typical for the winter months. Discharge observations at Lobith helped guide the selection to match hydraulic conditions across years as closely as possible. For 2018, an exceptionally dry year, measurements from slightly earlier in the year were used to better match the discharge conditions of the other survey periods. In 2020, no summer measurements were available, so October measurements were used instead. The following bed level measurements were used:

- 2016 week 39 (26 Sep - 2 Oct)
- 2018 week 26 (25 Jun - 1 Jul)
- 2020 week 42 (12 Oct - 18 Oct)
- 2025 Q3 around August

Additionally, measurements from Q1, Q2 and Q4 of 2025 were used to investigate morphological development near the inlet through the seasons, seen Appendix A.2.

The data provided by Rijkswaterstaat has a resolution of 1 m × 1 m and was analysed using QGIS. Model simulations were compared with observed bed-level trends and spatial sedimentation patterns rather than exact values, given the limitations of the model and the measurements. Focus was placed on:

- overall sedimentation and erosion patterns in the auxiliary bank channel in similar magnitudes and spatial distribution,
- long-term morphological tendencies,
- propagation of local scour holes or sedimentation bumps.

The purpose of the field analysis and validation was not full calibration, but to evaluate model performance in capturing key morphological processes. Therefore, the focus was not on matching exact bed levels, but more on trends and patterns in morphological development.

3.2. Numerical modelling

3.2.1. Model set-up

This study employs Delft3D-4 for 2D morphodynamic simulations using the DVR instrumentation developed by Deltares. Although the newer generation D-HYDRO (Delft3D-FM) offers a flexible mesh and improved hydrodynamic performance, there is not yet a released calibrated morphological model of the Waal. Employing the DVR model ensures consistency with previous work on LTWs in the Waal and direct relevance to ongoing decision-making regarding the morphological development of LTWs in the Waal within the RfR2.0 programme (Barneveld et al., 2025; Chavarrías et al., 2021; Huthoff et al., 2011; Omer et al., 2019b; Paarlberg et al., 2021; Sloff et al., 2024; Van der Niet, 2026; Van Linge, 2017).

Numerical modelling is carried out using two Delft3D-4 models:

1. A coarse model that contains the 3 subdomains of the Waal from Rkm 867 (the Pannerdensche bifurcation) to Rkm 953 (Gorinchem) of the DVR model revised by Sloff et al. (2024). The grid cells in this model are approximately 80 m in the streamwise direction and 20 m in the transverse direction. The model has been calibrated and validated, the riverbed has been spun up and there are hydrological restart files.
2. A refined model of a limited reach of the Waal containing the pilot LTWs. The model starts at Rkm 888 (downstream of Nijmegen) to Rkm 934.7 (Zaltbommel). This model was generated for this research with the grid of the model developed by Omer et al. (2019b) and utilised by Paarlberg et al. (2021). To correctly capture the geometry of the walls and sills, the grid was locally refined to a resolution of approximately 20 m in the streamwise direction and 4 m in the transverse direction at the walls.

How the LTW fits in these grids is shown in Figure D.1.

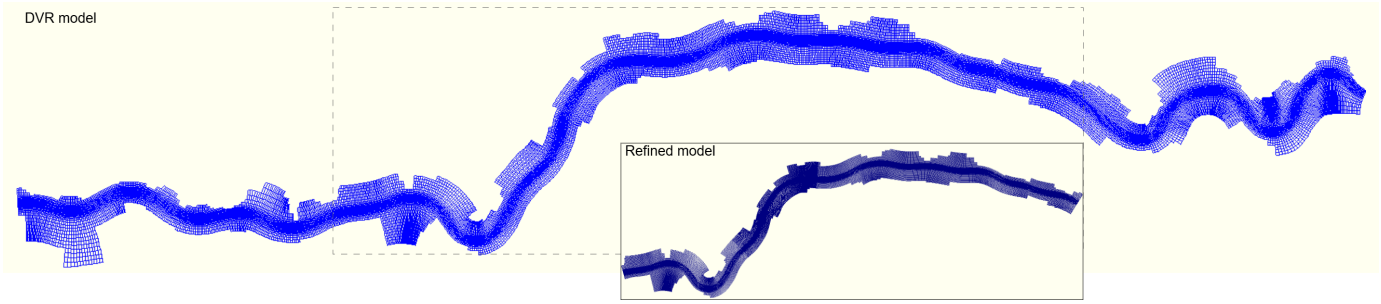


Figure 3.1: Computational grid of two used models of the Waal.

The following adjustments were made to the DVR model:

- **Boundary conditions:** A different hydrograph was used to simulate the discharge in the Waal for 2016-2025. Instead of one representative hydrograph that is repeated annually, measurements at Lobith were used to schematise a stepwise hydrograph. Instead of using a representative annual repeating hydrograph, this one follows annual variations. This decision was made to better match the hydrological conditions the LTWs faced in the real-life system, making comparisons with monitoring data more reliable. Standard discharge values were used to be able to reuse pre-existing hydrological restart files. The full hydrograph used is shown in Appendix C.

- **Schematisation methods:** Different schematisation methods to represent the LTWs were tested in the coarse model to be able to investigate the influence of this decision and identify key processes. For the walls, the two methods discussed in section 2.5.1 were used:
  1. The original way that the walls are included in the DVR model and Baseline: with 2D weirs at the centre of the crest and a slight increase in bed level that remained from interpolating the bed level in front of and behind the wall; see the top cross-section in Figure 2.10 and a top view in Figure D.3.
  2. The crest height is incorporated inside the bathymetry in the row of cells located into main channel against the 2D weir, which is aligned with the crest of the wall. The 2D weirs now become inactive as they are submerged in the bathymetry. See the bottom cross-section in 2.10 and a top view in Figure D.2.

  For the inlet sill, three different schematisation methods were used to test the influence of including the heightening. The following schematisations for the inlet sills were used:
  1. For reference, the inlet sill was left open during the entire simulation as schematised in the DVR model; the bathymetry from Baseline (no 2D weirs), see Figure D.2 or D.3 without the white line.
  2. Adding 2D weirs at the centre of the crest that are heightened during the run, see Figure D.2 or D.3.
  3. Inside the bathymetry with the as-built crest height. To represent the heightening of the inlet sill during the simulation, a nourishment was performed in the cells that represent inlet sill, see Figure D.4. This was done with the dumping-and-dredging option in Delft3D. For the nourishment, a tracer sediment fraction was used to be able to separate the sediment from the rest and make sure the inlet sill would stay in place and not erode away. For the nourishment, large stones (diameters between 1.5 – 1.8 m, larger than typical riprap, in Dutch *"stortsteen"* were used with a critical shear stress of 0.1 instead of the 0.025 used for the rest of the sediment in the model.

- **Transverse bed slope adjustment parameter A_{sh}:** The gravitational sediment transport deflection due to transverse bed level differences is represented in the model with the Koch and Flokstra formulation, extended by Talmon (1995). Delft3D allows tuning of this process with the calibration parameter A_{sh}, shown in Equation 2.9. The parameter was varied to see the effect on sediment transport over the LTW. A_{sh} is only variable per model domain, not locally. The parameter was varied for the second domain of the Waal (wl2b), the domain that includes the LTWs.

As monitoring data remains limited and there is no data that quantified the amount of sediment passing the structure, a refined model was used as a benchmark in analysing the coarse variants and to increase insights into how coarse grid schematisation decisions limit model results. To generate a refined model that operates in a similar way as the DVR model, the same model settings and calibration parameters were used. Additionally, the same spin-up procedure was followed. Just like with the coarse model, refined model spin-up was performed with a depth profile obtained from Baseline, before LTW schematisation alterations were done. Appendix E explains in depth how the refined model was set up and what spin-up procedure was followed.

Initial river bed

Although both models followed the same spin-up procedure, a difference remains in the resulting initial river bed and sediment availability in the auxiliary bank channel. Figure 3.2 shows the bed level and available sediment at the start of the coarse and refined simulations. It can be seen that the bed level in the main channel along the upstream reach of the LTW is deeper in the refined model than in the coarse model. In the downstream reach of the LTW near Wamel, the coarse model shows a deeper river bed than the refined model.

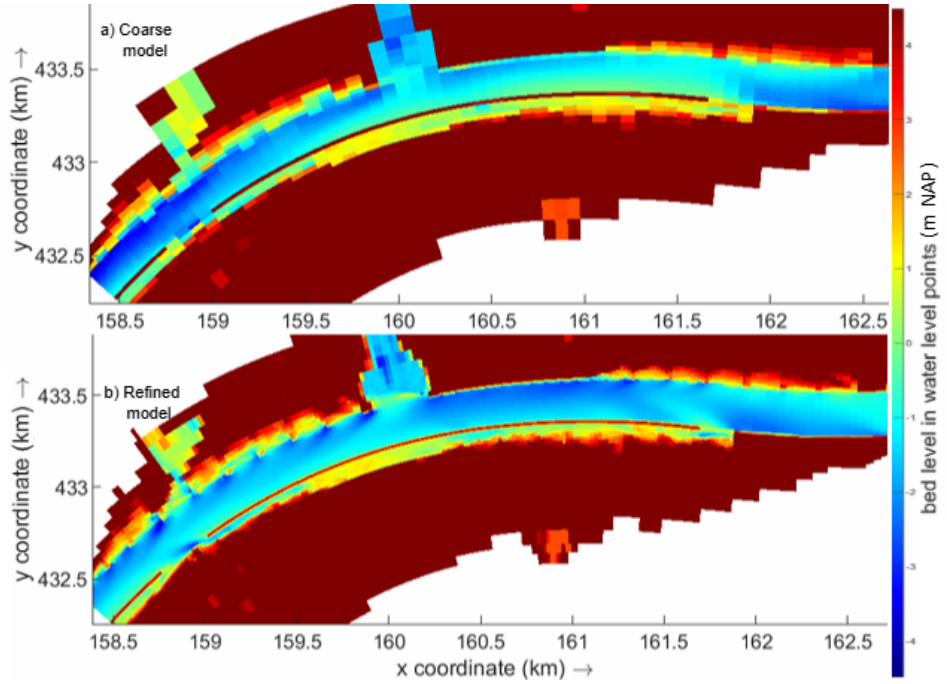


Figure 3.2: Bed level after the spin-up procedure that is used at the start of the model simulations for the coarse (a) and the refined model (b).

The auxiliary bank channels have a non-erodible fixed river bed (Section 2.5.4). During the spin-up procedure, some sediment was deposited on top of this fixed layer, which is shown in the available sediment thickness on the right in Figure 3.3. Bedload transport and morphological development are directly constrained by how much sediment is available in the grid cells. As the river bed can not erode below the fixed layer, the initial sediment thickness gives the maximum possible erosion. The total volume of available sediment in the auxiliary bank channel at the start of the simulations was 63998 m^3 for the coarse model and 63907 m^3 for the refined model. Although the total amount of available sediment (and possible erodibility of the auxiliary channel) lies very close together, the spatial distribution shows that the refined model has less available material in the upstream reach of the auxiliary channel and more in the downstream reach compared with the coarse model.

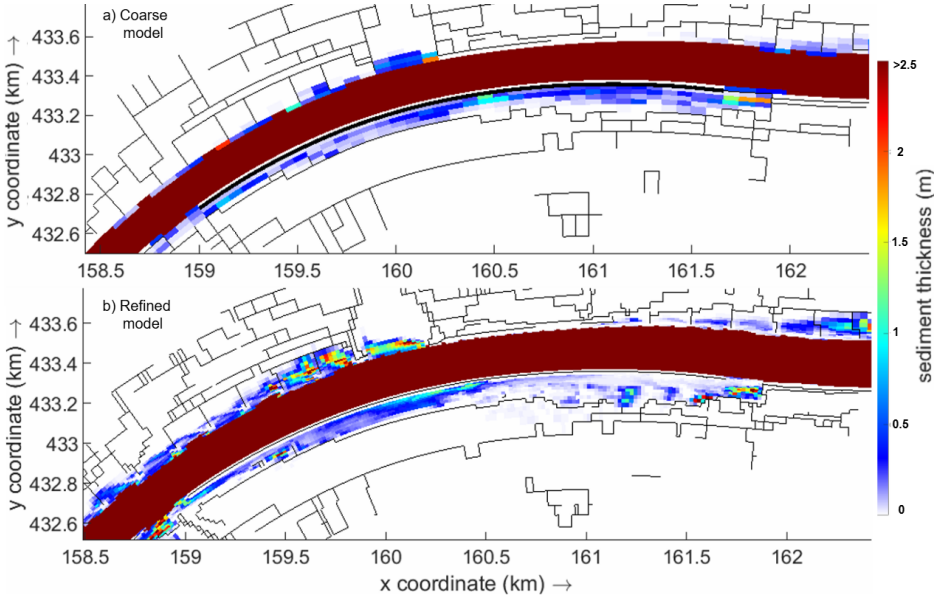


Figure 3.3: Sediment availability in the auxiliary bank channel at the start of the simulations for the coarse (a) and the refined model (b).

3.2.2. Modelling workflow

Two types of simulations were performed. First, ten-year simulations were run for the alternative schematisation methods, including one with altered A_{sh} parameters to test the model's sensitivity (see Table 3.1). Two additional ten-year simulations were performed in the refined model to help interpret these results: one with a milder wall and inlet sill slope, to verify the importance of the steep slope not captured in the coarse grid, and one with an alluvial (non-fixed) auxiliary bank channel bed, to gain insight into how the system would behave without the constraint of the non-erodible bed used elsewhere in this research. Following their analysis, short stationary test runs and simple hand calculations were performed to further examine coarse grid limitations.

Ten-year simulations

Table 3.1: Overview of model variants for ten-year simulations of the Waal.

Run ID	Grid	Wall schematisation	Schematisation heightening inlet sill (2018)	A_{sh}	Comment
W1	Coarse	Bathymetry	–	1.1	
W2	Coarse	2D weirs	–	1.1	
W3	Coarse	Bathymetry	2D weirs, height updated	1.1	
W4	Coarse	2D weirs	2D weirs, height updated	1.1	
W5	Coarse	Bathymetry	Nourishment (in bathymetry)	1.1	See Figure D.4
R1	Fine	Bathymetry	–	1.1	
R5	Fine	Bathymetry	Nourishment (in bathymetry)	1.1	
R5_M	Fine	Bathymetry, mild slope	Nourishment (in bathymetry) mild slope	1.1	See Section 5.2.5
R5_E	Fine	Bathymetry	Nourishment (in bathymetry)	1.1	Erodible auxiliary bank channel
W3a	Coarse	Bathymetry	2D weirs, height updated	0.2	
W3b	Coarse	Bathymetry	2D weirs, height updated	0.85	
W3c	Coarse	Bathymetry	2D weirs, height updated	1.45	

Analysing hydrodynamics
In order to properly model morphological development, representing hydrodynamics well is key, as hydrodynamics drives morphodynamics. The hydrodynamic performance of the model was considered by looking at the discharge distribution and the flow patterns based on depth-averaged flow velocity vectors around the inlet.

The discharge distribution in the model simulation between the main and auxiliary channel was measured every 0.5 rkm. The distributions are assessed by comparing them with ADCP measurements from 30-09-2025 to verify that they remain realistic across the different schematisation methods. Four different moments with a discharge at Lobith of approximately 2500 m^3/s were selected for this comparison. This discharge gave the best match with the available data, which lies slightly below this value. At this discharge, the wall is not yet submerged, whereas the inlet sill is submerged, also after the heightening. The first two moments are before the inlet was heightened in 2018, the last two after.

The depth-averaged flow velocity around the inlet was checked to see if the models were able to simulate the recirculation expected at the onset of the LTW, and whether the transverse distribution of flow velocity was as expected.

Analysing morphodynamics
To analyse the morphological development of the simulations, the following results were analysed:

- The spatial distribution of cumulative sedimentation/erosion over the ten years.
- Cumulative bedload transport through different pathways entering and exiting the auxiliary bank channel per discharge step. This was done using defined cross sections in the model domain. The obtained values were corrected by multiplying with the morphological acceleration factor (Morfac)

used for that step, see table C.2. With these transport rates, the pathways sediment took were analysed for varying schematisation variants, and sediment balances of the auxiliary bank channels were made. Separate balances over different time spans were used to see trend changes after inlet adjustments and to identify an initial response. To compare transport rates per discharge step, the cumulative transport values were recalculated to daily transport values based on the duration of the discharge step (-0.5 days, as each step has an initial spin-up time where it is morphologically inactive).
- bedload transport and depth-velocity vectors over the inlet sill were plotted to observe the distribution along the inlet sill length. This provided more insight into local effects of the schematised inlet geometry.
- Bed levels around the inlet were observed to see how local deposition and accumulation changed the bed level slopes that play a key role in sediment entering the auxiliary bank channel.

For model diagnostics, the following parameters were considered:

- A resulting sediment balance per variant was also made following a different procedure; based on cumulative bed level change, multiplied by the grid cell surface area and the porosity (0.6).
- Available sediment in the auxiliary channel was observed to evaluate the fixed layer constraint and the effect of the difference in initial available sediment between the refined and coarse model.

Short stationary runs: local sediment transport over inlet sill
After the ten-year simulation, hand calculations and short stationary runs were performed to analyse possible coarse grid sediment distribution corrections.

Based on the bed level in the cell centres and the width of the cells, the transverse bed slope resolved in the model was calculated. . This was compared with the as-built slope of the structure to quantify the missing ratio. An adjusted Comparing this with the as-built slope of the structure, a missing ratio was quantified. An adjusted A_{sh} parameter accounting for this ratio was then calculated by hand for a few cross-sections and moments during the simulation.

The test runs consisted of short stationary simulations, representing 25 days of morphological development. A discharge of 4350 m^3/s at Lobith was selected for the test runs, as for lower discharge there was too little sediment transport over the sill to compare the refined model with the coarse model. The threshold value for the Struiksma (1999) correction, equation 2.10, was lowered from 0.7 m to 0.001 m. The reduction factor on the sediment transport in cells with limited available sediment (a fixed layer) was turned off to avoid sediment interfering with the comparison between the sediment rates over the inlet sill in the coarse and refined model. The sill was represented inside the bathymetry, made of similar graded sediment as its surroundings (not riprap), so that the increased hiding-and-exposure effects present after dumping very coarse riprap in W5 and R5 did not influence the test results.

To improve the side-weir geometry and simulated inflow in the test runs, the bed level upstream of the inlet was adjusted in schematisation S2, placing the bank further into the river. This alteration, compared to the ten-year coarse grid simulations, was not done to improve the representation of the real system, as it moves the coarse grid geometry constraints upstream, but merely to study a local specific effect.

An overview of the short stationary test runs is given in Table 3.2. To analyse the resulting sediment distribution, focus was placed on the sediment transport rates over the inlet sill when comparing the test runs.

Table 3.2: Overview of short stationary test runs for the sediment transport over the inlet sill at Wamel.

Run ID	Grid	Wall schem.	Inlet sill schem.	A_{sh}	Local A_{cal}	Comment
WS1	Coarse	Bathymetry	Closed, in bathymetry	1.1	–	S1: W5 geometry
WS2	Coarse	Bathymetry	Closed, in bathymetry	1.1	–	S2: adjusted geometry
WS2a-e	Coarse	Bathymetry	Closed, in bathymetry	1.3/0.8/0.5/ 0.45/0.4	–	
WS2-A_{cal}	Coarse	Bathymetry	Closed, in bathymetry	1.1	0.5	See Figure D.8
RS	Fine	Bathymetry	Closed, in bathymetry	1.1	–	Benchmark

4

Field observations of the LTW near Wamel

This chapter presents MBES bed-level measurements of the auxiliary bank channel of the upstream LTW in the Waal near Wamel over nine years. Patterns in the observations are discussed to identify key processes and to validate model results.

4.1. Bed level observations in the auxiliary bank channel

Figure 4.1 shows the bed level of the auxiliary bank channel and a part of the adjacent main channel above it for four moments in the past decade, with the upstream end on the right and the downstream end on the left. Along the channel's reach, the bed level alternates between deeper and shallower zones: the bed is deeper directly behind the inlet at the upstream end, shallower between transects a and b, deeper again between b and c, shallower between c and d, and deepest in the downstream section beyond d. This pattern becomes stronger over time. Downstream of transect a, the channel widens, corresponding with lower flow velocities and sediment transport capacity, explaining the shallower bed level. The channel narrows around transects b and d, and the bed level directly downstream becomes relatively deeper again.

Looking at transverse bed level differences, the auxiliary bank channel flattens over time, losing the deeper dredged channel that was also forced back into the system in January 2018 with dredging along the wall (point 1). The dredged channel was filled up again before the summer of 2020. The flattening of the transverse bed level is mainly seen between transects c and d.

At the upstream start against the fixed bank, a deep scour hole becomes progressively deeper and more pronounced over time; see point 2. The clear pit occurs after the summer measurements from 2018, so after high flows occurred once the inlet sill was heightened. This deviates from the expected low-velocity shallow zones shown in Figure 2.6, indicating a strong recirculating flow vortex formed here. An expected shallower zone against the wall from the onset can be seen in 2025 (see line x).

In the measurements from 2020 and 2025, it can be seen that the vessel went close to the shallow sections near the bank, as the bright yellow line becomes visible. The measurements from 2016 and 2018 do not seem to go as close to the shallow parts near the banks. This can be due to higher water levels, improved monitoring, or erosion in these zones allowing the vessel to come closer.

4.2. Cumulative sedimentation/erosion observations in the auxiliary bank channel

Subtracting the bed level data of the different moments gives the bed level change between them, showing where sedimentation and erosion took place. This is presented in Figure 4.2. The bottom map shows that most of the channel experienced slight erosion (≤1.0 m) over the nine years, with deposition in the downstream half.

Looking at the upstream reach of the auxiliary channel after heightening of the inlet sill in April 2018, patterns changed significantly. Between the summer of 2018 and 2020, a scour pit against the upstream bank

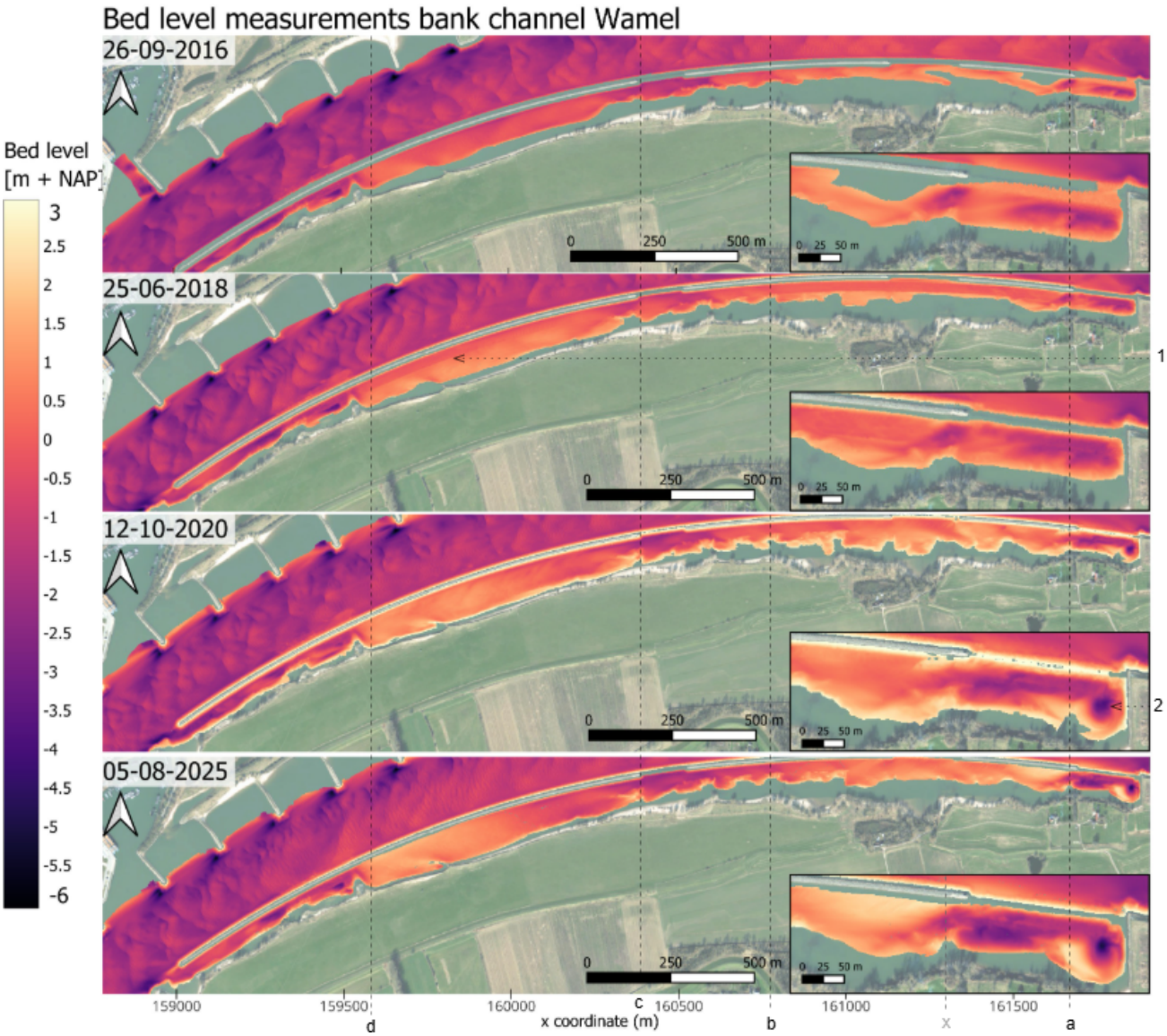


Figure 4.1: Multi-beam measurements of the bed level in the auxiliary bank channel near Wamel in the summers of 2016, 2018, 2020 and 2025. The upstream end is on the right, the downstream end on the left. Point 1 marks the dredged channel along the wall, point 2 the scour hole at the upstream end. Data from Rijkswaterstaat (2026).

formed. As measurements of 2018 were already after the heightening of the inlet sill and the measurements in 2020 after the extra opening was added at the upstream end of the sill, it can be that the scour pit is caused by the small opening added at the upstream end of the sill in April 2020. However, the lack of high-discharge events between May and June 2018 can also be the reason for the pit forming after the summer of 2018. It is interesting to see that just downstream of this pit, sedimentation occurs. Over the total nine years, this sedimentation is in the same order of magnitude as the erosion.

Not all monitoring transects reach close enough to the inlet sill to capture deposition directly in front of it; where they do, deposition is visible. Appendix A.2 shows the formation of a wedge at the downstream toe of the sill, where sediment accumulates as it overcomes the steep slope, forming a milder ramp over which sediment can eventually pass.

In the middle section, it can be seen that the 2016-2018 period shows clear green (sedimentation) across the full width. This is the reach known to have an eroding bank after protection was removed when the LTW was constructed (see Figure A.1). The findings of Flores et al. (2022) and Collas et al. (2020) in Table A.2 indicate that between 2016 and 2020 the bank line retreated around 7 m along a 1 km stretch shown in Figure A.1. Between 2018 and 2020 this was around 2.2 m. Figure 4.2 shows that sedimentation in this reach reduces over time. The erosion seems to be propagating in downstream direction. This can be from banks stabilising. Between 2018 and 2025, it can be seen that the transverse cross sections are changing,

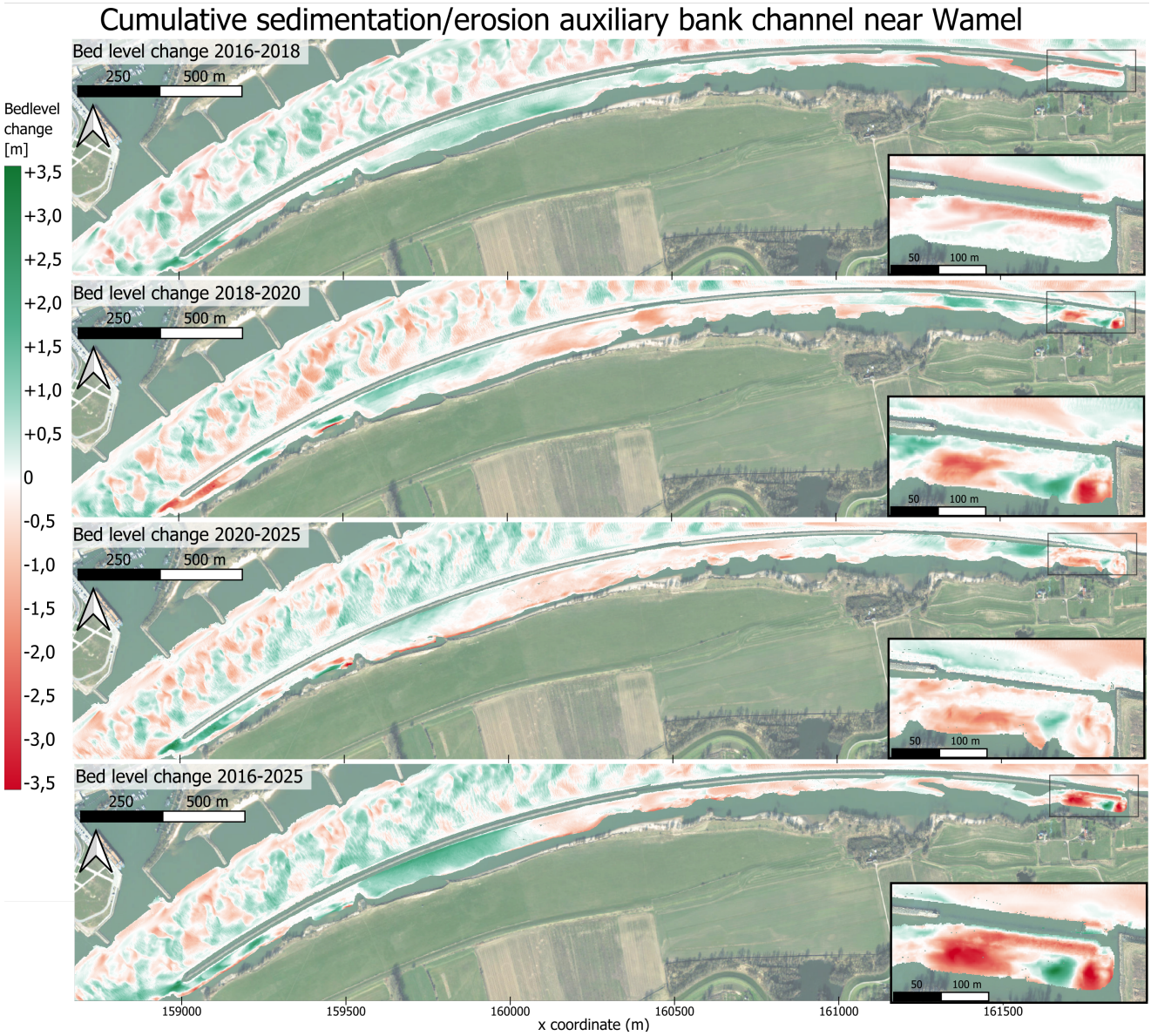


Figure 4.2: Bed level change from multi-beam measurements of the auxiliary bank channel near Wamel between the summers of 2016 and 2018, 2018 and 2020, 2020 and 2025, and cumulatively over the entire nine years. Green indicates sedimentation, red indicates erosion; insets show the upstream end at the inlet sill. Data from Rijkswaterstaat (2026).

with sedimentation in the deeper parts and erosion in the shallower parts.

The downstream reach shows very different behaviour between the years: waves of sedimentation turn to erosion and back to sedimentation. Also in this reach, it can be seen that near the bank erosion occurred, changing the transverse cross section.

4.3. Synthesis of the field observations

Figures 4.1 and 4.2 show that the system does not exhibit strongly unstable behaviour, like the filling up within a few years that was seen in models (described in section 2.4.2). Over the decade, strong erosion was seen behind the inlet at the upstream end of the auxiliary bank channel. After the heightening of the inlet sill and the addition of the small upstream opening in the closed sill, the morphological development directly behind the sill changed significantly, with a strong erosion pit forming at the upstream end. Strong sedimentation was seen along the stretch where the bank retreated after its protection was removed. The sedimentation rate in this zone reduced over time as the bank stabilised, indicating that bank processes are an important control on the morphological development of the channel.

5

Modelling results and analysis

This chapter shows the results of the model simulations. Section 5.1 first presents the hydrodynamic results, since representing the hydrodynamics well is a condition for interpreting the morphodynamic results that follow. Then, Section 5.2 shows the results of simulating 2016-2025 with the different schematisation methods for the LTW applied, comparing coarse model simulations with the refined model and field data. Section 5.3 presents results for different W3 variants with varying A_{sh} parameters to assess the domain-wide response over the simulated decade. Section 5.4 focuses on the local sediment transport over the closed inlet sill while varying calibration parameters (A_{sh} and A_{cal}) to account for slope schematisation limitations in the coarse model. Finally, a short summery of the findings is given in 5.5.

Table 5.1: Schematisation overview per variant

	Wall 2D weir	Wall in bed	Inlet sill open	Closed inlet 2D weir	Closed inlet in bed	Refined grid
W1		✓	✓			
W2	✓		✓			
W3		✓		✓		
W4	✓			✓		
W5		✓			✓	
R1		✓	✓			✓
R5		✓			✓	✓

5.1. Hydrodynamic performance

Discharge distribution

The discharge distribution between the main and auxiliary channels provides a first check on model performance. Figure 5.1 shows the discharge distribution at four moments with a Q_{Lobith} of 2500 m^3/s, compared with ADCP measurements from 30-09-2025 (red circles). The first two moments are before the inlet was heightened in 2018, the last two and field measurements after.

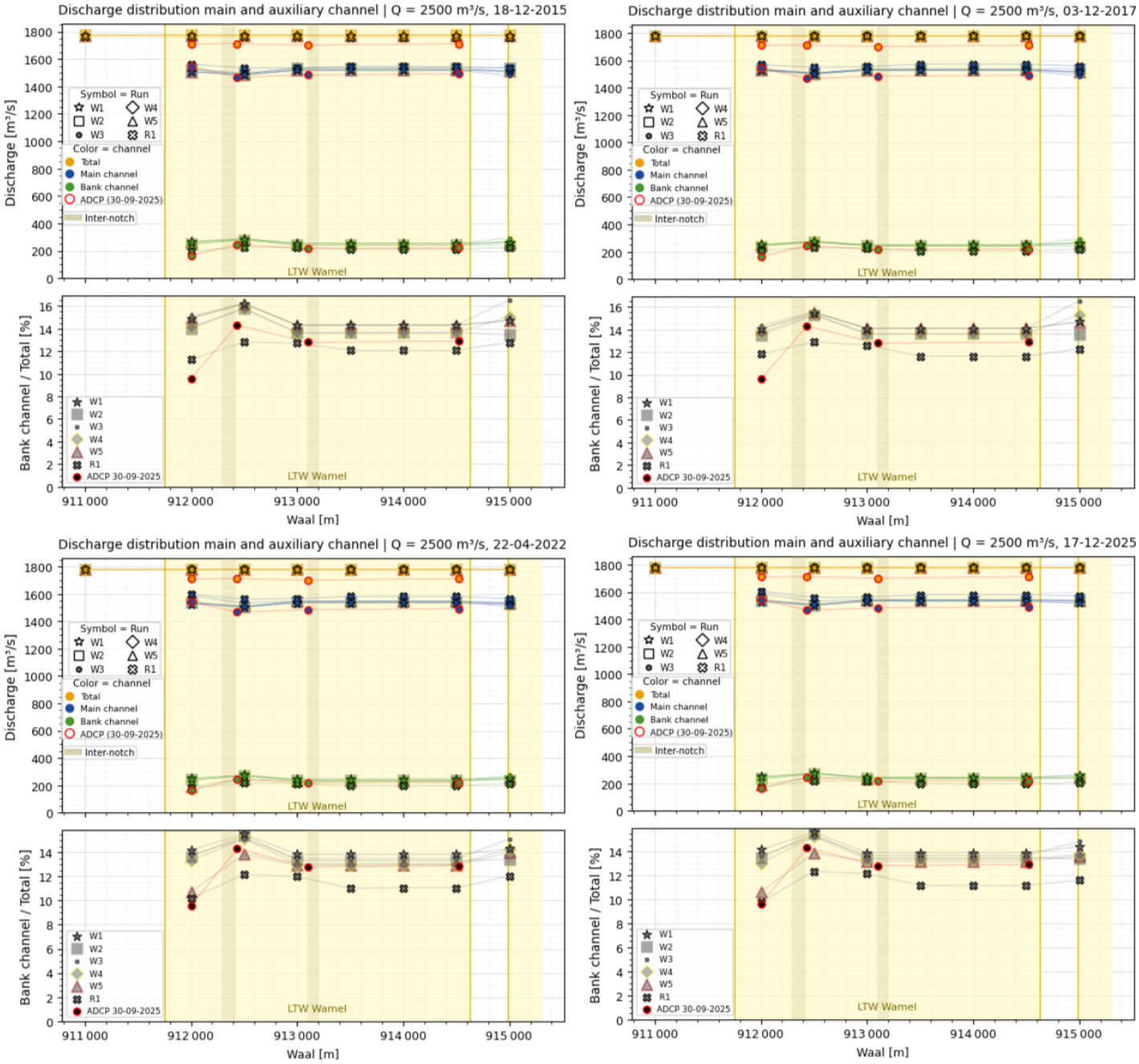


Figure 5.1: Discharge distribution between main channel and auxiliary bank channel

The discharge distributions of the simulations show overall a good match with the field measurements, with the values lying close together. The coarse model simulations show a slightly larger ratio to the auxiliary channel than the field measurements, while the refined model shows a slightly lower ratio. This can be explained by the width of the inlet; in the coarse model this is 245 m and in the refined model 188 m, in real life the sill is 200 m. Of the coarse simulations, Variant W5 shows the closest match with the field measurements. This variant incorporates both the wall and the heightened inlet into the bathymetry, which is expected to best represent the morphological processes.

The ADCP measurements show a change in the discharge distribution ratio over the upstream kilometre of the LTW where two inter-notches are present. The model results follow a similar trend, with an increasing share of the discharge diverted into the auxiliary channel, followed by a slight decrease over this stretch, but the magnitude still deviates a bit. This pattern can be explained by the inter-notches that allow for exchange of water at this discharge while the wall is submerged, and the non-prismatic geometry of the river reach. The upstream reach has a wider main channel with groyne fields on the other bank, and halfway along this stretch lie the Prins Bernhardsluizen that connect the Waal to the Amsterdam-Rijn Kanaal. Both factors alter the width ratio between the main and auxiliary channels along the reach. The model simulations reproduce a similar trend in the discharge distribution along the reach.

A clear discrepancy between the model simulation and the field data can be seen at the upstream end of LTW. The field data from 2025 reflects a situation after the inlet sill was heightened. This explains the mismatch in the first two moments in the simulations, as the inlet was still open in the model runs at those moments. Variant W1 and W2 did not include the heightening at all, and as seen, the discrepancy remains for these two variants throughout. For the two later moments shown (2022 and 2025), variant W5, in which the inlet sill adjustment was incorporated through nourishment in the bathymetry, matches the data more closely than variant W3 and W4, in which the adjustment was represented using heightened 2D weirs.

Looking at the two first moments (2015 and 2017), the variants in which the wall is incorporated in the bathymetry (W1, W3, W5) show a slightly higher ratio towards the auxiliary channel than the 2D-weir variants (W2, W4). This can be explained by the additional narrowing of the main channel in the wall-in-bathymetry schematisations.

Small differences remaining between the data and model simulations with the inlet adjustment incorporated can be due to geometry differences from schematisation limitations: the width of the inlet and inter-notches are limited by grid cell sizes. This plays a role especially in the coarse model, where the cells that form the LTW are roughly 80 m wide.

In the refined model variant, a consistently smaller share of the discharge is diverted to the auxiliary bank channel than in the field measurements. This can be due to differences in geometry: it is known that in the field, bank erosion has altered the width of the auxiliary channel, which could attract more water. Slight errors in the field data are also possible: the measurements are sensitive to how they are performed, as the measurement vessel must navigate each transect while avoiding excessive interference from passing ship traffic, and must try to start and stop at a similar, estimated distance from the banks at each cross-section.

Flow velocities around inlet

Figure 5.2 shows the depth-averaged flow field around the inlet for the different model variants, at a discharge for which the heightened inlet sill is submerged but the wall remains emergent. All variants reproduce the expected recirculation zone at the upstream end, generated by flow separation at the inlet. For the refined model, this eddy extends over approximately 7/9 of the inlet sill length. Based on the vector rotation at the indicated cell (point a), W5 develops the most pronounced eddy of the coarse variants, most closely resembling R5. The CFD results (Appendix F) show a primary and secondary gyre spanning the full length of the inlet sill; the secondary gyre (Figure F.2, point 1) is not reproduced in any of the model simulations, nor is the smaller eddy against the wall just downstream of the inlet sill, indicating that the grid resolution remains too coarse to capture these features even in the refined schematisation. The pronounced secondary gyre in the CFD results may further be linked to a local depression near the upstream end. Although the CFD model does not include the May 2020 inlet sill adjustment, the local scour pit that formed after this adjustment was present in the CFD bathymetry based on 2025 field data, but not represented in the Delft3D model simulations.

That the eddy is weaker in W1–W4 than in W5 and R5 can be attributed to differences in local geometry. In the coarse model, the wall is placed further into the main channel than as-built, so the side-weir geometry is not properly captured and water can enter the auxiliary channel in the longitudinal direction rather than being deflected. In W5, the last bank cell upstream of the sill was extended to connect the sill to the bank (see Appendix D.2, which improves the side-weir geometry and enhances flow separation. The flow direction at the entrance in W1–W4 therefore shows weaker curvature towards the bank than W5 and R5 (see the direction of the vectors at the entrance), as less deflection is required to enter the auxiliary bank channel.

The wall's crest schematised in the bathymetry (W1, W3, W5, R5) forms a local obstruction that reduces flow velocity on the downstream part of the inlet sill.

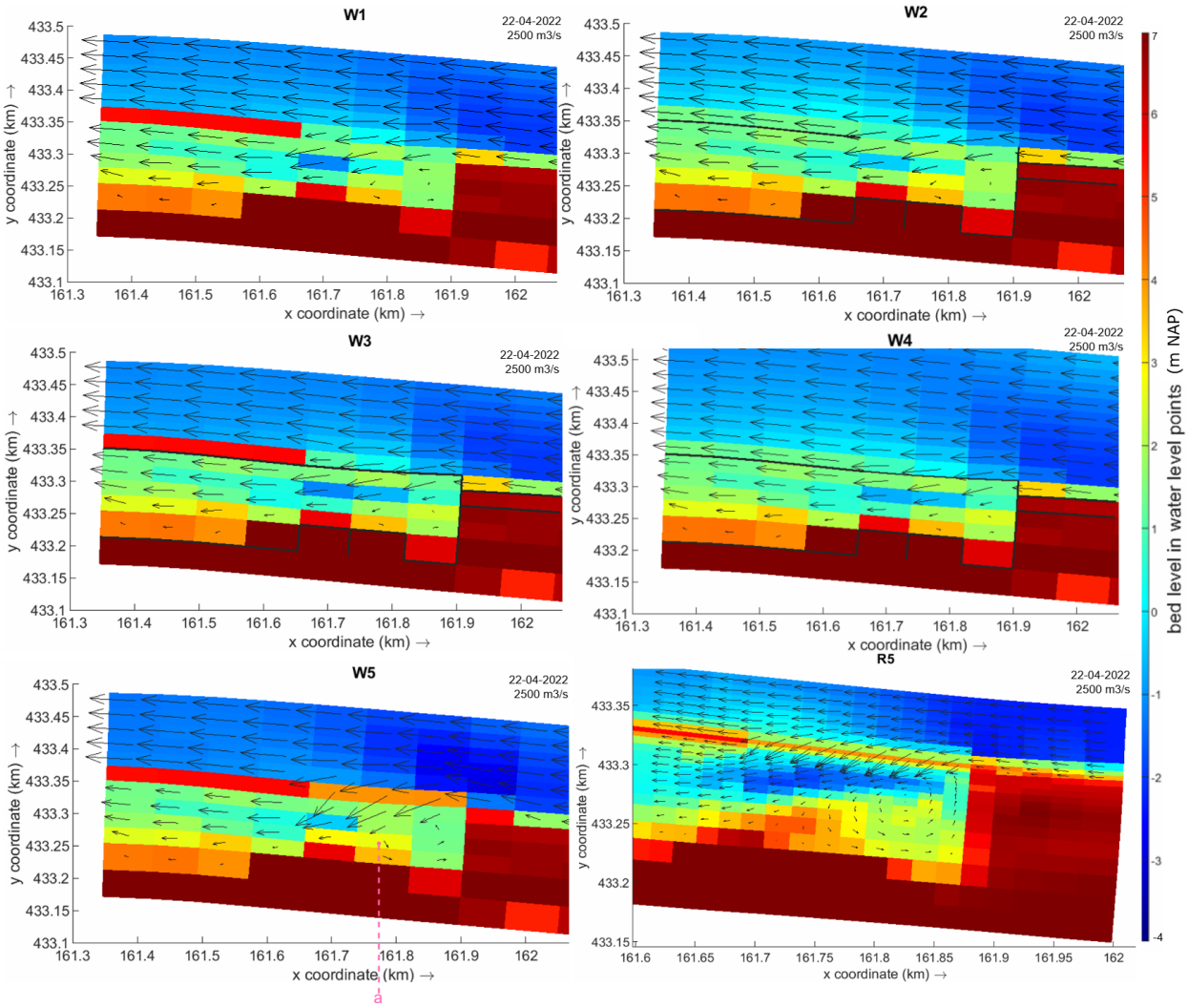


Figure 5.2: Depth-averaged flow velocity in rooted arrows on the bed level after the inlet adjustment, when Q_{Lobith} of 2500 m^3/s.

Synthesis of hydrodynamic results

Overall, the models show expected behaviour and match the field measurements sufficiently close to investigate morphodynamic development under these flow conditions. Of the coarse variants, W5, which reduced the cross-sectional flow area of the main channel due to schematisation of the structure inside the wide grid cells, gives the closest match to the measured discharge distribution after the inlet was heightened, closer than the variants that represent the heightening with 2D weirs. W5 also develops the widest eddy and the strongest transverse curvature at the entrance, matching the refined model and CFD findings better. All coarse variants, however, still allow water to enter the auxiliary channel longitudinally due to coarse grid schematisation limitations, requiring less deflection towards the bank than in the refined model.

5.2. Varying schematisation approaches for the LTWs

This section shows the results of the model simulations from the past decade for the different model variants with varying schematisation methods and grid resolutions. 5.2.1 looks at the overall morphological development of the different variants of the model. 5.2.2 and 5.2.3 dive into sediment transport effects of the schematisation methods for the wall and the inlet sill. 5.2.4 looks at behaviour change after the inlet adjustment in April 2018. Finally, 5.2.5 shows a mild slope test in the refined model, and 5.2.6 summarises the overall findings of the section.

5.2.1. Sediment balance and spatial patterns in the auxiliary bank channel

To analyse morphological development under the different schematisation methods, the spatial distribution of cumulative sedimentation/erosion over the ten years is shown in Figure 5.3. Using cross sections that outline the auxiliary bank channel, a sediment balance for 2016-2025 through these pathways is quantified in Table 5.2.

Auxiliary bank channel observations

Clear distinctions are seen in the morphological development of the auxiliary bank channels for the different variants. Variants with the wall's crest schematised as a 2D weir (W2, W4) show net sedimentation over the ten years, while variants with the wall's crest height in the bathymetry (W1, W3, W5, R5) show an overall erosional trend (Table 5.2). None of the coarse grid variants reaches the erosion magnitude of the refined model that incorporated the inlet adjustment (R5). W1 and W3 come closest in matching the total sediment balance. However, W5 and R5 show more similarity when looking at the magnitude of sediment transported through the different cross-sections entering and exiting the auxiliary bank channel.

Table 5.2: Cumulative bedload transport in and out of the auxiliary bank channel and the resulting sediment balance in [m^3] between the end of 2015 and the end of 2025 for model variants W1–W5, and R1 and R5. Positive values indicate import of sediment and negative values indicate export.

Run	Inlet_WA	Wall_WA1	Notch_WA1	Wall_WA2	Notch_WA2	Wall_WA3	Outlet_WA	Balance crs	Balance $\frac{\partial z_b}{\partial t}(1-p)A$
W1	46002	5911	82	1.62	1.55	-234	-55859	-4091	-5137
W2	77239	13302	8701	656	61	-8262	-75822	+15874	+14628
W3	43271	5206	73	1.26	1.10	-229	-52138	-3814	-4545
W4	64672	11349	7844	596	72	-7800	-66003	+10729	+9763
W5	36542	2751	624	6.35	-0.07	-173	-41001	-1250	-2674
R1	37207	358	0.04	0.00	0.00	0.00	-33604	+3960	+4025
R5	22688	624	0.12	0.00	0.00	0.00	-35119	-11806	-12008

Looking at the spatial distribution of the cumulative sedimentation/erosion in the auxiliary bank channel in Figure 5.3, the sedimentation of variant W2 and W4 mainly occurs in the downstream reach. This distribution for variant W2 and W4 shows the most similarity to the field data observations in Chapter 4: light erosion dominating in the upstream reach and sedimentation in the downstream reach, although the sedimentation onset is a little more upstream in the simulations than in the field. In the observations from the data, this was linked to bank erosion, a process not included in the model. In these model variants, the wall has no physical presence when overflown, and bedload is easily exchanged between the main and auxiliary channel along the LTW. Table 5.2 shows that variants W2 and W4 have significantly more bedload transport over the wall entering the auxiliary channel than the other variants. Most likely, the possible sediment exchange with the main channel, together with the widening due to the Prins Bernhardsluizen on the other bank, causes the sedimentation seen here in the channel in these simulations.

In the variants where sediment exchange along the LTW is reduced by the elevated wall in the bathymetry (W1, W3, W5, R5), clear erosion is seen in the middle of the channel. This spatial distribution links directly with the distribution of available sediment at the start of these simulations (see Figure 3.3). The coarse variants show more erosion upstream, where more sediment was initially available than downstream, while the refined model shows more erosion downstream, reflecting its lower initial sediment availability upstream. The pronounced erosion for W1 and W3 compared to W5 appears to stem from erosion just behind the inlet at the upstream end. As this erosion is not seen in R5, W5 matches the spatial distribution of morphological change of R5 better than W3. Differences in the distribution of the erosion between W5 and R5 are directly related to the available sediment at the start of the simulation.

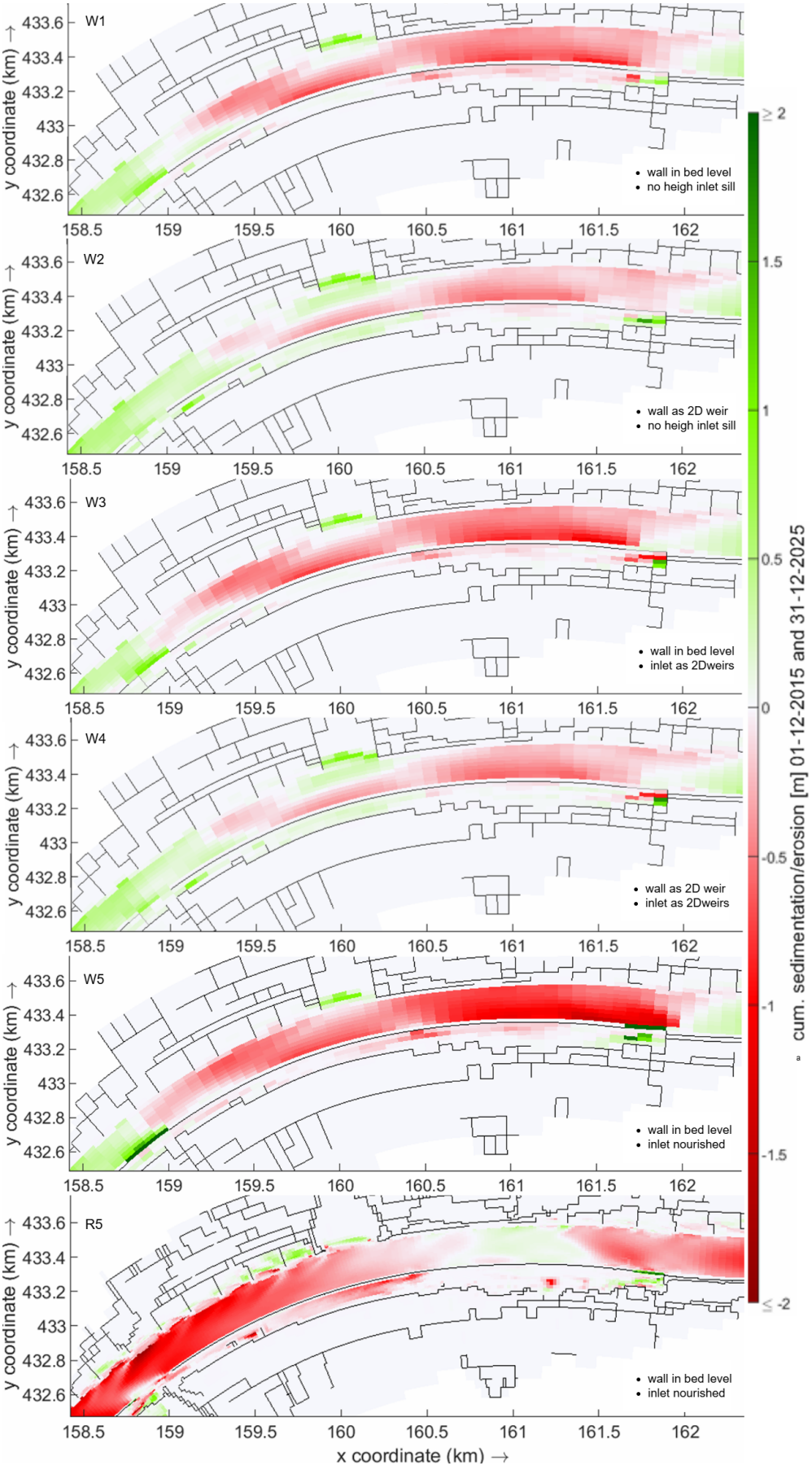


Figure 5.3: Cumulative erosion/sedimentation between the end of 2015 and the end of 2025 in the auxiliary bank channel for variants W1–W5 and R5

All variants show sediment deposition near the bank at the upstream end, consistent with the low-velocity recirculation zone from flow separation identified in Figure 2.6 and 5.2. The smaller sedimentation areas against the upstream end in variants W3 and W4 are consistent with the smaller eddy formations seen in Figure 5.2.

The field data in Figure 4.2 likewise show erosion directly behind the inlet sill, along with a pit at the upstream bank that is not reproduced by any model variant. This is likely because the small lowered section added to the inlet sill in May 2020 was not included in W5 and R5. In W3 and W4 this was included, which can explain more erosion seen. However, the scour is placed at a different location than the scour pit in the field data pointed out in Figure 4.1, point 2.

One clear anomaly is seen at the outlet where the two channels reconnect; variant W5, shows strong sedimentation here. It appears as if the outlet is closing off to an extent not seen in any other simulations. Figure G.1 shows that indeed a bump formed in the bed level at the end of the simulation for W5. However, as detailed in Appendix G.5, this sedimentation accumulates during periods of low discharge and is flushed away again at higher discharges within a year. This is in line with the described cyclic behaviour of Czapiga et al. (2022) of scour at the outlet during floods. The strong sedimentation seen in Figure 5.3 is related to the last moment being after a prolonged period of low discharge (last 15 days Q_{Lobith} 1400 m^3/s and last eight months Q_{Lobith} ≤2500 m^3/s). It is expected that if the simulation were extended a few weeks, the final cumulative bed level changes would not have shown such strong erosion. Figure G.12 shows that there is no unexpected blocking of sediment leaving the auxiliary channel. It was checked that the riprap dumped in the inlet sill in W5 and R5 had not been transported through the auxiliary channel from the heightened inlet, ruling out a potential cause of the sedimentation seen so strongly only in W5.

Main channel observations

All coarse model variants show erosion in the main channel in the upstream reach of the LTW over the ten years (Figure 5.3). The discharge abstracted from the main channel was insufficient to halt the ongoing erosion. This can be explained by the mild hydrodynamic conditions during the ten years; Appendix C.4 shows that the number of days the wall was submerged was lower than the LTWs were designed for. Milder hydrological conditions led to relatively less discharge passing the inlet sill, keeping the active flow width reduced and increasing flow velocities and erosion in the main channel.

For the variants with the wall in the bathymetry (W1, W3, W5), the erosion increased and extended downstream. This is likely due to the narrowing of the main channel from incorporating the wall's crest height a full cell-width, which raises flow velocities and the sediment transport capacity. W5, where the inlet sill is also schematised in the bathymetry, shows the strongest main-channel erosion of all coarse variants, as the narrowing extends further downstream.

Comparing the coarse runs (W) with the refined model run (R5), a different pattern is seen along the river reach. After erosion at the upstream end, the refined model shows a stretch of sedimentation in the main channel. As the simulation ends following a prolonged period of relatively mild hydrological conditions, this may reflect a bump, created by the widening at the upstream start of the LTW, that has migrated downstream. It is important to note that the bed level at the start of the coarse and refined model runs deviated (see Figure 3.2). The refined model had a deeper initial bed level in the area that experienced sedimentation. Figure G.1 shows that the bed level difference here has become less at the end of the ten years.

The expected deposition and scour due to the water abstraction shown in Figure 2.5 are not seen in the coarse model runs. However, the bed level at the start, resulting from the spin-up procedure, already showed elevated bed levels just downstream of the LTW onset, and a deeper section at the confluence. During the spin-up, the LTW was only schematised with 2D weirs for the wall sections; no wide elevated bed levels to represent the crest height. This means that the initial bed level was already adjusted to the widening of the system with a secondary channel, but not yet to the narrowing caused by schematising crest heights inside the bathymetry. This explains the more intense erosion seen in W1, W3 and W5, and also the lack of the expected deposition after the LTW onset. Additionally, the mild hydrological conditions explain why clear signs of water abstraction are not visible in the morphological development.

At the downstream end of the LTW near Wamel lies the harbour of Tiel. The local widening of the river could explain the sedimentation seen here instead of the expected erosion. However, the refined model does show erosion here. It remains unclear why the morphological development in the main channel for the downstream reach of the LTW shows so distinct behaviour.

5.2.2. Influence of wall schematisation

In all of the coarse model variants, sediment exchange over the wall takes place. Comparing variants W3 and W4, where the inlet schematisation is the same (updated 2D weirs), isolates the effect of schematising the wall the effect of wall schematisation – bathymetry (W3) versus 2D weir (W4). Figure 5.4 shows that the sediment exchange between the main and auxiliary channel is substantially larger when the wall is a 2D weir. In variant W4, the amount of sediment overtopping the wall in the first wall section (Wall_WA1) is 2.2 times larger than in variant W3. Along the second half of the LTW reach (section Wall_WA3), a large sediment flux went back into the main channel over the wall. This reduced the balanced sediment exchange over the wall, bringing the total flux for W4 close to that of W3.

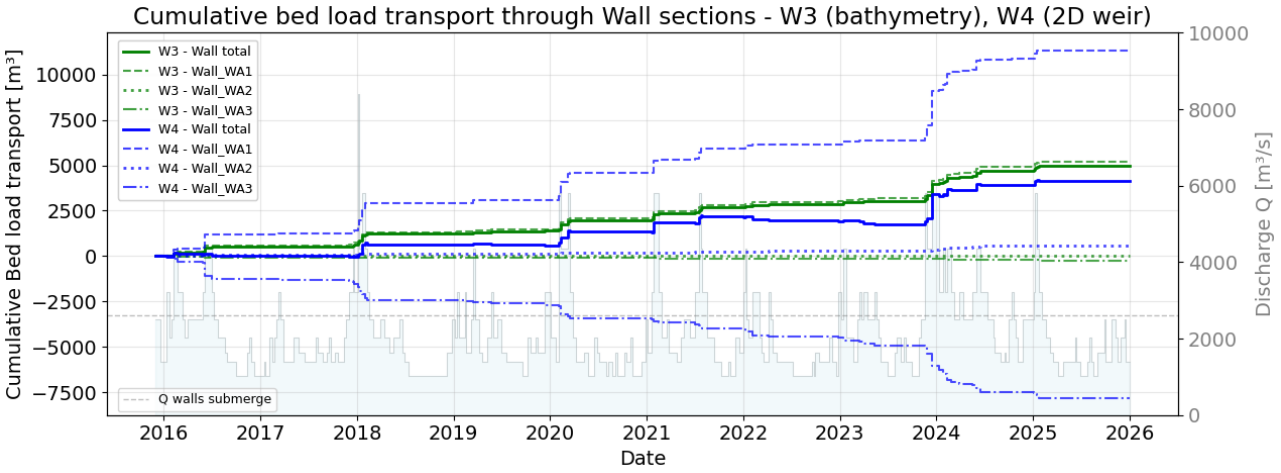


Figure 5.4: Bedload transport over the wall for variant W3 (crest in bathymetry) and W4 (2D weir). **Sediment through the inter-notches is not included*

For all simulations, the largest amount of sediment transport over the wall occurs at the upstream section of the wall. This is understandable, as the transverse flow velocities are largest closer to the onset of the widening. The total over-wall flux for W3 closely matches the flux through the first section, since the transverse flow velocities decrease along the wall, the velocities become too low to overcome the physical barrier formed by the crest height represented in the bathymetry. This results in barely any sediment exchange over the later sections of the wall.

The schematisation of the wall also influenced the amount of sediment entering through the inlet; Table5.2 shows that with the walls as 2D weirs in W4, there is more sediment going through the inlet than with the walls in the bathymetry, although both variants have the inlet schematised with adjusted 2D weirs. The physical presence of the wide wall creates a larger flow separation, slowing down the flow velocity at the downstream part of the inlet sill and reducing the sediment transport into the auxiliary channel.

Although the variants where the crest height is incorporated in the bathymetry (variant W1, W3 and W5) show a reduction in sediment exchanges over the wall, still a significant amount of bedload sediment overtops the wall when looking at the relative influence on total sediment balance; in variant W3 the amount of sediment that entered the auxiliary bank channel over the wall is -139% of the sediment balance and 12.2% of the sediment that entered over the inlet sill, for W5 this is -321% and 11.0%. These percentages are a lot larger for the refined model R5, where there is barely any transport over the wall; only 5.29% and 0.002%.

Like mentioned when discussing the cumulative sedimentation/erosion in the main channel, the incorporation of the structure in the bathymetry reduces the effective flow width, increasing erosion and lowering the bed level. The reduction of the bed level of observation points along the auxiliary bank channel is shown in the Appendix in Figure G.3.

5.2.3. Influence of inlet schematisation

Sediment entering

Comparing the variants where the walls are schematised in similar ways but the inlet sill differs (W1 vs W3 and W5, and W2 vs W4), it can be seen that keeping the inlets open results in the most sediment passing the inlet sill, using updated 2D weirs reduces transport somewhat, and the dumping riprap leads to a stronger reduction, see Table 5.2 and Figure 5.5. The variant with dumping in the refined model, where proper schematisation of the side-weir geometry and the steep slope that became possible, shows the strongest reduction.

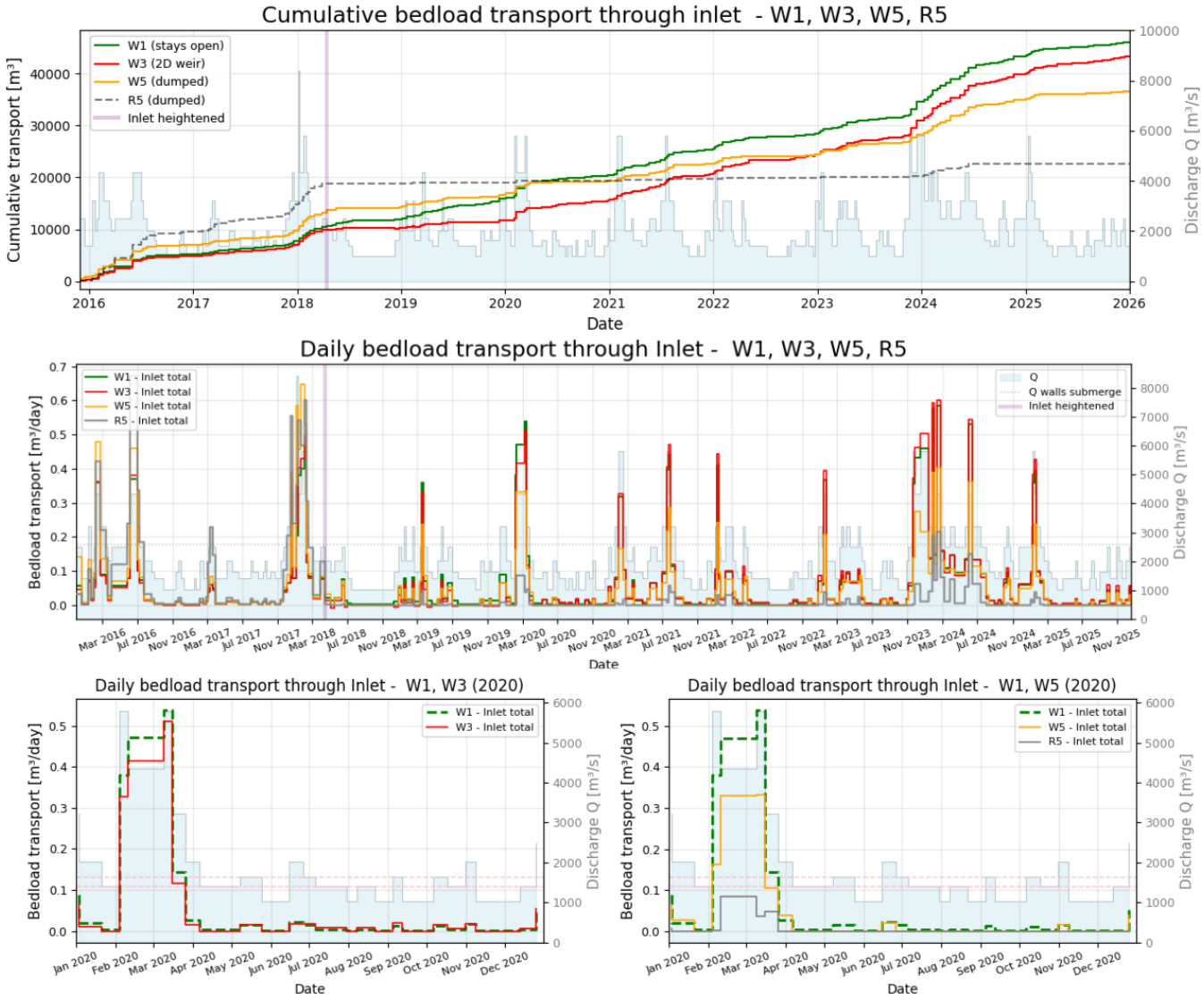


Figure 5.5: Bedload transport through inlet for variant W1 (-), W3 (2D weir) and W5 and R5 (in bathymetry nourished)

Based on the workings of the 2D weirs on the sub-grid, the difference in sediment transported through the inlet between W1 and W3 was expected to arise at discharges where the flow into the auxiliary channel is strong enough to enter the originally low open inlet sill, but too low for water to overflow the 2D weir. Figure 5.5 shows that this is not the case: there are no discharge steps in the simulation at which W1 has sediment entering while W3 does not, because the schematised hydrograph covers only a limited number of discrete discharge steps, none of which fall in this window. Only the transport rates differ, with W1 generally showing larger rates, as the 2D weirs included an energy loss in their formulation. The cumulative bedload transport shows that W1 and W3 grow apart in the first few years after the inlet was heightened, and move closer together again after the upstream cell is lowered in May 2020.

For W5 a discharge of ≥1630 m^3/s is needed before sediment transportation over the sill starts, while W1 already shows transport at 1400 m^3/s. During higher discharges, the amount of sediment for W5 is reduced.

The refined model shows even more sediment entered during its open state. Most likely, this links back to the effects of grid size limitations in capturing the inlet geometry correctly. The reduction on sediment entering after the inlet is heightened and is even stronger than in the coarse model (W5).

Distribution of sediment passing the refined model inlet sill

Figure 5.6 shows the distribution of bedload transport over the closed sill for three different discharges at which overtopping occurs. The grid cells of the coarse model are too large to properly see a magnitude distribution along the sill, whereas the refined model does show distinct distributions of the bedload passing the sill. From the CFD research carried out at Deltares shown in Appendix F, it was learned that sediment concentrations are highest not at the downstream end of the inlet sill, but more around the middle part. This is reflected in the results for a discharge of 3220 m^3/s in R5. Similarly, the moment chosen in 2025 at 4350 m^3/s shows higher transport towards the middle, whereas the moment in 2024 at the same discharge shows the highest rates at the downstream section. The sediment transport over the inlet sill is surprisingly lower for the higher discharge at Lobith of 5800 m^3/s than for the two lower discharge steps shown for R5. This was seen for other same-valued discharge steps too. It should be noted that this concerns instantaneous bedload transport, which, due to the fixed layer, is highly dependent on the amount of sediment available at that moment, as sediment transport occurs in pulses.

The third row of Figure 5.6 shows the depth-average velocity vectors over the sill. It can be seen that the angles of the depth-averaged velocity vectors change: at the lower discharges, the flow is turned more towards the auxiliary bank channel. This could explain the higher transport rates. Looking at the cumulative transport recalculated to daily transport values in Figure 5.9, the sediment passing the inlet sill during a discharge of 5800 m^3/s is sometimes larger, sometimes lower than during discharges of 4350 and 3220 m^3/s.

For W5, the vectors are shown at a different scale for the two higher discharge values, as the vectors otherwise became too large to plot. For W5, the vectors for a discharge of 3220 m^3/s were not larger than those for 5800 m^3/s. For the coarse variant, the direction of the vectors reveals that sediment enters the top of the sill in the longitudinal direction, clearly showing that the geometry of the side-weir, even with the alterations made, is not captured properly and increases sediment transport into the auxiliary bank channel. The longitudinal transport onto the crest is facilitated by the very mild longitudinal slope to the crest (only roughly around 1:15) resulting from the wide grid cells (80 m in longitudinal direction). This shows that not only does losing the slope in the coarse grid cells increase sediment transport, but also the schematisation of the wall and sill into the main channel causes the loss of the side-weir entrance.

Additionally, for W5, most sediment enters the auxiliary bank channel at the downstream third of the sill: the sediment transport vectors on top of the crest are not yet oriented towards the auxiliary channel, and only undergo strong turning upon impinging on the wall.

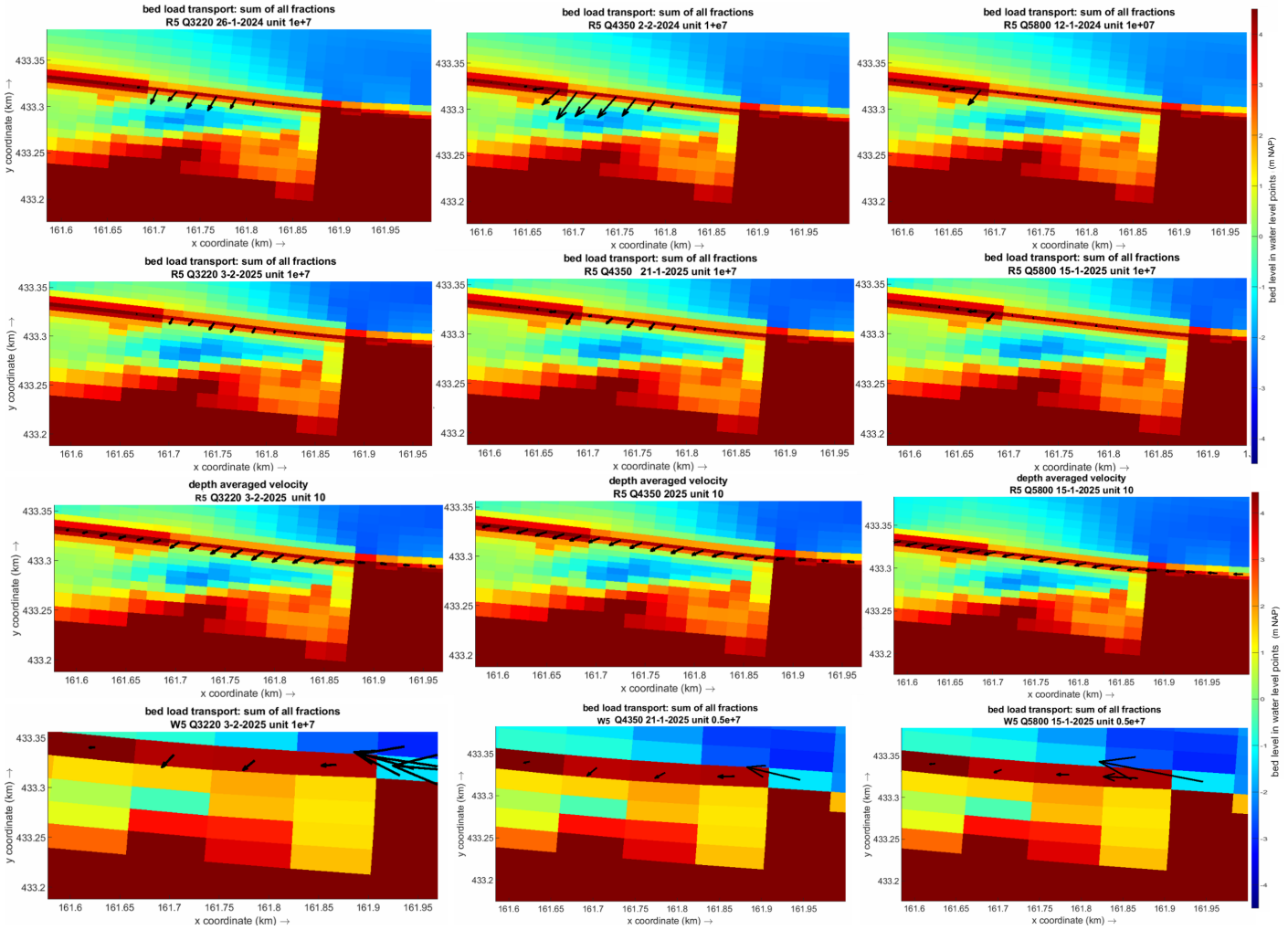


Figure 5.6: bedload transport and depth-averaged flow velocity over the closed inlet sill for three discharges at Lobith (Q = 3220, 4350 and 5800 m³/s, columns left to right). The first two rows show bedload transport for variant R5 at two different moments (2024 and 2025). The third row shows the corresponding depth-averaged flow velocity for the 2025 moment (row 2). The fourth row shows bedload transport for variant W5 (2025). Colour shading shows bed level (m NAP)

Morphological development directly behind inlet

Figure 5.7 shows the bed level at the end of the simulations around the inlet. All variants show elevated bed levels in the cells directly in front of the inlet sill, with the bed level increasing in the downstream direction (there was more deposition left of point a and b than on the right in Figure 5.7). This matches what was seen in field measurements, where a triangular deposition pattern formed in front of the inlet sill with its base at the downstream end of the sill. W5 shows the elevation less clearly and less pronounced, but it is difficult to judge as the grid is coarse and the crest extends quite far into the main channel. The refined model shows a higher bed level in front of the sill at the upstream end.

Behind the sill, in the auxiliary channel, the refined model variants both clearly show the shallow low-velocity recirculation zone consistent with the expected flow separation pattern. In the coarse grid, it is more difficult to see. In W5, an elevated bed level is observed in the cells directly behind the inlet sill (point c). This is unexpected, as W3 shows a much lower bed level for this cell (point d). Although W5 matched the cumulative sedimentation/erosion pattern of R5 more closely than W3 in this area, the cause of this local elevation remains unclear.

In the field data, a deep scour pit was observed (Figure 4.1 point 2). The pit started forming after a small section at the upstream end of the sill was lowered in 2020 (B.1). This adjustment was only incorporated in variants W3 and W4, which explains the scour seen at point d. However, the location differs from what was observed in the field data, most likely due to the coarse-grid amplification of the lowered section. None of the model simulations show the scour pit located closer to the upstream end.

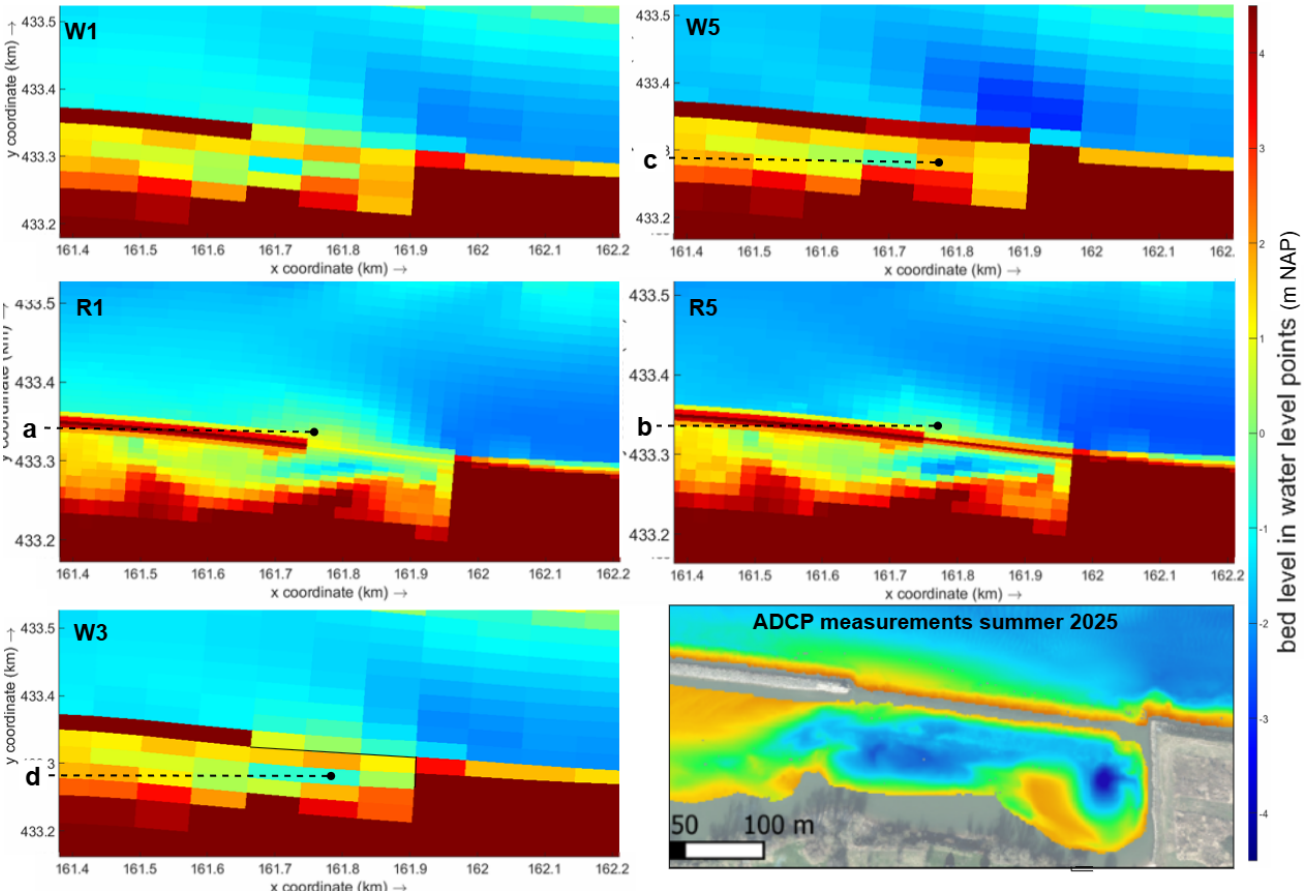


Figure 5.7: Bed level around the inlet sill at the end of the simulations for the different inlet sill schematisation methods.

5.2.4. Trends before and after the 2018 inlet adjustment

Comparing the transport through different pathways with the resulting sediment balance for the auxiliary channel from before and after the inlet heightening in Figure 5.8, the effect of the inlet adjustment on the overall morphological development of the auxiliary channel can be considered. Variants W1, W2, and R1, which did not include any alteration to the inlet sill and remained ”open”, can be used as reference simulations. The trends seen in these runs should be considered when analysing the other effects of the inlet adjustment in the other variants.

Trends in reference variants

The changes between 2016-2017 and 2019-2022 for variants W1 and R1 show that due to different hydrodynamic conditions and/or initial responses, a behaviour change also took place if the sill had remained open. Looking at the hydrograph in Appendix C; on average 2019, 2020, 2021 and 2022 were slightly drier than 2016 and 2017. However, the difference is small, as 2017 was also dry year. As the change is different for W1 and R1, likely, the effect of sediment availability at the start and the initial morphological response are at play. It takes time for sediment to travel through the auxiliary channel, and Figure 3.3 showed more sediment was already closer to the outlet at the start of the refined model simulations. The different reactions in W1 and R1 should be considered when analysing the change in trends for the other schematisation variants. The coarse model variants showed less sediment entering the auxiliary channel in the first two years, leading to an erosive trend that changed into a slightly sedimentating trend for 2019-2022 due to a strong reduction on the amount of sediment leaving. So for W3 and W5, one should keep in mind that regardless of the inlet adjustment, more sediment is already expected to remain in the auxiliary channel between 2019-2022 (W reference balance went ↑). While R1 shows more sediment entering in 2016-2017, and less of that sediment (has jet) left the auxiliary channel in April of 2018, leading to cumulative sedimentation for the first few years that turned into an almost stable, very little eroding trend or 2019-2022. When considering R5, one should keep in mind that without the heightening of the inlet, there would also have been a strong reduction in the amount of sediment entering, halting the strong sedimentation to a stable sediment balance. (R reference balance went ↓).

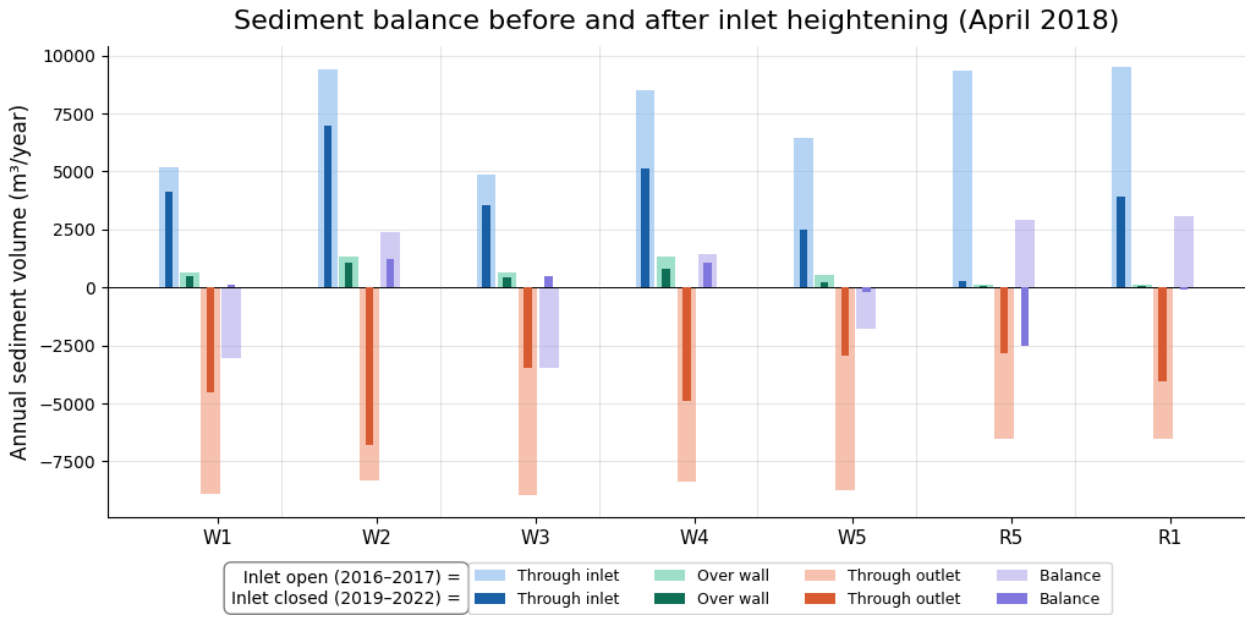


Figure 5.8: Sediment transported in and out of the auxiliary bank channel through different cross sections and the resulting volume balance before and after the inlet was closed in April 2018. In this figure, all sections of the wall, including the inter-notches, are taken together.
**The sediment fluxes and total balance shown in this histogram are highly dependent on the fixed nature of the bed level in the auxiliary channel.*
***The histogram shows small differences before the inlet adjustment between variants where this is the only varying parameter. These stem from small alterations made at the start of the simulations, needed to properly incorporate the 2018 adjustment (visible in Figures D.2 to D.4):*

- *W1 vs W5: In W5, the inlet sill cells used to represent the sill inside the bathymetry were raised to match the as-built crest height. Also, the adjacent upstream river bank cell was raised to keep the sill connected to the bank, keeping the side-weir geometry and preventing flow entering longitudinally. These changes resulted in more sediment entering through the inlet before the 2018 adjustment.*
- *W1 vs W3: variant W3 additionally included a 2D weir matching the as-built crest height (1.05 m NAP) from the start. This slightly reduced sediment entering through the inlet before the adjustment.*

****Sediment that passed through the inter-notches is included in the transport rates over the wall.*

Inlet heightened from ”open” to ”closed”

Comparing the dark blue lines (representing 2019-2022) of variant W1 with W3 and W5, W2 with W4, and R1 with R5, it is seen that heightening the inlet in all schematisations reduced the amount of sediment entering through the inlet, with incorporation in the bathymetry showing the strongest reduction. However, despite all showing a reduction in the amount of sediment entering, the total sediment balance shows different overall trends for the closed years.

The refined model shows the expected change in trend from heightening the inlet: the initial sedimentation changed to erosive behaviour once the inlet was closed. As the sill blocks the deepest part where most sediment is in motion, less sediment enters. The flow through the auxiliary channel continues, able to erode the bed behind the sill. This causes relatively more sediment to leave the system than to enter. It should be noted, however, that the amount of sediment exiting in these model simulations is strongly limited by the fixed nature of the bed level in the model. The total sediment balances should therefore not be used to judge the overall morphological development of the system, but merely to understand how the inlet adjustment altered the development across the different variants.

In the coarse model, variant W3 showed sedimentative behaviour, more so than the reference W1, as the amount of sediment exiting through the outlet showed a stronger reduction. The reduction of sediment exiting can be explained by the 2D weirs reducing the flow through the auxiliary channel. The 2D weirs do not manage to block sediment entering when overflown, causing the reduction in the amount of sediment entering to be too little to show the expected decrease in the total sediment balance when the inlet is closed.

Variant W5 also showed a slowing down of the initial erosive behaviour, but not as strong as the reference W1, as W5 did not start sedimentating. For W5, more sediment was blocked at the inlet. Comparing W5 with R5, W5 appears to show opposite behaviour, as the sediment balance for W5 increases. However, when the reference trend is abstracted out (which showed a strong increase in the sediment balance), it can be seen that the heightened inlet actually reduced the sediment balance, but not as strongly as for R5. Sediment balances remain difficult to judge, as the amount of sediment leaving through the outlet is distorted by the fixed layer in the auxiliary bank channel. Looking at Figure 5.9 makes it easier to see that the W5 still allows more sediment to enter through the inlet than leaves through the outlet compared to R1. The smaller reduction on sediment entering in W5 than in the refined model, indicates again that the coarse

grid that loses the steep slope and localises the LTW further into the main channel, missing the erosional response seen from the heightening in the auxiliary channel that was captured in the refined model. To properly capture the response, a realistic slope is needed to steer the bedload back into the main channel.

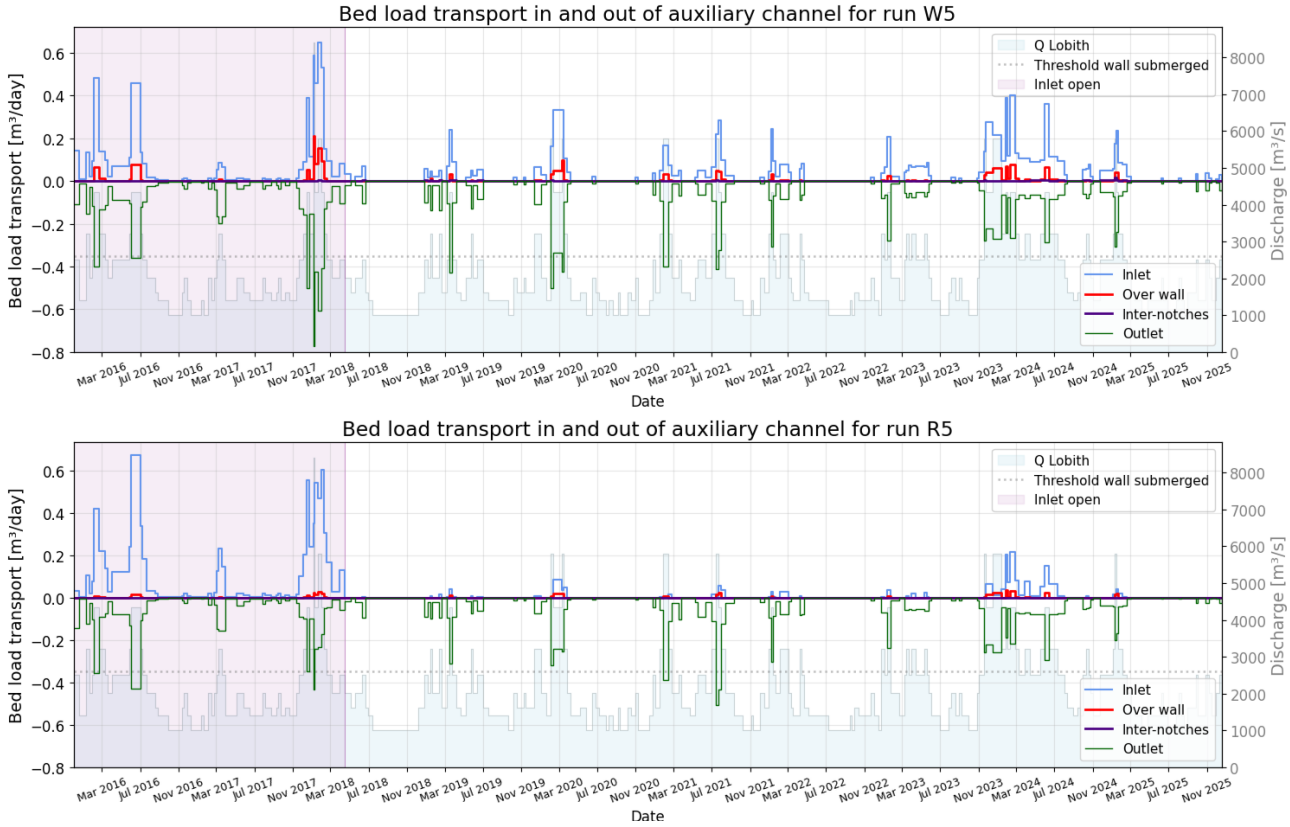


Figure 5.9: Bedload transport into auxiliary bank channel through different cross sections over time for variants W5 and R5

5.2.5. Testing a mild slope in refined model

To test whether the steep slope is indeed key to properly representing the sediment exchange between the main and auxiliary channels, a test was conducted in the refined model with a milder slope. The slope of the wall and the inlet sill on the side of the LTW with the main channel were made milder from 1:2.5 to 1:4.3 by heightening the cells directly touching the crest in the main channel, see Figure 2.11.

Table 5.3 shows that indeed less sediment passes over the wall in the refined model when schematised with a milder slope similar to the coarse model. However, the increase in exchange is not as strong as that shown by the coarse model, indicating that it is not only the slope that plays a key role, but also the geometry: the wall is placed too far in the main channel, and is no longer in line with the bank line, allowing longitudinal inflow (also seen and discussed with Figure 5.6).

Table 5.3: Bedload transport in and out of the auxiliary bank channel and the resulting sediment balance in [m³] between the end of 2015 and the end of 2025 for model variants W5, R5 and R5_M. Positive values indicate import of sediment and negative values indicate export.

Run	Inlet_WA	Wall_WA1	Notch_WA1	Wall_WA2	Notch_WA2	Wall_WA3	Outlet_WA	Balance crs	Balance $\frac{\partial z_b}{\partial t}(1-p)A$
W5	36542	2751	624	6.35	-0.07	-173	-41001	-1250	-2674
R5	22688	624	0.12	0.00	0.00	0.00	-35119	-11806	-12008
R5_M	21435	1262	1.50	0.00	-0.01	0.00	-33139	-10441	-10257

Unexpectedly, the amount of sediment passing through the inlet has slightly decreased compared to the steep-sloped case. Figure 5.10 shows that the difference in the amount of sediment entering over the sill originates from the first year of the simulations; R5_M has less sediment entering while the inlet is still open, and once the inlet is closed the amount of sediment entering over the mild-sloped inlet sill becomes larger again, as can be seen from the decreasing difference between R5 and R5_M. During the first two years of the simulation, the only difference is the schematisation of the slope of the wall; the inlet sill is schematised identically for R1, R5 and R5_M before the heightening in 2018. Repetition of the simulations led to the

same results. The difference must therefore stem from different flow velocities downstream of the inlet sill, due to the slightly wider schematisation of the wall into the main channel at the downstream end of the sill.

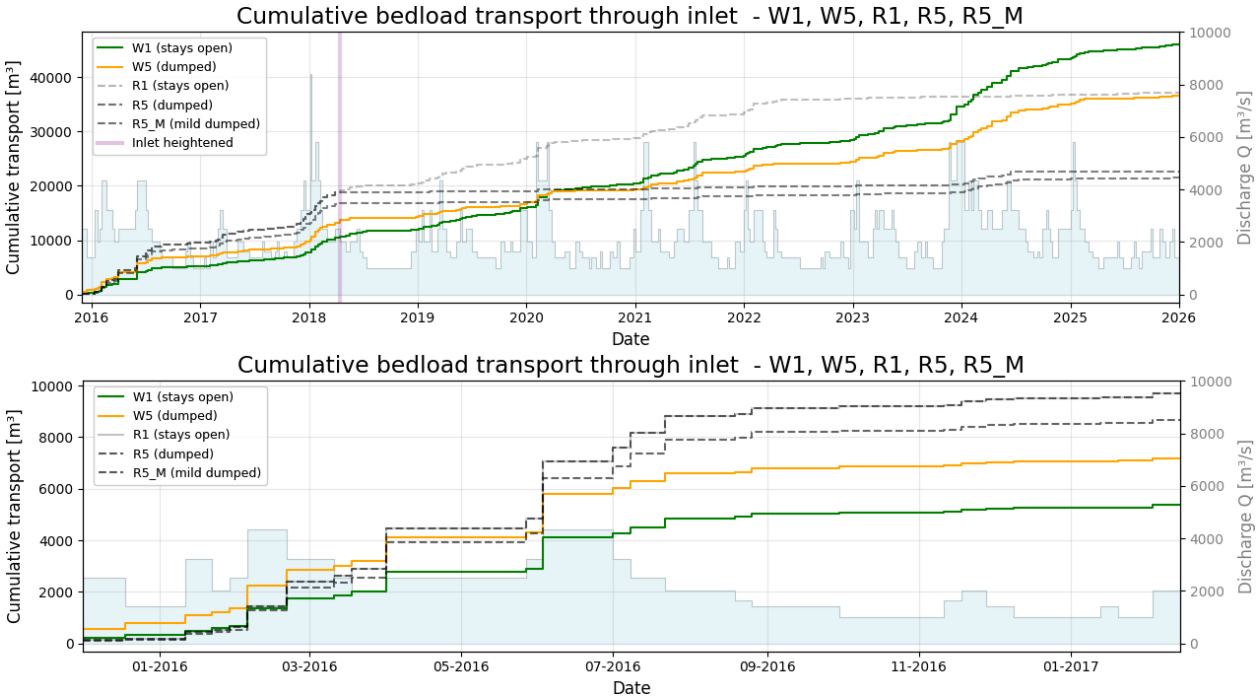


Figure 5.10: Bedload transport over the inlet sill for variants W1, W5, R1, R5 and R5_M.

5.2.6. Alluvial auxiliary bank channel

This section provides the results of a test run in which the auxiliary bank channel was schematised with an alluvial bed instead of a fixed layer (R5_E). Previous research with the coarse model showed unstable behaviour when the bed in the auxiliary bank channel was made erodible, which was linked to the sediment transport parameters being calibrated for the main channel. The run presented here tests whether the same occurs in the refined model, where the geometry of the structure is resolved and the channel is represented with more cells and detail.

The cumulative bed level change over the ten-year simulation, shown in Figure 5.11, shows erosion in the upstream half of the channel and in the shallower zones near the bank, while the deeper sections in the downstream half show deposition. This resembles the patterns observed in the field data discussed in Chapter 4, including the change in the transverse profile, with deposition in the deeper parts closer to the wall and erosion in the shallower areas near the bank. This differs strongly from R5, where the locations of erosion were governed by the limited sediment available on top of the fixed layer, which was concentrated in the downstream reach, so the alluvial run reproduces the observed patterns considerably better.

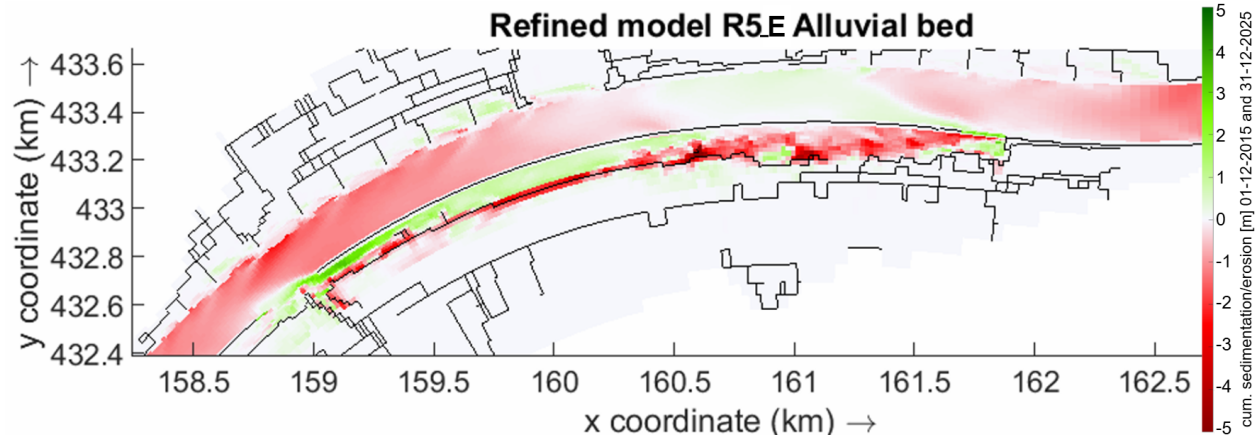


Figure 5.11: Cumulative sedimentation/erosion for the refined model simulation without the fixed layer in the auxiliary bank channel (R5_E).

Table 5.4 shows that allowing the bed to erode increases the total erosion over the ten-year simulation by roughly a factor of seven compared with R5, from a balance of −11806 m^3 to −80835 m^3 over the entire channel. This exceeds the total amount of possible erosion with a fixed layer, which was limited to the available sediment that entered the channel during spin-up, 63907 m^3 for the refined model. The alluvial bed simulation started from the same spun-up model as R5. During the spin-up, the auxiliary bank channel still had a fixed layer and only sedimentation was possible. Compared to the initial sedimentation in R5, the alluvial test simulation shows an eroding system from the start (see Appendix G.7). The bed was therefore not in equilibrium for this configuration at the start of the run, so part of the initial erosion is likely an adjustment to the changed setting rather than a response to the LTW itself.

The effect of the heightening of the inlet sill on sediment transport rates and overall morphological development of the channel is less dominant in the already eroding system; see Figure G.14. The heightening still has a strong effect on the amount of sediment entering the channel over the sill, but since the amount of sediment leaving through the outlet increased as well, the eroding trend remains similar. Compared to R5, the total amount of sediment entering the system over the inlet sill is larger when the bed is alluvial, indicating that the eroding channel increases its conveyance capacity and the discharge and sediment extraction from the main channel.

Table 5.4: Bedload transport in and out of the auxiliary bank channel and the resulting sediment balance [m^3] between the end of 2015 and the end of 2025 for model variants R5 and R5_E (alluvial bed). Positive values indicate import of sediment and negative values indicate export.

Run	Inlet_WA	Wall_WA1	Notch_WA1	Wall_WA2	Notch_WA2	Wall_WA3	Outlet_WA	Balance crs	Balance $\frac{\partial z_b}{\partial t}(1-p)A$
R5	22688	624	0.12	0.00	0.00	0.00	-35119	-11806	-12008
R5_E	51374	1987	0.45	0.00	-0.00	0.02	-134198	-80835	-85356

These results are promising for future research. They indicate that with local grid refinement, a fixed layer in the auxiliary bank channel may not be necessary to obtain realistic morphological behaviour, even with transport parameters calibrated on the main channel. Only one test run was carried out here, in an unvalidated refined model, so whether the same holds in a large-scale model with local refinement cannot be concluded from these results alone.

5.2.7. Summary of findings of the subchapter

None of the coarse model variants reproduces the magnitude of erosion seen in the refined model (R5). Although W1 and W3 match the total eroding sediment balance most closely, W5 and R5 correspond more closely when looking at sediment transport rates over the structure, behaviour change after the inlet was heightened and the spatial distribution of erosion and sedimentation in the auxiliary channel.

Open inlets result in the most sediment passing the inlet sill; heightening the inlet with the use of 2D weirs reduces transport somewhat, but dumping riprap to create a physical barrier for the sediment shows a significantly higher reduction in the amount of sediment that enters the auxiliary bank channel. The refined model showed a significantly stronger reduction, indicating that the missing steep slope results in an underestimation of the deflection on the sediment transport vector due to the gravity force at play on the slope of the sill. This limits the coarse model from properly modelling the sediment distribution between the main and auxiliary bank channel.

The schematisation of the wall proved to be of key importance to properly model morphological development as well. The refined model shows almost no sediment exchange over the wall (occurring only locally at the upstream end where transverse velocities are strongest), whereas in the coarse model this pathway remains a substantial contributor to the sediment balance, even when schematised inside the bathymetry. This indicates that loss of the steep slope of the wall, just like the sill slope, allows excessive sediment exchange along the LTW.

The influence of losing the steep slope in the coarse grid was confirmed with a test run in the refined model in which the slope was made milder. However, this variant also showed that it is not only the milder slope that limits the coarse model's performance, but also the geometry. The increase in sediment exchange with a milder slope was not large enough to match the transport rates seen in the coarse model, indicating that the slope is not the only key limitation; the geometry — with the LTW placed this far into the main channel — allows longitudinal inflow. Plotting sediment transport vectors showed sediment entering the crest of the sill in a longitudinal direction over a very mild slope. This likely contributes to the coarse model showing more sediment through the inlet, not just missing the steep transverse slope.

5.3. Sensitivity to transverse bed slope parameter (W3a-W3c)

Figure 5.12 shows the bed level and cumulative erosion/sedimentation for variants W3a–W3c, in which the transverse bed slope parameter (A_{sh}) was varied while keeping all other settings equal to variant W3. The A_{sh} parameter is originally calibrated based on observations of the bed level in the main channel.

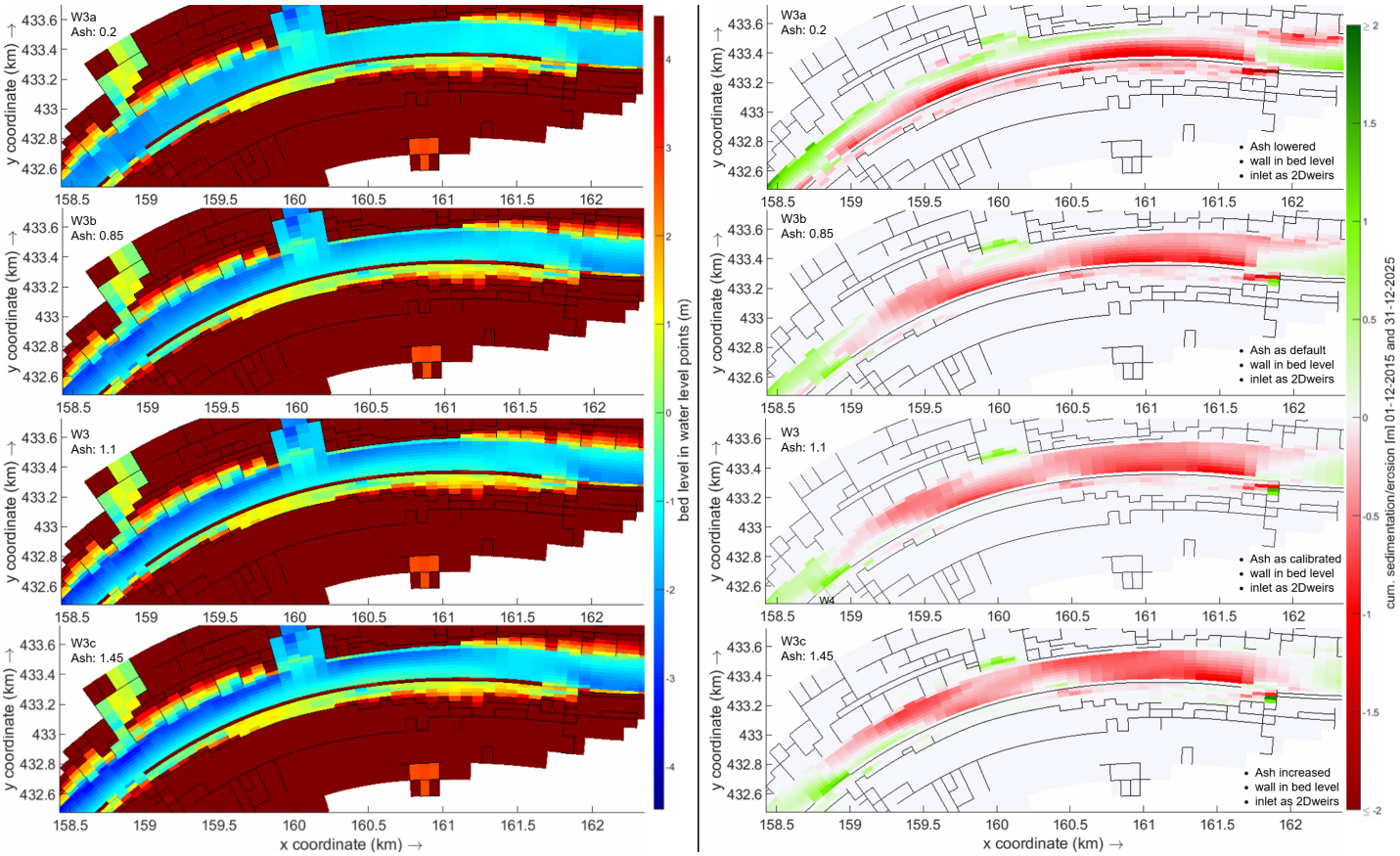


Figure 5.12: Bed level after and cumulative erosion/sedimentation at the end of the simulation from December 2015 to 2025 for variant W3 with different A_{sh} values

Main channel changes

The parameter is defined for the entire domain, which results in bed level changes throughout the main channel. A lower A_{sh} increases the transverse bed slope adjustment on the sediment transport vector, pulling sediment to the deeper parts, flattening the transverse cross-sectional profile of the main channel. Figure 5.12 shows the resulting strong sedimentation in the outer bend and strong erosion in the inner bend, and consequently a more uniform bed level, for variant W3a. Increasing A_{sh} has the opposite effect; variant W3c shows slightly deeper outer bends and shallower inner bends.

Table 5.5: Bedload transport in and out of the auxiliary bank channel and the resulting sediment balance in [m^3] between the end of 2015 and the end of 2025 for varying A_{sh} values in variant W3. Positive values indicate import of sediment and negative values indicate export.

Run	Inlet_WA	Wall_WA1	Notch_WA1	Wall_WA2	Notch_WA2	Wall_WA3	Outlet_WA	Balance crs	Balance $\frac{\partial z_b}{\partial t}(1-p)A$
W3a	-237	2272	0.9	0.00	0.00	0.00	-34267	-32231	-32304
W3b	35781	4936	29	0.3	0.3	-46	-50507	-9806	-10489
W3	43271	5206	73	1.3	1.1	-229	-52138	-3814	-4545
W3c	50675	5567	242	5.8	20	-688	-52631	+3190	+2399
R5	22688	624	0.1	0.00	0.00	0.00	-35119	-11806	-12008

Sediment exchange with the auxiliary bank channel

As a lower A_{sh} increases the correction on the sediment vector towards deeper parts, it steers sediment trying to get over the sill with the flow away from the inlet back to the deeper main channel. The reduction on the amount of sediment that passes the sill and wall entering the auxiliary bank channel can be seen back in the amount of sediment fluxes shown in Table 5.5. Considering the transport through the inlet, it should be pointed out that in variant W3 the heightened inlet sill was not incorporated in the bathymetry. For W3a, the sediment flux through the inlet even became negative, indicating sediment leaving the auxiliary through the inlet. Figure G.4 shows the sediment transport through the inlet for W3a on a zoomed-in scale, revealing that the negative transport comes from the beginning of the simulation; sediment tumbles due to the stronger gravity correction than applied during the spin-up into the main channel. Sediment does not transport against the flow direction.

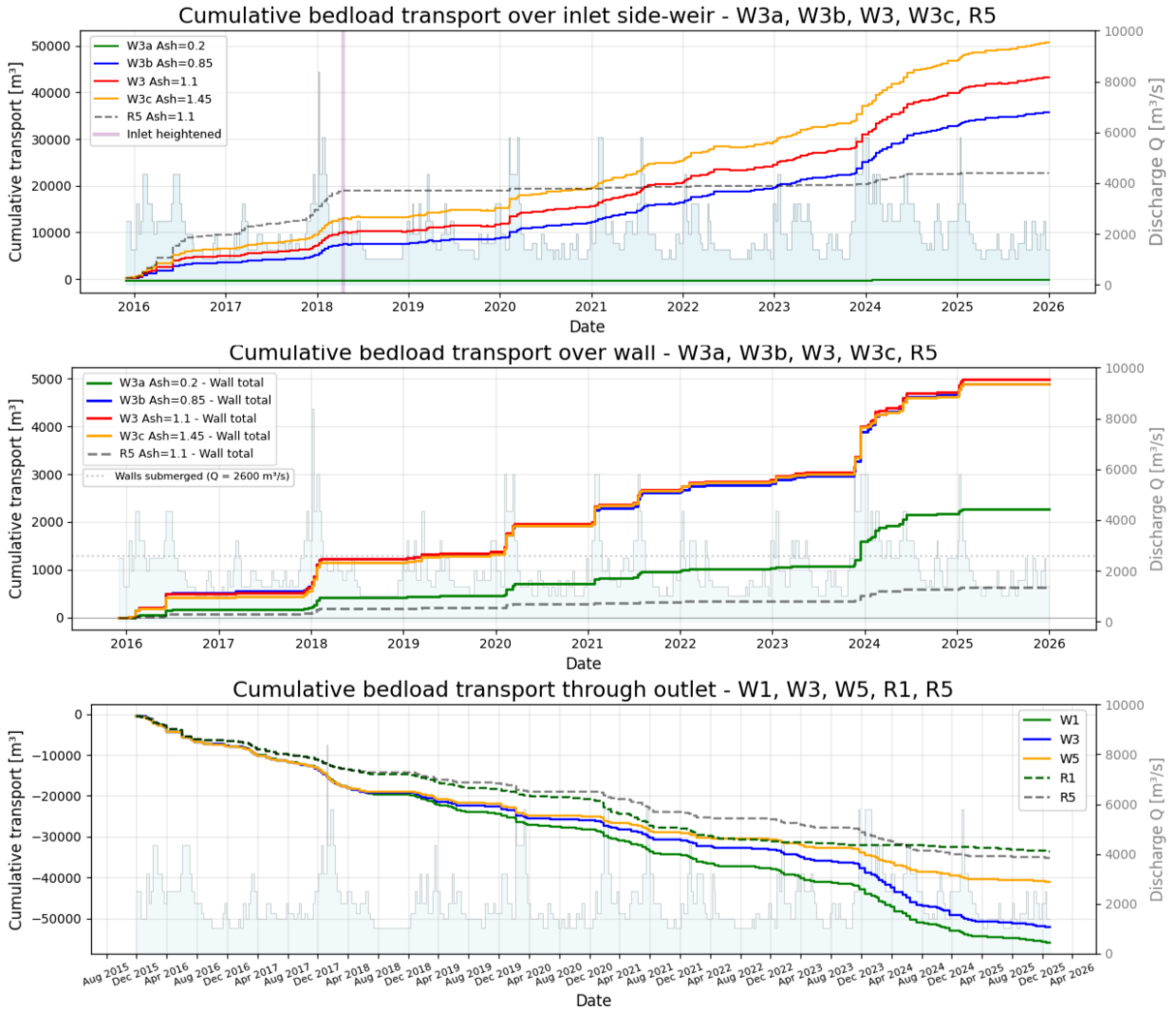


Figure 5.13: Bedload transport into bank channel Wamel through different cross sections for W3 runs with different A_{sh} values

Figure 5.13 shows how the cumulative sediment transport through the cross sections grows over time for the varying A_{sh} values compared to the R5 variant. It can be that the biggest influence on varying the A_{sh} is seen through the (in bathymetry open) inlet. Varying between 0.85 and 1.45 seems to have relatively less effect on the transport through the other cross sections; only when lowered to 0.2 is a strong reduction seen. The reduction on the amount of sediment exchange over the wall when the A_{sh} is lowered to 0.2 is still not strong enough to match the exchange in the refined model that did incorporate the steep slope. This can indicate that potentially the geometry, schematised into the main channel, is causing the excess transport over the wall and that a local A_{sh} correction might not be enough to mimic the low sediment exchange over the wall observed in the refined variant. An explanation for the difference can be a stronger transverse flow direction at the onset of the widening. Possibly, the difference at the inlet has to do with the lower sill height, which has a very mild slope of 1:20 at the start of the simulation compared to the 1:4.3 for the wall.

Additionally, one should keep in mind that the changes in the main channel directly affect the amount of sediment available to enter the auxiliary channel. As the flattened main channel bed effectively forms a barrier relative to the (unchanged) inlet and wall crest levels, less sediment reaches the inlet to begin with. This is most clearly seen for variant W3a, where sediment through the inlet is reduced strongly, despite the wall transport remaining substantial.

Potential of combining A_{sh} and E_s corrections

Potentially, the flattening of the main channel bed due to lowering the A_{sh} can be counteracted by adjusting the spiral-flow intensity (secondary flow).

In river bends, surface water is mildly forced to the outer bend and water near the bed to the inner bend by a balance of centrifugal forces and hydraulic pressure. This so-called spiral-flow effect or helical-flow, causes sediment load near the bed to be slightly deflected towards the inner bend. This generally leads to a transverse slope in cross-sections in bends, with a shallow inner bend and deep outer bend. In a depth-average model, this spiral flow is not simulated, but to still account for its effect, a spiral flow deflection is added. This effect deviates (rotating) the bedload transport direction towards the inner bend to simulate the formation of pointbars in river bends.

The formation of the transverse bed slope in river bends is a balance between the spiral flow and the gravity-caused bed slope term. In Delft3D this formation is calibrated with use of the A_{sh} parameter for the gravitational force (see eq. 2.6 and 2.10) and the E_s parameter for the spiral flow;

$$\tan(\phi_\tau) \propto \alpha_I = \frac{2}{\kappa^2} E_s \left(1 - \frac{\sqrt{g}}{\kappa C}\right) \tag{5.1}$$

A higher E_s increases the intensity of the spiral motion's effect on bedload direction and pushes sediment transport towards the shallower inner bend increasing the transverse bed slope. This suggests that the unwanted changes to the main bed level from lowered A_{sh} could, in principle, be counteracted by raising E_s. Whether a value for E_s exists that reverses the effect of the altered A_{sh} on the main channel highly depends on how strong the A_{sh} reduction has to be, and on the local curvature and transverse bed slopes of the Waal.

This is complicated by the now standard calibration practice: A_{sh} is typically calibrated first, on the pattern and location of the point bars, and the E_s afterwards, on their amplitude (E. Mosselman of Deltares, personal communication, August 21, 2026). A_{sh} is moreover the only parameter that governs the spacing between the point bars, E_s cannot fully substitute for it, although the bends in this domain of the Waal show relatively mild curvature. Even if a workable combination could be found, it would mean recalibrating the entire domain in order to account for a single local process at one location. A locally applied adjustment or formulation would be more efficient and more robust.

5.4. Parameter adjustments for local transport over the inlet sill

5.4.1. Quantifying the missing slope and corresponding A_{sh}

Previous results showed that the loss of the steep slope of the structure in the coarse grid allows too much sediment to pass due to an underestimation of the gravitational correction on the direction of the sediment transport vector. For a few cross sections of the wall and inlet sill in simulation W5, the transverse bed slope ($\delta z_b / \delta y_m$) used in calculating this gravitational correction is compared to the as-built slope of the structure, see Figure D.6. Based on equations 2.5 and 2.10, an A_{sh} parameter is calculated that can account for the missing slope ratio, such that $\frac{1}{f(\theta)} \frac{\partial z_b}{\partial y_m}$ results in the same correction as when the model would have been able to incorporate the real steep slope in its sediment transport calculations. For the wall, only cross sections of the upstream and downstream ends are considered, at the start and end of the simulation. For the inlet sill, only the heightened, "closed", geometry is considered; right after the heightening in April 2018 and at the end of the simulation. Table 5.6 shows the resulting reduced local A_{sh} values needed.

Table 5.6: Missing steep slope of wall and inlet sill in W5 and corresponding corrected A_{sh} to account for it.

Moment	Location	Schematised slope	As-built slope	Ratio missing	Original A_{sh}	Corrected local A_{sh}
Start	Wall upstream end	1:4.3	1:2.5	1.72	1.1	0.64
	Wall downstream end	1:3.3	1:2.5	1.32	1.1	0.83
End dump	Inlet sill, upstream cell	1:4.3	1:2.5	1.72	1.1	0.64
	Inlet sill, middle cell	1:5.3	1:2.5	2.12	1.1	0.52
	Inlet sill, downstream cell	1:5.8	1:2.5	2.32	1.1	0.47
End	Wall upstream end	1:3.4	1:2.5	1.36	1.1	0.81
	Wall downstream end	1:3.3	1:2.5	1.32	1.1	0.83
	Inlet sill, upstream cell	1:4.4	1:2.5	1.76	1.1	0.63
	Inlet sill, middle cell	1:4.1	1:2.5	1.64	1.1	0.67
	Inlet sill, downstream cell	1:3.5	1:2.5	1.40	1.1	0.79

The local corrected A_{sh} values show significant variation over space and in time; the downstream end of the inlet sill needs a correction factor of 0.47 at the start of the simulation, compared to 0.79 at the end. As the bed level against the upstream reach of the wall and inlet sill became deeper over time, the slope incorporated in the model became steeper, and the needed local A_{sh} reduction became smaller. This raises a concern regarding the implementation of this method to account for the loss of the steep slope: the row of cells along the bed level might have to be fixed, losing even more width of the alluvial main channel.

5.4.2. Short stationary test runs

This section provides the resulting transport over the inlet sill for the short stationary test runs performed to see if sediment transport rates over the inlet sill in the coarse model can match refined model rates when altering A_{sh} for the domain or A_{cal} locally.

To improve the side-weir geometry, the bed level upstream of the inlet was adjusted compared to the ten-year coarse grid simulations. In the left two figures in Figure 5.14, it can be seen that for the adjusted S2 schematisation, eight cells were heightened to the crest of the wall (5.57 m NAP). This narrowed the river, but improved the representation of the side-weir entrance geometry. The alteration changed where the flow velocities over the sill are the highest. The reduction in the high flow velocity for the upstream cell of the sill better matches what was seen in CFD calculations (Figure F.3). The alteration did not seem to change the discharge distribution between the main and auxiliary bank channel; see Figure H.1.

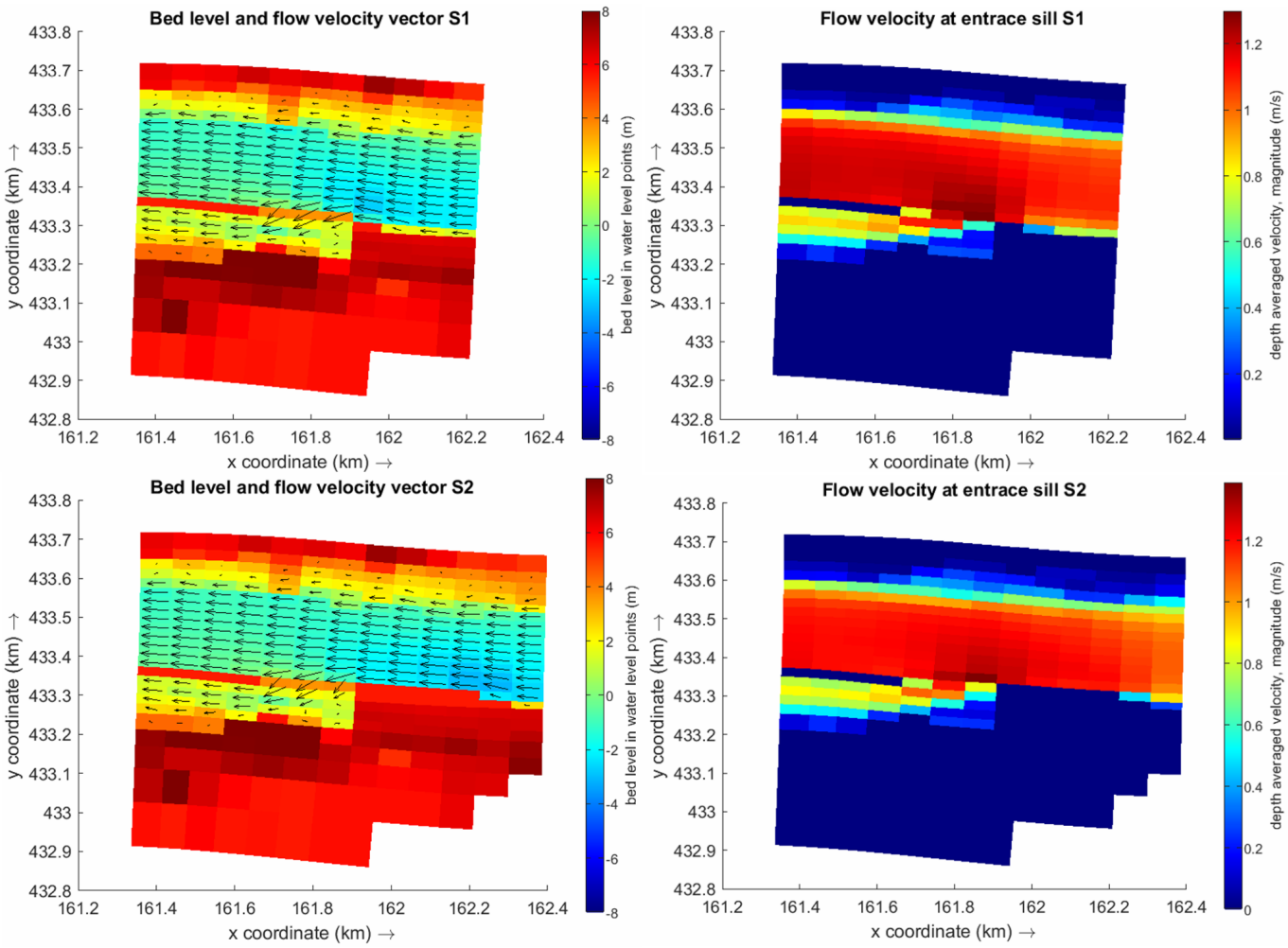


Figure 5.14: Flow velocity at inlet sill with Q_{Lobith} of 2500 m^3/s for original inlet geometry S1, and improved S2.

Table 5.7 shows the resulting cumulative and instantaneous bedload transport for the coarse (WS2-coarse) and refined (RS-refined) grids. The instantaneous transport rates were determined based on the trend of the cumulative transport during the simulation.

Table 5.7: Bedload transport over the inlet sill in short stationary test runs, Q_{Lobith} 4350 m^3/s, 25-day cumulative sediment volume.

Run	A_{sh}	$A_{cal,local}$	Cumulative (25 days, m^3)	Ratio run/RS
RS (refined)	1.1	2.4	272	
WS2	1.1	2.4	1897	7.0
WS2a	1.3	2.4	2307	8.5
WS2b	0.8	2.4	1105	4.1
WS2c	0.5	2.4	366	1.3
WS2d	0.45	2.4	202	0.74
WS2e	0.4	2.4	97	0.4
WS2-A_{cal}	1.1	0.5	378	1.4

Adjusting A_{sh}

The local reduced A_{sh} needed to match the refined model transport rates from the model runs is quite close to the calculated values based on the missed steep slope in Table 5.6. The short test runs showed that to match the refined model, a value between 0.45 and 0.5 is needed, and calculating the missed ratio gave values of 0.47, 0.52 and 0.64 from the downstream to the upstream end of the sill. The value is a little lower in the test runs than the averaged value calculated along the sill. This may be because most of the transport goes over the sill at the downstream end or due to remaining geometry differences between the coarse and refined model (although S2 included a side-weir improvement, the structure remains placed too

far into the main channel).

The shown values needed in the hand calculations and test runs are far below the calibrated 1.1, based on pointbars in the Waal. Since A_{sh} is defined for the entire domain, applying such a reduction flattens the main channel as shown in Section 5.3. Recovering a realistic main channel bed alongside this reduction is maybe possible, but would require recalibrating the whole domain to compensate for a local effect at the structure, moving away from using parameters for the physical meaning and process they were meant to represent. It also raises the question of whether the missed process at the steep slope should be adjusted with this parameter: the Koch and Flokstra formulation was derived for the gradual transverse slopes of river bends, not for slopes as steep as those of the wall and inlet sill. A locally applied adjustment with a formulation based on a steep-slope side-weir would be more efficient and more robust.

Adjusting A_{cal} locally

An alternative approach is adjusting the sediment transport magnitude instead of the deviation. Unlike the bed slope deviation parameters, the parameters that determine the magnitude of transport, such as the critical Shields parameter or the MPM calibration parameter A_{cal}, are locally adjustable. This allows the transport over the inlet sill and wall to be reduced directly without needing a domain-wide correction. However, this approach does not address the same underlying process: it reduces the amount of sediment in transport in those cells in both transverse and longitudinal directions, rather than correcting the deflection that determines where that sediment goes. Instead of the sediment being carried further by the main flow, it accumulates in front of the inlet sill, see Figure 5.15. The accumulation leads to an increase in sediment passing the side-weir over time, see Figure 5.16, creating further flaws in the model that would have to be resolved.

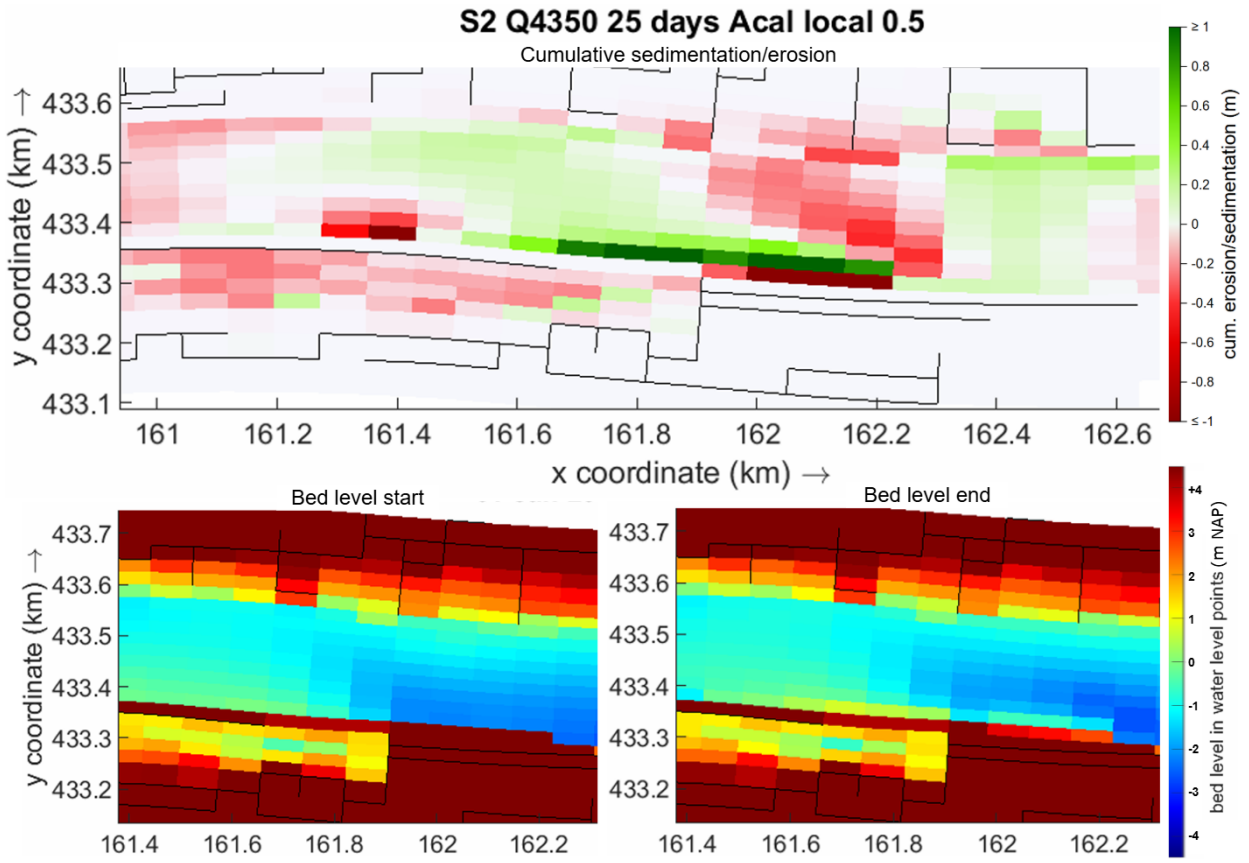


Figure 5.15: Bed level development in front of the inlet sill during 25 days for S2 with a locally adjusted A_{cal}

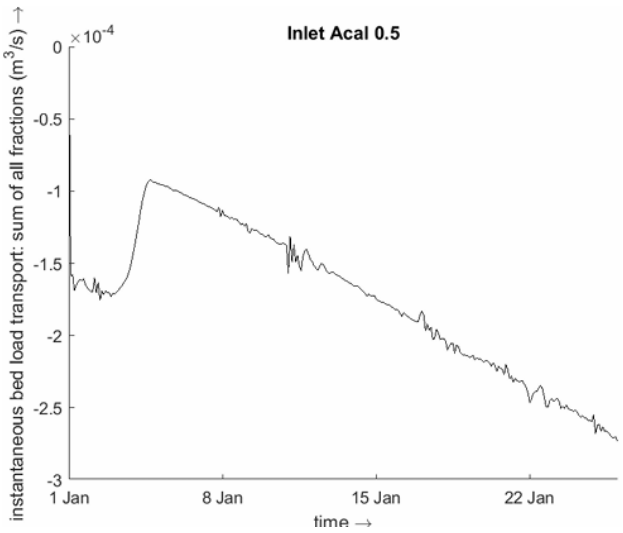


Figure 5.16: Instantaneous bedload transport over the inlet sill during the 25 days for S2 with a locally adjusted A_{cal}

5.5. Summary of the modelling result analysis

The hydrodynamic results showed that the models reproduce the measured discharge distribution and flow patterns well enough to investigate morphodynamic development, with W5 matching the measurements and the refined model most closely of the coarse variants. All coarse variants, however, still allow water to enter the auxiliary channel longitudinally.

Comparing the coarse variants with the refined model, incorporating the wall and inlet sill crest directly into the bathymetry (W5) was shown to be needed to reproduced the reduction in sediment transport into the auxiliary bank channel at the inlet sill, as well as the sediment exchange along the wall. The reduction in W5 was, however, still weaker than in the refined model (R5), for two identified reasons. First, the side-weir entrance geometry is lost, as the wall placed into the main channel no longer aligns with the upstream bank. Allowing longitudinal inflow into the auxiliary bank channel. Second, the steep slope of the structure is lost in the coarse grid, which reduces the gravitational deflection on the sediment transport.

Attempts to compensate for the resulting loss of gravitational deflection, represented through the Koch and Flokstra formulation, required reducing the domain-wide calibration parameter A_{sh} so strongly that the main channel lost its transverse bed level pattern, leaving an unrealistic bed. The alternative, locally reducing A_{cal}, does not act on the deflection but instead directly lowers the transport rate through the inlet. This produced deposition in front of the sill, which in turn increased sediment transport over the sill again over time, alongside unrealistic bed level changes upstream of the structure.

6

Discussion

Model set-up: initial state and scenario
This research simulated the morphological development of the Wamel inlet and auxiliary bank channel over the period 2016–2025. The already built and revised DVR model, however, has a restart date in 2018 on Baseline version j18. This means that the geometry (bank lines and structures) corresponds to as-is beginning of 2018. The calibration and spin-up procedure were aimed at reproducing the observed trajectory-averaged trends, the long-term gradients in annual sediment transport that determine the rate of erosion or sedimentation, rather than the riverbed exactly as it was at the start of 2018. A spin-up is not intended to reconstruct the conditions preceding the simulated period: a wet average yearly hydrograph was used, since wetter forcing lets the bed adjust to what the model computes as equilibrium more quickly, and removes noise from features the model does not reproduce, such as dunes. As a result, the model is not being re-exposed to the specific dry conditions of 2016–2018, but to a generalised long-term forcing representative of that period.

As bank erosion is not simulated in the model, the bank lines remain fixed throughout the simulations. One could argue that using the 2018 geometry of the auxiliary bank channel as this fixed baseline is, in this respect, preferable for simulating 2016-2025 to a 2016 baseline: the strong bank retreat that occurred in the auxiliary bank channel near Wamel between 2016 and 2018 is already incorporated into the 2018 geometry. The channel is therefore wider at the start of the simulations than it was in 2016, which lowers flow velocities and can cause more sedimentation.

Furthermore, it should be pointed out that the simulated period (2016–2025) was relatively dry compared to the wet averaged hydrograph used during spin-up. Part of the response of the system can be interpreted as a reaction to this shift in hydrological forcing; the erosive response seen when comparing the initial and final bed levels may reflect a reaction to this specific, drier period, which kept more discharge in the main channel, rather than solely a response to the LTW schematisation itself. Comparisons between the schematisation variants, which this research focused on, remain valid, as all variants were forced with the same discharge series; however, no conclusion can be drawn on whether the LTW design is sufficient to accomplish its intended purpose under different hydrological conditions for decades to come.

Schematisation methods applied
This research tested a limited number of schematisation methods due to time constraints. The following paragraphs describe other options and improvements that could have been made, and whether these are expected to affect the findings

The 2D weirs used to represent the wall sections were not created specifically for this study; the weirs already present in the DVR model were not adjusted, on the assumption that these had already been tested and produced satisfactory hydrodynamic results (Paarlberg et al., 2021). The weir file contained a different height for each wall section per grid cell, resulting in an irregular crest height along the wall's length. The schematisation of variant W2 therefore remained identical to the original DVR model. A version with improved weir heights based on as-built crest heights of the structure was not tested. However, most findings regarding sediment transport distribution and exchange are not expected to change.

When schematising the wall's crest inside the bathymetry, the height was linearly interpolated between the as-built upstream and downstream end crest heights, resulting in a smooth crest along the LTW. For schematising the inlet in the bathymetry, more alterations were needed to connect the wall, sill and bank; see Appendix D.2. This resulted in small differences in the geometry of the inlet between variant W5 and the other coarse model runs, even before the heightening was added. In retrospect, these alterations could have been included in W1-W4 as well for consistency. These geometry differences are visible in the first years of the simulations; before the inlet sill was heightened, the amount of sediment entering through the inlet already differs between W5 and W1 and W3, but the general trend in the channel stays similar (see Section 5.2.3 and Figure 5.8).

The dimensions of the LTWs in the model depended on the grid resolution. The inlet sill was designed to be 200 m long, but with cells of roughly 80 m in the longitudinal direction, it was schematised as 245 m in the coarse model. In the refined model it was schematised as 188 m. Similar differences were present in the total length of the wall and inter-notches. These discrepancies led to small differences in water distribution between the models, and could have contributed to a different sediment distribution. An inconsistency in schematisation variants concerns the small opening made in the inlet sill in May 2020. This adjustment was incorporated in variants W3 and W4, where the upstream 2D weir section was lowered, but was not incorporated in variants W5 and R5. The opening itself was difficult to represent accurately in the coarse model: in reality, the opening is 15 m wide at a level of +2.8 m NAP, with the sloped connection stretching over 35 m to come back to the +4.05 m crest height of the rest of the sill. With the 80 m wide coarse model grid cells, the small opening could not have been properly schematised. The inconsistent incorporation of this adjustment across variants should be considered when comparing the variants. However, from analysis of the period in which neither included it (2018-2020), the findings regarding the effects of the schematisation variants are not expected to change if both included or did not include the small opening. Including the small opening showed more erosion behind the inlet sill than the closed scenario without it in variant W5 (see Figure 5.7 points c and d).

The schematisation of the crest heights in the bathymetry was not incorporated in the spin-up of the model. During the spin-up, the coarse model resembled the schematisation of variant W2 (the original DVR schematisation, the same as the first 2 years of W4). Including the crest height of the wall in the bathymetry reduced the cross-sectional flow area. At the upstream end of the wall near Wamel this reduction was around 7% when comparing the wall in the bathymetry (W1, W3, W5) vs schematising with 2D weirs (W2, W4). It is expected that this narrowing in the model after the spin-up procedure would cause an erosive response and likely explains the strong erosion seen in the first two years for W1, W3 and W5, shown in Figure 5.8. It should be noted that this 7% is from comparing model schematisations, not with the real-life system, as the wall in real life also takes up cross-sectional flow area. Compared to the real-life system, the 2D weirs with a slight bathymetry increase underestimate the flow area, while schematising the crest height inside the bathymetry overestimates it.

An extra schematisation variant, not implemented in this study, would be to combine the wall crest in the bathymetry with a 2D weir that protrudes slightly above it so that the weir remains active and continues to account for the associated energy losses, thereby improving the flow velocities over the structures. In this study, the weir file was instead kept as it was in the DVR model, with the weir crests positioned slightly below the bed level that incorporated the wall's crest height. As a weir below bed level is not active, this energy loss was therefore not accounted for.

A further option could be to place the bed level partway up the slope of the structure rather than at its crest, and the 2D weir at the as-built crest height. This would improve the representation of the cross-sectional flow area of the main channel, but would reduce the physical barrier against sediment passing. A lower crest in the bathymetry results in a milder transverse bed slope and an even weaker deflection on sediment transport in the coarse model.

Sediment balance quantifications

The sediment balances were determined in two independent ways: from cumulative bed level change, and from cumulative sediment transport. Although the two methods produced reasonably close values and the same behaviour response, they slightly differed. This discrepancy can be due to the output of sediment transport at specific time steps not corresponding entirely to the numerical fluxes with which the model updates the bed level between those steps. What causes this difference is not further investigated. Using either method does not change the findings or conclusions drawn in this research. The absolute magnitudes remain a big uncertainty in this research, as there are no measurements available to verify

them. Additionally, the model is not capable of reproducing bank processes, and it is known that there are sections where the bank line retreated. This additional sediment input was not accounted for in the model simulations.

Sediment transport modes

The Meyer-Peter–Müller (MPM) formula was originally derived for situations where bed-load transport is dominant, such as gravel rivers with low Shields values. The Waal, however, has a bimodal river bed of gravel and sand; due to the finer sand fraction, a substantial portion of sediment transport occurs in suspension, particularly during high-water conditions with high Shields values. Since the sediment transport parameters are calibrated against field observations that inherently include the combined effect of both transport modes, it can be argued that the calibrated bedload transport in the model implicitly represents more than bedload transport alone.

The distinction between the two transport modes is particularly relevant at the LTW site, where they behave differently. The blocking effect of the inlet sill and wall means that mainly suspended sediment enters the auxiliary bank channel, whereas bedload transport is largely blocked and remains in the main channel (De Ruijsscher et al., 2020). The CFD modelling carried out at Deltares (Appendix F) shows the same: the largest contribution to the sediment flux over the inlet comes from suspended load, as bedload is mostly deflected down-slope by the transverse slope effect against the steep slope of the structure. In the DVR modelling approach, bedload and suspended load are lumped into a total load that behaves as bedload only. The transport over the structure is therefore governed by the sediment available in the cells on the slope and crest of the wall, and is fully subject to the slope effect. Modelled as a suspended concentration, through the advection-diffusion solver, sediment can instead pass over cells without available sediment, and is not as strongly affected by the transverse slope because it is mixed with the fluid phase. Calibration can only absorb the magnitude of the missing mode into the transport parameters; it cannot reproduce a mechanism the formulation does not contain, so this selective blocking is not captured. Although the model may already implicitly capture part of this suspended sediment exchange through calibration, rather than missing it entirely, it likely still underestimates the total exchange between the main and auxiliary channel during high-flow conditions, when the suspended fraction increases the most. Recalibration of a new sediment transport formulation would be needed to confirm this. The grain-size composition of the sediment entering and depositing in the auxiliary bank channel was not analysed in this research, although the model calculates transport per fraction. This could provide more insight into the limitations of the MPM formulation used.

Non-erodible bed level

The auxiliary bank channel was schematised with a non-erodible bed level layer, set at the start of the spin-up procedure. This constrains the amount of possible erosion during the simulations to the available sediment deposited on top of the fixed layer during the spin-up. None of the ten-year simulations reached the maximum amount of possible erosion; R5 showed 18-19% of the initial available sediment left the channel, while for W5 this was only 2-4%. However, it can be expected that there was still a significant constraint on erosion at certain locations and discharges.

The threshold for the Struiksma formulation (1999) to account for local bed forms and avoid erosion below a certain fixed layer within a time step is set at 0.7 m. This, in combination with the limited available sediment, activates a reduction factor on the transport almost constantly throughout the channel, affecting how sediment moves through the channel, with bed perturbations moving in the downstream direction with a higher celerity. The reduction factor is also applied on the crest of the wall and inlet sill, since these have a fixed layer too. This means that sediment first needs to come on top of the crest before it can be transported over it, interfering with the sediment magnitudes collected in the cross-sections.

Since the wall and sill are made of rough coarse riprap in real life, some sediment trapping is expected. For the wall, this effect is not yet in the model as the wall is represented with similar graded sediment and roughness as the surrounding river bed. The reduction factor may therefore somewhat compensate for roughness or trapping effects that are not otherwise represented, although the Struiksma formulation was not derived for this purpose and whether the two are of the same order was not investigated. At the heightened inlet sill in R5 and W5, the dumped material is treated as available sediment, which means that the threshold is never met and no reduction factor applies there. However, the dumped material consisted of unrealistically large stones (diameters between 1.5 – 1.8 m) to not erode. Since hiding effects are included in the used transport equations, a strong correction for sediment trapping is nonetheless expected in this

case as well.

Although the sediment transport magnitude may be limited by the reduction factor added, this is the case across all variants, so the results remain usable for comparing them, which is what this research focused on. As already mentioned, the lack of field data on the actual amount of sediment passing over the inlet sill and wall means that neither verification nor an estimate of the error introduced by this reduction is possible, and the absolute quantifications are not usable on their own.

Refined model limitations: lack of validation and compatibility

The refined model was assumed to be the best available representation of the system and used as a benchmark to evaluate the coarse model variants. However, the refined model itself was not independently validated. All tuneable parameters, calibrated and validated for the coarse DVR model, were assumed to remain valid when applied to the refined model. Since these parameters were calibrated for this specific system, they most likely represent it correctly to some extent in the refined model as well, but this still needs to be validated.

Additionally, although the refined and coarse models followed the same spin-up procedure, the initial bed level, bed composition and available sediment distribution differed. Because sediment is scarce on top of the fixed layer, the results depend strongly on the initial availability. As this availability differs between the two models, it limits how well they can be compared. The difference was mainly relevant at the beginning of the simulations up until the high discharge event in January 2018 with Q_{Lobith} 8400 m^3/s. Appendix G.6 shows that after this event, the distribution of available sediment has become more similar between W5 and R5. Figure G.12 shows that the cumulative transport through the outlet diverges up to January 2018, after which it grows with a similar trend in both models. This means the sediment fluxes and balances over the first two years are not directly comparable between W5 and R5. For comparisons over the remainder of the simulation, the effect of the different initial available sediment between the coarse and refined model has diminished, although the totals reported in Table 5.2 still carry this early difference.

Mild slope corrections

This research examined ways to account for the loss of the steep slope of the structure in the coarse grid, which would otherwise have caused a stronger deflection of the sediment transport vector towards the main channel. Tests were done where calibration parameters were altered to compensate for the underestimated slope and the resulting overestimation of sediment transport into the auxiliary bank channel. The relevance and the method of these approaches can, however, be questioned for several reasons.

The A_{sh} parameter in the transverse bed slope correction based on the Koch and Flokstra formulation, as extended by Talmon (1995) was reduced to strengthen the gravity forcing. This parameter governs the process that the missing slope would otherwise have driven. It is, however, applied uniformly across the domain rather than per cell, and accounting for the missed slope factor in this formulation or matching the transport rates of the refined model both required a reduction strong enough to move the main channel bed away from a realistic representation. Model developers might in future make A_{sh} locally adjustable in Delft3D, but this would not be a straightforward addition: locally adjustable parameters are currently defined at cell centres, whereas the transverse bed slope correction is applied after the transport vectors have been moved from the cell centres to the cell faces. A test with a locally lowered A_{cal}, the calibration parameter for the magnitude of transport in the MPM formula, avoids a domain-wide transport calculation adjustment, but does not redirect the sediment at a steep slope; it limits how much is transported in both the transverse and longitudinal directions. Results showed that this caused deposition in front of the structure, increasing the sediment passing the structure again over time.

Neither approach addresses the whole of what the coarse grid misrepresents. The limited increase in transport in the refined model run with a milder slope indicates that the schematised geometry, with the wall placed further into the main channel allowing longitudinal inflow, is also a cause for the higher rates of sediment entering the auxiliary bank channel in the coarse model. A correction acting on the slope alone cannot compensate for both, indicating that local refinement would be needed anyway.

More fundamentally, both approaches tune a formulation towards a target that is itself uncertain. The reductions applied here were based on the transport rates of the refined model and on the ratio missing from the slope in the Koch and Flokstra formulation, as extended by Talmon (1995). That formulation was derived for the transverse slopes that form naturally in river bends, not for steep slopes on longitudinal structures. Laboratory work found a vortex that develops along a longitudinal structure (De Ruijsscher et

al., 2020; Van Os, 2020). The vortex could be argued to be partly contained within the transverse bed slope adjustment, since both describe sediment being deflected back down-slope, but this cannot be assumed for slopes outside the range the formulation was calibrated for. Local grid refinement would resolve the real slope and remove the need for these corrections, but the deflection would still be calculated with the same formulation.

What is missing is therefore not only the slope, but knowledge of what the correction should reproduce. It is known that sediment is deflected back into the main channel against the structure, but not how strongly, and no field data on the amount of sediment passing the inlet sill and wall exist to calibrate against. The corrections tested here should be read accordingly: as an indication of how large the missing effect is in this model, not as calibration values, and the quantification carried out remains useful mainly for showing the size of the discrepancy between the coarse and refined schematisations.

7

Conclusion

This chapter draws the findings of this research together to answer the research questions. The main research question was:

> ***How can the schematisation of longitudinal training walls in 2D morphological models be improved to better assess the stability of auxiliary bank channels?***

Sediment exchange between the main and auxiliary channel is governed by the deflection of the sediment transport vector at the steep slope of the structure, which the coarse grid does not resolve. Incorporating the crest of the wall and inlet sill in the bathymetry improves the representation of the physical barrier and reduces sediment entering the auxiliary bank channel, bringing the simulated sediment distribution closer to that of the refined model. Two limitations remain in the coarse grid: the steep slope of the structure cannot be resolved, which weakens the gravitational deflection, and the entrance geometry risks being lost in the wide cells; both of which increase the sediment transport into the auxiliary bank channel. Tuning the existing calibration parameters to compensate for this caused unrealistic development in the main channel. Local grid refinement, or a sub-grid formulation for the sediment deflection along a steep-sloped longitudinal structure, is therefore needed. Local refinement allows proper schematisation of the geometry of the LTW. A sub-grid feature for morphodynamics would allow a sediment transport deflection formulation based on the local processes observed along such steep-sloped longitudinal structures to be applied even when the steep slope is not resolved, rather than a domain wide formulation calibrated on main channel point bars.

The remainder of this chapter sets out how this answer was reached through the four sub-questions, covering the key processes, how these are represented in the model, and the morphological development seen in the real system and in the simulations.

1. What processes play a key role in morphological development of the auxiliary bank channels of LTWs?

The wall and the inlet sill block near-bed flow, which carries the bulk of the sediment in transport. Sediment passing the wall or inlet sill results from a balance between curved inflow and gravity pulling it back down-slope. Where the bed rises steeply toward the crest, gravity deflects the sediment back to the deeper sections of the main channel and sediment exchange is strongly suppressed. Where the rise is gradual, this resistance is weaker and more sediment is carried across. The gravitational deflection against the flow is stronger on the bedload that moves in contact with the bed than on suspended sediment that travels within the fluid. This selective blocking of bedload and natural sorting in the Waal leads to coarsening of the main channel bed, whilst fine sediment is deposited in the auxiliary bank channel near Wamel.

Due to the longitudinal nature of the structure, sediment does not pile up in front of the sill to eventually be transported over once a mild slope forms, but is taken along with the flow in the main channel. Laboratory work has shown a vortex developing against the slope that deflects sediment back into the main channel. The local geometry of the inlet and the steep slope of the wall and sill are critical to reproducing these processes and the resulting sediment distribution.

Two-dimensional, large-scale river models such as the DVR model do not have a formulation specific for representing these morphological processes against a steep slope, but do include a transverse bed slope

correction on the sediment transport vector. The DVR model uses the Koch and Flokstra formulation, as extended by Talmon (1995), which is calibrated for main-channel bar and pool development, but not tuned for the sediment deflection on steep slopes at inlet structures for LTWs.

Initial rapid bed-level rise in the auxiliary bank channel raised concern about instability. Tranche 1 monitoring (2015–2020) showed deposition in the deeper parts of the channel and erosion near the shoreline. Flores et al. (2022) showed that once bank-retreat sediment is accounted for, the overall channel is eroding, rather than net-depositing, as the deeper-water data alone suggest. Extending the analysis with monitoring data from 2025 (Chapter 4) confirms this: the strong deposition of the first years has reduced, and after the heightening of the inlet sill more areas show erosion in the channel. Reaches of erosion and sedimentation succeed one another along the channel due to channel profile changes and inter-wall notches, which cause local widening that decelerates the flow and allows sediment from upstream to deposit. The deposition concentrated along and just downstream of the stretch where the bank line retreats remains, but is slowing down as the bank stabilises.

Taken together, these field observations identify bank processes as an important control on the morphological development of the auxiliary channel: bank retreat supplies the channel with additional sediment and alters the channel profile. Local deflection of sediment at the steep slope of the structure plays a key role in the sediment distribution between the two channels. Neither of these mechanisms can be reproduced in a coarse grid model with fixed bank lines, such as the DVR model.

2. How reliable is the current DVR (revised 2024) schematisation of LTWs for representing morphodynamic development?

The current DVR model, as schematised in Baseline, does not represent the physical barrier formed by the wall and inlet sill with sufficient accuracy, allowing more sediment exchange between the main and auxiliary channels than is likely to occur in reality. Models relying on this schematisation therefore risk misrepresenting the main channel sediment budget and overestimating dredging costs in the auxiliary bank channel if this exchange is not explicitly accounted for. Although variant W2 reproduced a sedimentation pattern that resembles the field data the most closely among the coarse variants, it does not represent realistic morphological processes. The cause of this sedimentation differs: rather than reflecting the bank erosion-driven redistribution seen in the field data, it results from excess sediment exchange over the LTW. The model does not incorporate bank erosion, and the LTW schematisation has shown overestimated sediment exchange compared to variants that incorporated a more realistic physical barrier. The DVR model, though reproducing the water distribution between the two channels well, does not reliably reproduce either the sedimentation distribution at the inlet sill or sediment exchange along the wall. Since these are the key processes, the standard DVR schematisation cannot be considered reliable for representing morphological development in the LTW reach.

3. How can the geometry of LTWs best be schematised in the coarse grid model to improve the representation of key morphological processes and the resulting development of the auxiliary bank channel?

A refined numerical grid can represent the entrance geometry and the steep slope of the LTW, and with that the hydrodynamics and sediment transport vectors around the structure, in more detail and closer to reality. The refined model was used as a benchmark to test the coarser schematisations. Sedimentation and erosion of the channel in the model are too strongly influenced by the non-erodible bed and by transport settings tuned for the main channel to conclude on the magnitude of the overall trends. The focus was therefore placed on comparing the computed sediment fluxes over the inlet sill and wall between the variants.

The refined model showed a strong blocking effect at the steep-sloped wall and the heightened inlet sill, which resulted in an eroding channel. Schematising the LTW in the coarse model with a slight bathymetry increase combined with a 2D weir was found to be insufficient: although 2D weirs showed some reduction in transport rates, this method still allowed significantly more sediment exchange over the LTW structure than the refined model and than is physically expected. Incorporating the crest height of the structure in the bathymetry reproduced a significantly stronger reduction in sediment transport over the structure than the other coarse variants. Of the coarse variants, W5 was therefore found to be the most suitable for morphological modelling, with the sediment transport rates through the different cross-sections and the spatial distribution of cumulative sedimentation/erosion in the channel resembling R5's most closely.

Nonetheless, W5 still showed considerably more sediment entering over the high inlet sill and exchanging along the wall than the refined model. Two causes were identified. First, placing the wall too far into the main channel loses the alignment with the bank, degrading the geometry of the side-weir entrance and allowing longitudinal inflow into the auxiliary bank channel. This is consistent with the limitation already noted by Barneveld et al. (2025), who applied a similar bathymetric schematisation of LTWs in the coarse DVR model. Second, the coarse grid cannot resolve the steep local slopes of the wall and inlet sill. Because the transverse bed slope directly governs the strength of the gravity term opposing sediment transport over the sill, this missing steepness, and not crest height alone, allows disproportionately more sediment to pass over the structure than expected to occur in reality. A refined model test with a milder slope confirmed this finding. Both shortcomings follow from the cell size. Local refinement therefore resolves both directly.

In the ten-year simulations performed, the heightening of the inlet sill had a significant effect on the overall trend in the morphological development of the entire auxiliary bank channel. The refined model showed that the initial depositional response changed to an erosive trend after the inlet was heightened, due to the increase in sediment blocked at the entrance. The inlet sill therefore forms an effective control knob on this trend. In the coarse model, the heightening showed a similar dominant effect on the amount of sediment entering, but not on the overall morphological development of the channel.

4. To what extent can existing DVR calibration parameters compensate for the loss of local processes at the wall and inlet sill in a coarse grid?

This research looked at tuning parameters to reduce the sediment flux over the LTW and its inlet, to compensate for the loss of the strong deflection due to the misrepresented transverse slope in the coarse grid. Neither the parameter governing the gravitational deflection nor those governing the transport magnitude could be applied in a way that accounted for this process without introducing unrealistic development in the main channel. The A_{sh} parameter goes directly into the formulation for sediment transport deflection due to the transverse bed slope and is therefore the most obvious candidate.However, Delft3D does not allow the parameter to be altered locally, and the A_{sh} reduction needed based on the misrepresented slope and refined model transport rates is strong. Ten-year simulations showed that such reductions significantly alter the main channel river bed: point bars in the river bends disappear, flattening the transverse bed and making the model unfit for representing the main channel. Potentially, increasing the spiral flow intensity could counteract the unwanted flattening of the river bed, although this would only restore the amplitude of the bar and pool pattern while moving its wavelength further from the observed values. Whether it would still be a viable option for the Waal would require additional research and new calibration strategies for the entire domain to account for a localised process occurring only at the LTW structures.

The alternative of locally adjusting parameters in the sediment transport formula, such as the critical Shields parameter or A_{cal}, does not provide an adequate solution for tuning the sediment fluxes at the LTW. These parameters can be varied spatially, but they do not address the same underlying process: they reduce the transport magnitude in both directions, rather than deflecting the transport. Short test simulations with a locally lowered A_{cal} showed this leads to accumulation in front of the inlet sill, which causes an increase in sediment entering the auxiliary bank channel again over time.

Both approaches try to compensate for a process the grid cannot resolve, but neither incorporates it through a formulation made for this situation. The Koch and Flokstra correction was derived for the mild transverse slopes of river bends, not for the steep slope of a longitudinal structure, and it does not represent the vortex that develops against it. Both also introduced new flaws in the main channel. Given the compromises required by either approach to reach a transport rate acceptable against the refined model results, local grid refinement or a new sub-grid formulation for the steep-sloped longitudinal weir is a more suitable solution for morphological modelling than continuing to compensate through these existing calibration parameters. A sub-grid feature would allow a formulation derived for such a steep-sloped longitudinal structure to act locally, in the same way that the current 2D weirs account for energy losses on the sub-grid.

8

Recommendations

The results of this research show that modelling LTWs in a coarse grid, such as the DVR model, requires additional schematisation effort to properly represent the physical barrier the steep-sloped structure forms and the resulting sediment distribution between the main and auxiliary bank channel. Local processes at the inlet sill and along the wall that play a key role in this distribution are missed. This research provides recommendations on how to improve the representation of this process. Part of the recommendations concern possible improvements within the current coarse model, while others regard further model developments and system knowledge needed.

Schematising LTWs in the current coarse grid

Schematising the structure with the current 2D weir formulation alone is insufficient, as it does not form a physical barrier blocking and deviating sediment when overtopped. Incorporating the crest height of the structure directly into the bathymetry does provide a physical barrier that limits sediment transport. A possible further improvement, not tested in this research, would be to combine the crest height in the bathymetry with a 2D weir protruding slightly above it, so that the weir remains active and continues to account for the energy losses. This could slightly reduce the flow velocities over the structure and, with that, the sediment transport rates, as seen in Figure 5.5 when comparing W1 and W3. Further research is needed to determine if this improves the hydraulic and morphodynamic simulation.

This research highlighted two remaining coarse-grid limitations when the crest is incorporated into the bathymetry that result in more sediment transport into the auxiliary bank channel than in the refined model: misrepresentation of the steep slopes, and placement of the wall too far into the main channel, which allows longitudinal inflow and degrades the side-weir entrance. The second can be improved by realigning the grid. In the grid of the DVR model, the crest centreline of the wall and inlet sill was aligned with a grid line rather than a cell centre. This is preferred when a 2D weir is the main representation of the wall, but when incorporating the crest in the bathymetry, it forces modellers to choose between placing the cell too far into the main channel, losing the side-weir inflow geometry, or too far into the auxiliary channel, affecting the channel's conveyance capacity and the discharge extraction. Realigning the grid such that the centreline of the crest falls on the cell centres instead, as done in the refined model, allows the structure to be incorporated into the bathymetry with a more accurate representation of its true position relative to both channels, see Figure 8.1b.

The misrepresentation of the steep slope reduces the deflection of sediment back into the main channel. No calibration parameter in the model intensifies the deflection locally, and the parameter adjustment needed in the case of Wamel caused unrealistic morphological development in the main channel. Although tuning existing parameters is a quick way to force a lower sediment transport into the auxiliary channel, it is neither robust nor widely applicable, and Something additional is needed in the coarse model if one wants to further improve the schematisation of the sediment distribution.

Beyond the current coarse grid

Local grid refinement around the structure in the coarse model can be such an addition. The refined model demonstrated that resolving the steep slope and the entrance geometry has a significant effect

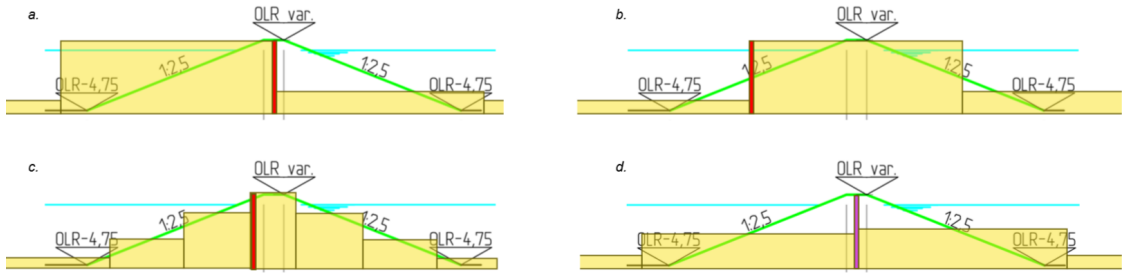


Figure 8.1: Cross-section of the wall showing schematisation options for the LTW, with the as-built geometry in green and the schematised bed level in yellow. (a) Crest height incorporated into the bathymetry with the current grid alignment of the DVR model. (b) Grid realigned so that the crest centreline falls on a cell centre rather than on a grid line. (c) Locally refined grid, in which smaller cells resolve both the steep slope and the entrance geometry. (d) A new sub-grid formulation that accounts for the sediment deflection along the structure, so that the bathymetry no longer has to carry the full crest height. The red line indicates a 2D weir with the current formulation; the purple line a 2D weir extended with a morphological formulation.

on the simulated sediment distribution between the two channels and showed promising initial results in simulating the changing geometry of the channel. Refining is therefore recommended where it is feasible. Local refinement is not yet widely applied in such large-scale river models, and further research is needed into how it can best be applied, and how it influences model stability and computation times.

However, it remains uncertain how much local refinement improves the representation of the process against the steep slope that determines the sediment distribution. The sediment deviation is still defined by the transverse bed slope adjustment calibrated on point bar formations in the main channel. The Koch and Flokstra formulation, as extended by Talmon (1995), used in the DVR model was not derived for slopes this steep and was never intended to represent the vortex that can develop along a longitudinal structure. A further avenue would be to develop a feature that includes the sediment transport deflection against the LTW on the sub-grid, similarly to how the current 2D weirs account for energy loss in the flow when overtopped. Such a feature would also remove the need for the bathymetry to carry the full crest height in order to incorporate the steep slope and represent gravitational deflection, see Figure 8.1d. With the deflection handled on the sub-grid, the cell representing the structure could instead be raised to an intermediate level reproducing a realistic conveyance capacity, while the sub-grid feature accounts for the blocking and deflection of the sediment. This requires further research into a suitable formulation that takes into account the steep slope and the angle and magnitude of the flow. In addition, building in such a feature would require a clear need from Rijkswaterstaat for this kind of addition to morphological modelling in Delft3D.

Further knowledge needed

Significant uncertainties remain in the quantification of sediment exchange between the main and auxiliary channels. Field measurements are recommended to quantify this exchange to validate potential formulations and to verify whether models represent realistic transport rates. Such data would clarify how much sediment models should realistically redirect from the main channel. Additionally, this would give more insight into how representative the current modelling with the MPM formulation is.

Related to this, further research could increase insight into the role of suspended sediment transport and its effect on the long-term stability of the auxiliary bank channel. Potentially alternative transport formulations that include suspended transport may better represent the morphological development of the Waal. Due to time constraints, the grain size of the sediment transported over the structure and the resulting grain size distribution were not examined in this research. Analysing the composition of the sediment entering the auxiliary bank channel, and its spatial distribution within the channel, is strongly recommended, as it would increase knowledge on the model's performance in reproducing the selective sediment blocking of the LTW and indicate how reliable the model is in predicting morphological development.

Finally, the refined model showed promising results in reproducing the morphological development of the auxiliary bank channel. With an alluvial bed in the channel, it reproduced the distribution of deposition and erosion seen in the field observations, including the transverse redistribution, with deposition in the deeper parts and erosion in the shallower zones near the bank. Investigating this further is strongly recommended, as the fixed layer is what most constrains what these models can say about the stability of the auxiliary bank channel: only a channel that is free to erode and accrete can show how its conveyance capacity and the discharge distribution between the two channels develop over time, and what dredging is needed to maintain them. Reducing this uncertainty would give the Room for the River 2.0 programme a firmer basis for assessing LTWs as a measure along the Waal.

Bibliography

Asselman, N. (2025). Hoe werken we aan een toekomstbestendig rivierengebied? https://www.deltares.nl/verhalen/toekomstbestendig-rivierengebied

Barneveld, H., Paarlberg, A., Van Denderen, P., & Kuiper, J. (2025). *Systeemmaatregelen beleidskeuze rivierbodemligging rijntakken* (tech. rep. No. PR5219.10). HKV.

Becker, A., Kosters, A., Nunes de Alencar Osorio, A. L., Chavarrias, V., & Ottevanger, W. (2023). *Morphological model for the river rhine: First (v0) model of the waal branch* (tech. rep. No. 11209261-003-ZWS-0002). Deltares.

Becker, A., & Mosselman, E. (2026). Monitoring pilot langsdammen tranche 1 [Unpublished presentation at the Longitudinal Training Walls Symposium, Driebergen, 2026. Deltares].

Chavarrías, V., Sloff, K., & Mosselman, E. (2021). *Eindevaluatie pilot langsdammen in de waal* (tech. rep. No. 11204644-012-ZWS-0001) ('WaalSamen' Werkpaket 10). Deltares.

Collas, F. P. L., Buijse, A., Van Den Heuvel, L., et al. (2017). Longitudinal training dams mitigate effects of shipping on environmental conditions. *Science of the Total Environment*, *619-620*, 1183–1193. https://doi.org/10.1016/j.scitotenv.2017.10.299

Collas, F. P. L., Flores, N. Y., van Aalderen, R., Bosman, F., Schoor, M. M., Verbrugge, L. N. H., Van Kessel, N., Achterkamp, B., Romeijn, W., Liefveld, W., Buijse, A. D., & Leuven, R. S. E. W. (2020). *Rapportage natuurgegevens langsdammen waal 2016 - 2020* (tech. rep. No. Verslagen Dierecologie en Fysiologie 2020-2) ('WaalSamen' Werkpaket 8). Radboud Universiteit.

Czapiga, M. J., Blom, A., & Viparelli, E. (2021). Impact of weir location on discharge partitioning in longitudinal training walls. *NCR 2021*.

Czapiga, M. J., Blom, A., & Viparelli, E. (2022). Efficacy of longitudinal training walls to mitigate riverbed erosion. *Water Resources Research*, *58*(12). https://doi.org/10.1029/2022WR033072

De Ruijsscher, T. V., et al. (2018). Flow bifurcation at a longitudinal training dam: Effects on local morphology. *River Flow 2018*.

De Ruijsscher, T. V., Vermeulen, B., & Hoitink, A. J. F. (2020). Diversion of flow and sediment toward a side channel. *Water Resources Research*, *56*(6). https://doi.org/10.1029/2019wr026750

De Wit, L. (2026, April 21). Cfd ltw progress meeting [Internal presentation, not publicly available].

Deen, L., Becker, A., Sieben, A., Beyer, D., & Krabbendam, J. (2026, June 9). Langsdammen waal met 2d morfologisch d-hydro model [Internal presentation, not publicly available].

Deltares. (2026). *Delft3d-flow user manual* [Version 4.07.01]. https://content.oss.deltares.nl/delft3d4/Delft3D-FLOW_User_Manual.pdf

Flores, N. Y., Collas, F. P. L., & Leuven, R. S. E. W. (2022). Geomorphological development of aquatic mesohabitats in shore channels along longitudinal training dams. *Remote Sensing in Ecology and Conservation*, *8*(5), 744–760. https://doi.org/10.1002/rse2.273

Huthoff, F., et al. (2011). *Rivierkundig onderzoek waalsamen: Pilotstudie langsdammen* (tech. rep. No. PR2096.10). HKV/Deltares.

Jammers, S. M. M. (2017). *Sediment transport over sills of longitudinal training dams* [Master's thesis, Delft University of Technology]. https://resolver.tudelft.nl/uuid:4570fe94-c2f2-4d4c-96a0-fb53d7e7dc3f

Koedijk, O., van der Sluijs, A., & Steijn, M. (2017). *Richtlijnen vaarwegen 2017* (tech. rep.). Rijkswaterstaat.

Le, B., Crosato, A., & Uijttewaal, W. (2018). Long-term morphological developments of river channels separated by a longitudinal training wall. *Advances in Water Resources*, *113*, 73–85. https://doi.org/10.1016/j.advwatres.2018.01.007

Mosselman, E., & Sloff, K. (2026). Insights in processes and modelling of the morphological evolution of the lower rhine. *Water*, *18*(3), 407. https://doi.org/10.3390/w18030407

Nijsse, L. (2025). *Optimizing longitudinal wall and multi-channel design at the ijssel river* [Master's thesis, Delft University of Technology]. https://resolver.tudelft.nl/uuid:2cb6166f-6476-4847-accd-b9ea970c2ec1

Omer, A., Ottevanger, W., & Yossef, M. (2019a, December). *Modelling the morphological effects of longitudinal dams in the midden-waal* (Tech. Rep. No. 11203681-002-ZWS-0001) ('WaalSamen' Werkpaket 1). Deltares. Delft, the Netherlands.

Omer, A., Ottevanger, W., Yossef, M., & Buschman, F. (2019b). *Case study of morphological modeling with delft3d4 and delft3d-fm* (tech. rep.). Deltares.

Osorio, A. L. N. A., Mosselman, E., Franca, M., & Creech, C. (2020). Longitudinal training walls on the waal river as a river training alternative. *XIV Encontro Nacional de Engenharia de Sedimentos*.

Paarlberg, A. J., Omer, A. Y. A., & Yossef, M. F. M. (2021). *Eindevaluatie pilot Langsdammen in de Waal Delft3D simulations* (tech. rep.) ('WaalSamen' Werkpaket 1). HKV Deltares.

Shields, A. (1936). *Anwendung der ähnlichkeitsmechanik und der turbulenzforschung auf die geschiebebewegung* (tech. rep.). Preussischen Versuchsanstalt für Wasserbau und Schiffbau. Berlin.

Sieben, A. (2020). *Overzicht afvoermetingen 2016-2019 project monitoring langsdammen* (tech. rep.). Rijkswaterstaat.

Sloff, K., Becker, A., Paarlberg, A., & van Denderen, P. (2024). *2d morfologisch model irm* (tech. rep. No. 11209264-001-ZWS-0005). Deltares.

Struiksma, N. (1999). Mathematical modelling of bedload transport over non-erodible layers. *Proceedings of the IAHR Symposium on River, Coastal and Estuarine Morphodynamics (RCEM)*, 89–98.

Swart, S. (2020). Luchtfoto waal met langsdammen. https://www.siebeswart.nl/image

Talmon, A., Struiksma, N., & Van Mierlo, M. (1995). Laboratory measurements of the direction of sediment transport on transverse alluvial-bed slopes. *Journal of Hydraulic Research*, *33*(4), 495–517. https://doi.org/10.1080/00221689509498657

Van der Niet, W. (2026, February). *Bed level changes in side channels of longitudinal training walls: Sensitivity analysis for the Waal River* (Technical Report No. RO:1215.10). Wageningen Univerist, HKV.

Van Linge, B. W. (2017). *Hydraulic evaluation of longitudinal training dams* [Master's thesis, Delft University of Technology]. https://resolver.tudelft.nl/uuid:63160c45-f3ed-4ad2-84c8-9a1db1e04f0a

Van Os, W. J. (2020). *Bed-load transport over inlet sills of longitudinal training walls* [Master's thesis, Delft University of Technology]. https://resolver.tudelft.nl/uuid:9b437435-05d8-43fb-a8f8-9ee9c5374a84

Van Weerdenburg, R. J. A. (2018). *Measured change in bed elevation and surface texture near longitudinal training dams in the waal river* (Honours Programme Master Thesis) (CIEAESM4015). Delft University of Technology. Delft, the Netherlands.

Wang, Z. B., De Vries, M., Fokkink, R., & Langerak, A. (1995). Stability of river bifurcations in id morphodynamic models. *Journal of Hydraulic Research*, *33*(6), 739–750. https://doi.org/10.1080/00221689509498549

Ylla Arbós, C., Blom, A., Viparelli, E., et al. (2021). River response to anthropogenic modification. *Geophysical Research Letters*, *48*. https://doi.org/10.1029/2020GL091338

Zanting, H. A., & Van Rijn, S. (2024). *Werkhypothesen ruimte voor de rivier 2.0* (tech. rep.). Arcadis Nederland B.V.

Zevenbergen, C., Rijke, J., van Herk, S., & Bloemen, P. (2015). Room for the river: A stepping stone in adaptive delta management. *International Journal of Water Governance*.

A

Appendix

Overview of the appendix:

- Appendix A: Shows additional field research regarding the bank erosion in Wamel found by Collas et al. (2020) and Flores et al. (2022) and sedimentation against the inlet sill
- Appendix B: Shows the adjustments made to the inlet sills of the LTWs in the Waal
- Appendix C: Stepwise hydrograph used as boundary condition for ten-year simulations
- Appendix D: Elaborates on the schematisation of LTW in the grids
- Appendix E: Elaborates on the set-up of the refined model and the spin-up procedure.
- Appendix F: Initial findings of CFD LTW project at Deltares
- Appendix G: Additional model results
- Appendix H: Discharge distribution for the short stationairy test run

A. Additional field observations

A.1. Bank erosion Wamel tranche 1

Table A.1: Change in sediment volume (m^3) in the three bank channels and the two groyne field locations in the period 2015–2019. + = sedimentation; − = erosion, from Collas et al. (2020)

Location	2015–2016	2016–2018*	2018–2019**	2015–2019	
	m^3	m^3	m^3	m^3	m^2/200 m
Bank channel Wamel	+60375	−23397	−42154	−5176	−335
Bank channel Dreumel	−19127	−106460	−31061	−156649	−8830
Bank channel Ophemert	−1483	−29372	+5132	−25724	−1614
Groyne field Tiel	−1543	−21560	+9164	−13940	−3765
Groyne field Heereawaarden	−29264	+663	−6151	−34751	−12353

* Estimate for the period 2016–2017 based on the difference between the 2016 and 2018 datasets.
** On Jan 23 2018 dredging took place in Wamel (15074 m^3) and Dreumel (23400 m^3).

Table A.2: Summary of the bank line retreat rates (m/year) of the erosion areas in the Wamel and Dreumel shore channels in the river Waal from Flores et al. (2022)

Period	Study site	Mean retreat rate (m/year)
2014–2015	Wamel	0.1 ± 1.2
2015–2016	Wamel	1.7 ± 1.0
2016–2018	Wamel	2.4 ± 2.2
2018–2019	Wamel	0.8 ± 0.8
2019–2020	Wamel	1.4 ± 0.8
2015–2020	Wamel	1.6

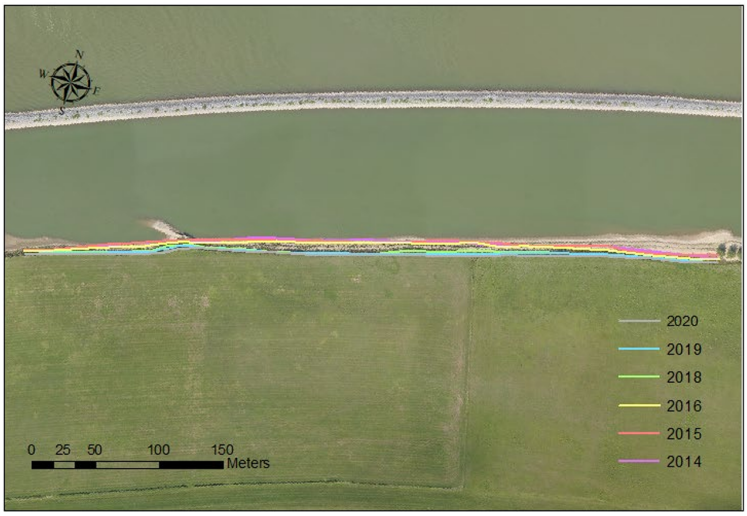


Figure A.1: Bank lines at the bank erosion area in the auxiliary bank channel at the LTW near Wamel, with aerial photograph as background 2019 (Flores et al., 2022)

A.2. Sedimentation against the inlet sill

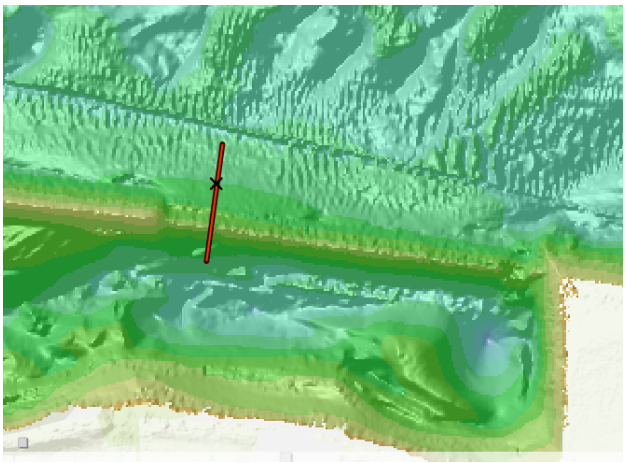


Figure A.2: Bathymetry around the LTW inlet near Wamel (L. Deen, Rijkswaterstaat, personal communication, June 12 2026)

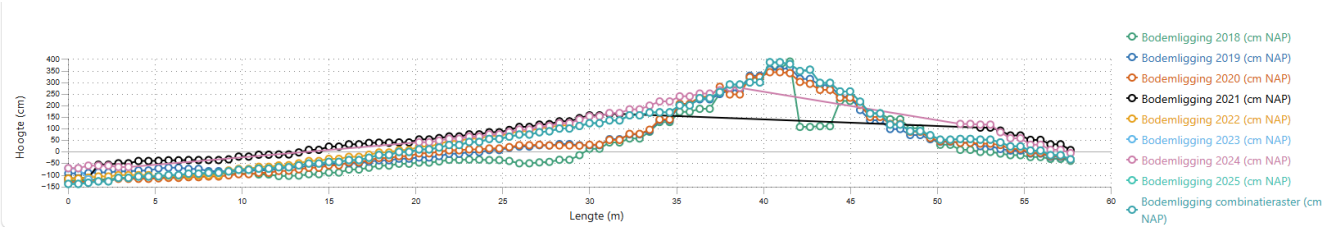


Figure A.3: Slope in front of inlet Wamel for 2018-2025 (L. Deen, Rijkswaterstaat, personal communication, June 12 2026)

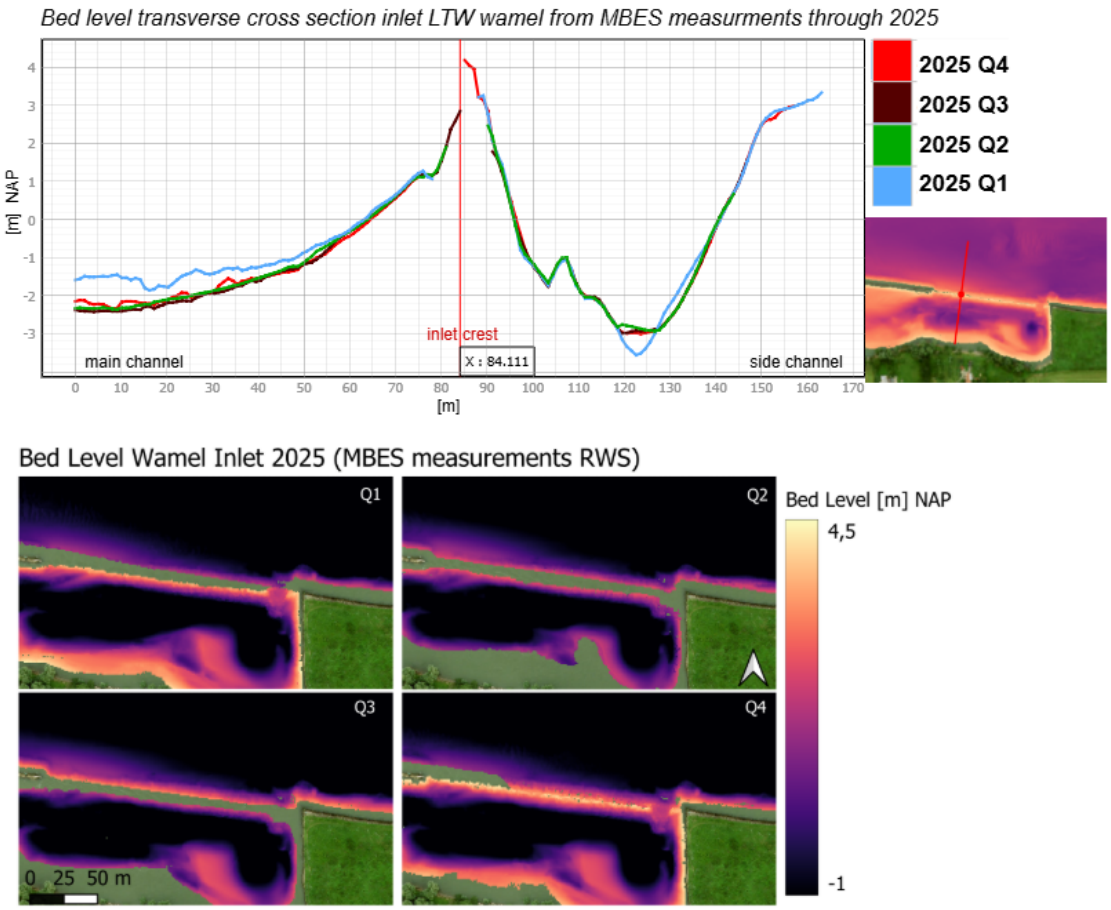


Figure A.4: Deposition in front of the inlet Wamel based on MBES measurements throughout 2025

B. Adjustments to inlet sills

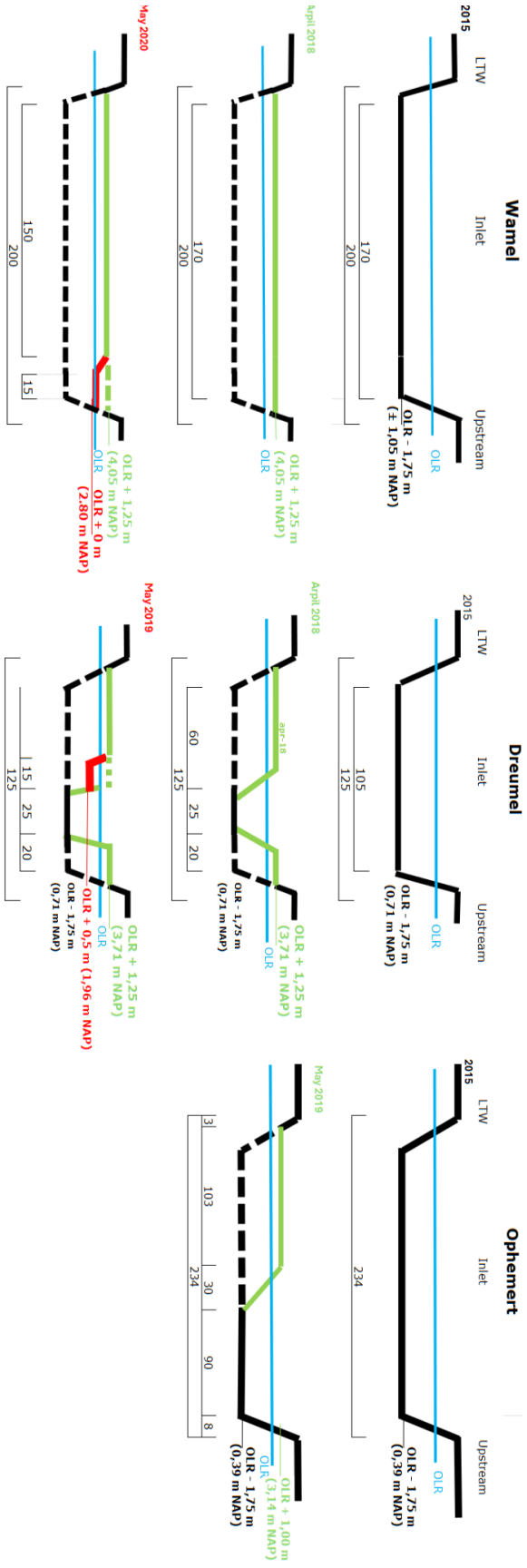
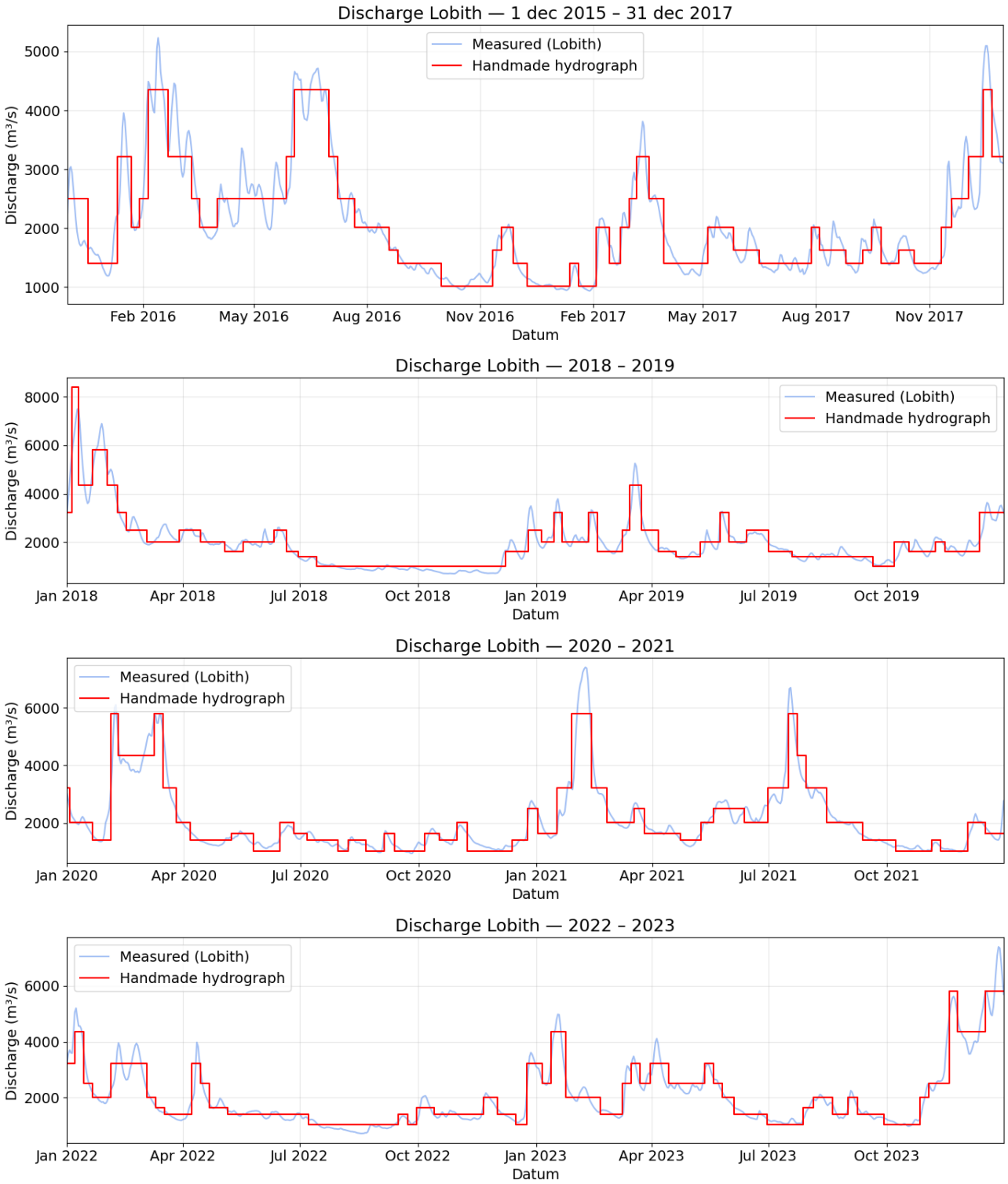


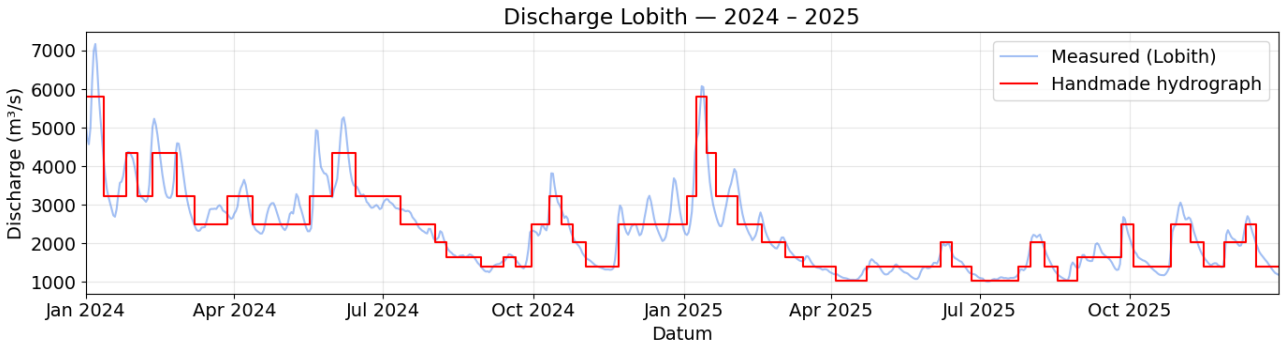
Figure B.1: Adjustments made to geometry of inlet sills

C. Hydrograph

C.1. Stepwise schematisation of discharge at Lobith

This appendix shows the annual-varying stepwise hydrograph used to represent the hydrological conditions in the Waal between 2016 and 2026. The hydrograph is based on daily observations at Lobith. Standard fixed discharge values were used for the steps to be able to reuse pre-existing hydraulic restart files for the DVR model. Since only the Waal is modelled, the Pannerdensche bifurcation is outside of the domain. A fixed discharge distribution commonly used by Deltares is used to determine the discharge to the Waal, shown in Table C.2.

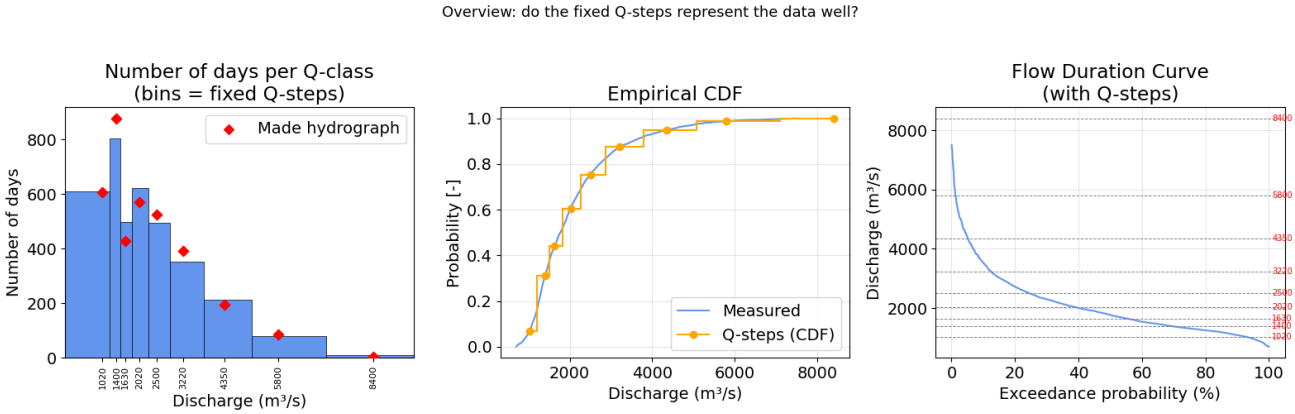




C.2. Fit of the schematised stepwise hydrograph

Table C.1: Annual volume comparison between measured discharge and made hydrograph at Lobith.

Year	Measured (10^9 m³)	Made hydrograph (10^9 m³)	Difference (10^9 m³)	Error (%)
2016	72.615	71.693	-0.922	-1.30
2017	57.748	57.707	-0.041	-0.10
2018	61.726	62.217	0.491	0.80
2019	61.623	62.123	0.500	0.80
2020	59.140	59.039	-0.101	-0.20
2021	70.503	71.019	0.516	0.70
2022	53.456	54.399	0.943	1.80
2023	74.263	74.474	0.211	0.30
2024	88.456	87.134	-1.322	-1.50
2025	56.644	56.457	-0.187	-0.30
Total	656.174	656.262	0.088	0.01



C.3. Discharge distribution to Waal and applied Morfac

Table C.2: Discharge [m^3/s] Boven Rhine with the fixed associated fraction that goes to the Waal, and the applied Morfac per discharge value

Q_{BR} (DVR steps)	Q_{Waal}	Applied Morfac
1020	830	1440
1400	1127	1440
1630	1307	720
2020	1581	720
2500	1778	240
3220	2244	240
4350	3014	120
5800	4001	120
8400	5671	120

C.4. Days a year discharge high enough for the wall to be submerged

The LTWs were designed to overflow approximately 100 days a year (De Ruijsscher et al., 2018). The past ten years showed mild hydrodynamic conditions, leading to fewer submerged days. Table C.3 shows how many days the discharge at Lobith was high enough to submerge the wall in the model simulations and in real life.

Table C.3: Number of days per year for which the wall is submerged ($Q_{Lobith} > 2600\ m^3/s$)

Year	Stepwise hydrograph $Q_{Lobith} > 2600\ m^2/s$	Discharge measured at Lobith > 2600 m^2/s
2016	88	117
2017	39	44
2018	46	63
2019	49	47
2020	53	56
2021	86	94
2022	55	52
2023	87	104
2024	145	203
2025	31	44
Total	679	824

D. Model grids

D.1. Schematization of inlets and walls

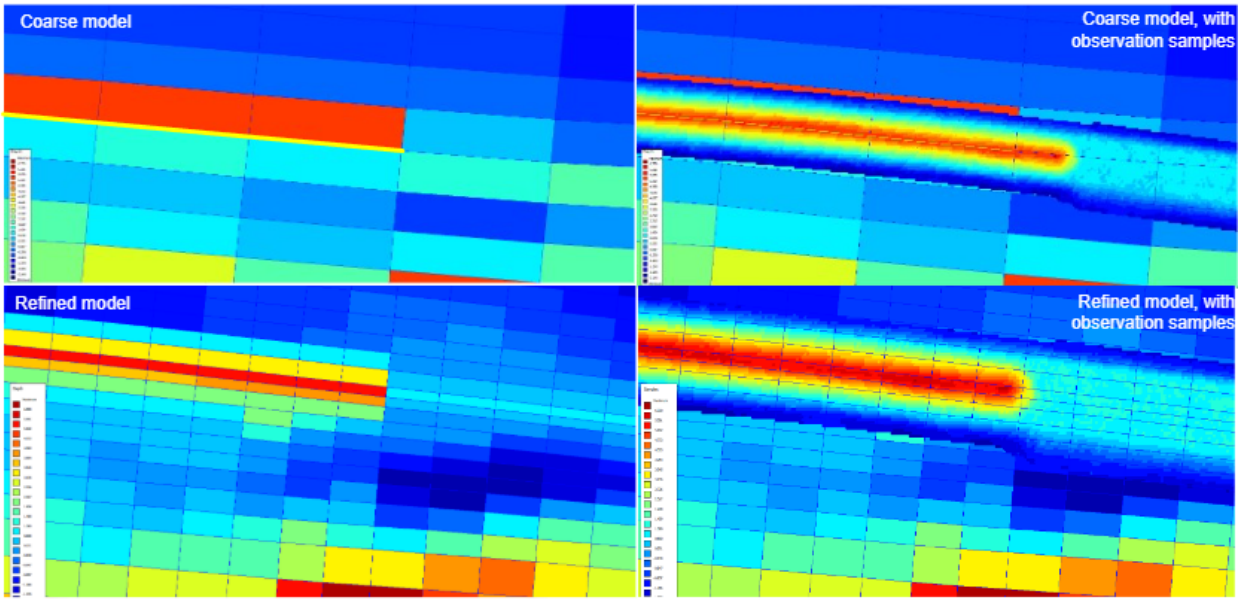


Figure D.1: The onset of the wall schematised with the crest height inside the bathymetry in the coarse and refined grid compared with observation samples. The finer grid is locally refined to 4 m for the crest of the wall.

D.2. Schematization of inlets and walls

This appendix helps understand the ways that the walls and inlet sills of the LTWs are schematized.

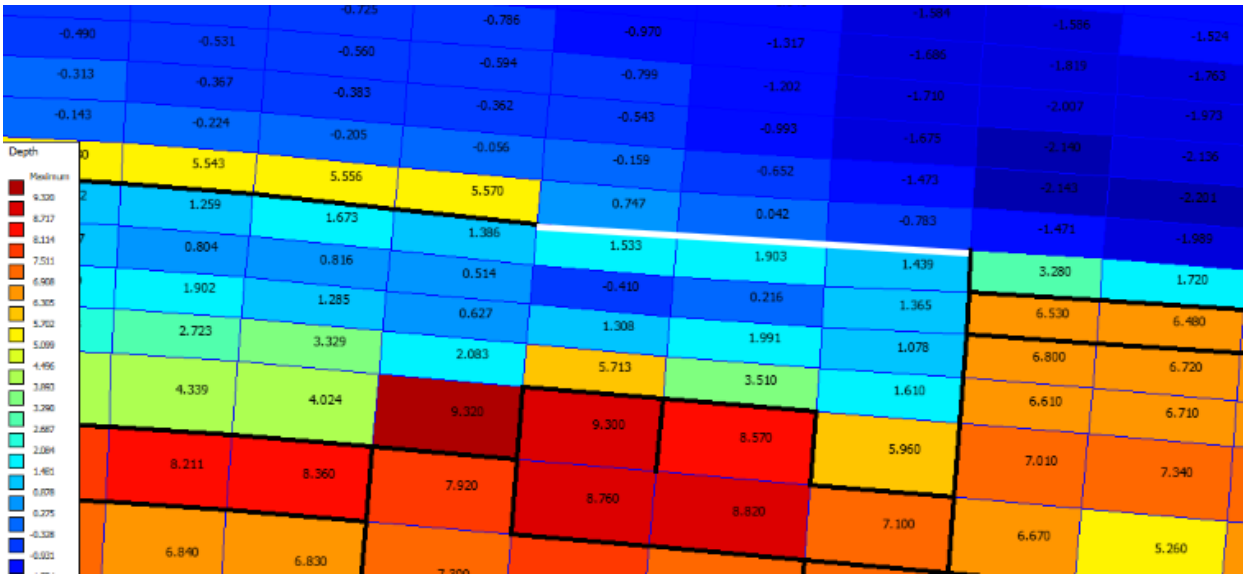


Figure D.2: Grid with depth and 2D weirs around inlet Wamel used in run W1 and W3; wall in bathymetry and with 2D weirs. In white the 2D weir used on the inlet that is heightened in 2018 is shown for run W3. In run W1 no 2D weir for the inlet is used and the heightening is not included.

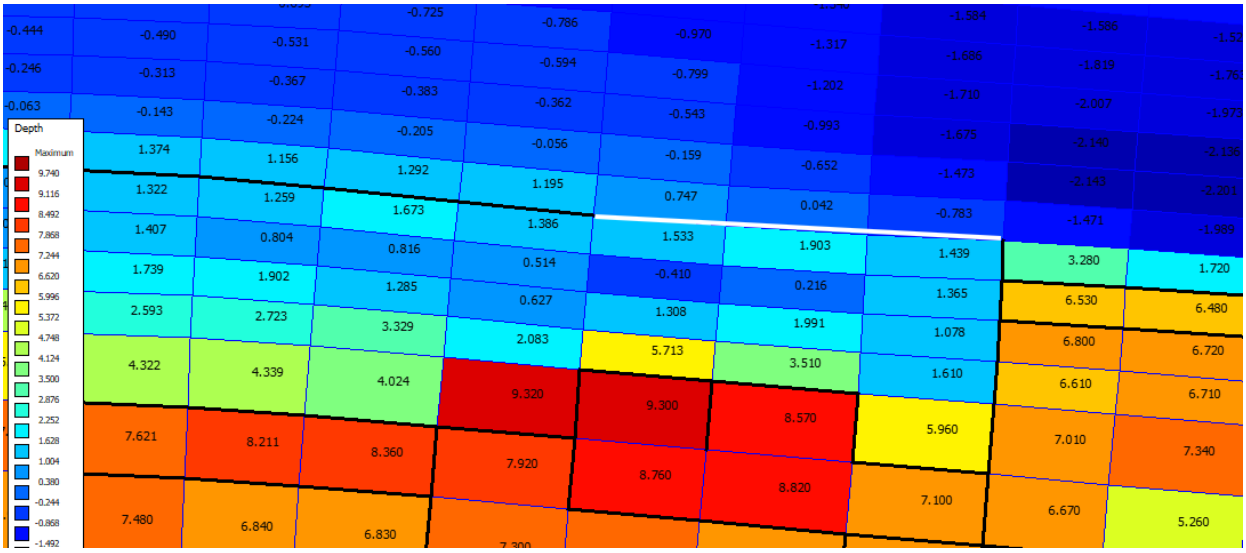


Figure D.3: Grid with depth and 2D weirs around inlet Wamel used in run W2 and W4; wall is schematized with 2D weirs that came from Baseline j18 like they where in the DVR model from Sloff et al. (2024). In white the 2D weir used on the inlet that is heightened in 2018 is shown for run W4. In run W1 no 2D weir for the inlet is used and the heightening is not included.

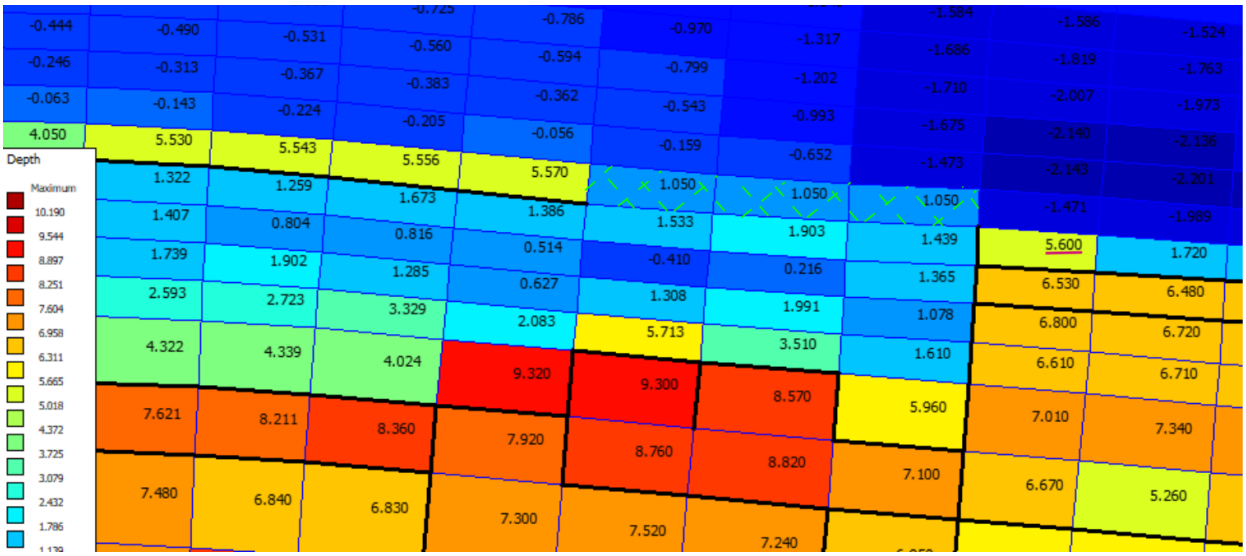


Figure D.4: Grid with bed level values and 2D weirs around inlet Wamel used in run W5; wall in bathymetry and with 2D weirs. The cells with the green dashed lines represent the crest of the inlet sill and are heightened with nourishment of coarse riprap to represent the adjustment made to the inlet. The start height of the inlet crest cells was altered to match the inlet height as built in 2016. Additionally, to connect the inlet sill with the bank, the height of the cell upstream of the inlet sill was increased, see the pink line.

D.3. Cross sections and observation points locations

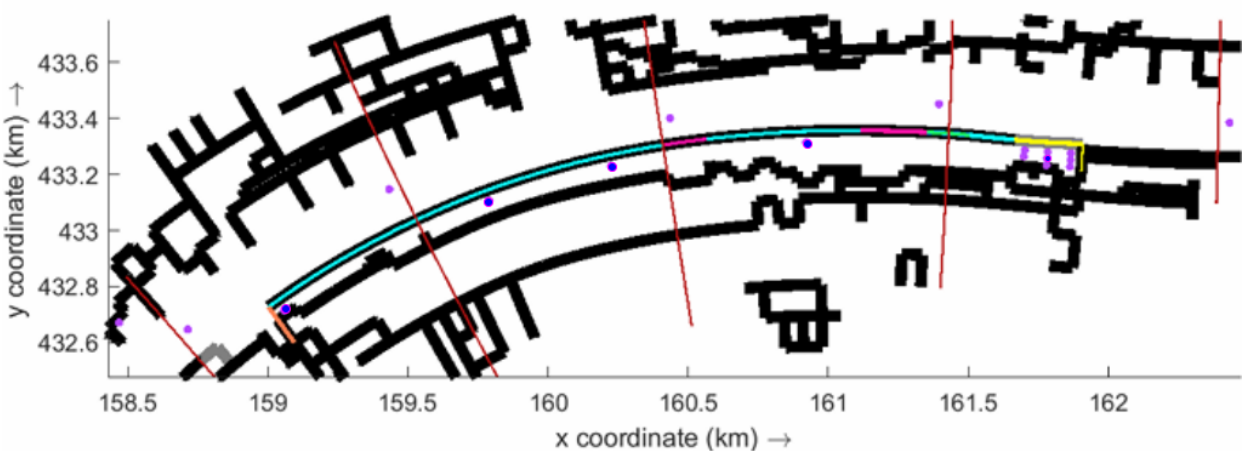


Figure D.5: Cross sections and observation points used to asses morphological development of the coarse model runs in the bank channel near Wamel. On top of the lines of the wall (in black) and added 2D weir (run W3 and W4, in grey).

The cross sections shown are:

- yellow: the inlet with in the flow directec part 1 and in the transverse direction part2
- teal: the parts of the wall with 1, 2, 3 are from right to left in downstream direction. The righest part is 1A and greener shade is part 1B
- pin: the inter-notches, also counted from right to left
- orange: the outlet
- red the river kilometres (rkm 911, 912, 913, 914 and 915).

The observations points are shown in lilac:

- the main channel matching the rkm from the cross sections,
- the bank channel the points behind the inlet are measured and with a dark blue centre the LTW 1, 2, 3, 4, 5 points are shown from right to left.

D.4. Nourishment on inlets for run W5 and R5)

Nourishments were added to the cells with the inlets to incorporate the adjustments made in rile-life. Only the heightening performed in 2018 and 2019 were added, as the little gaps made in 2019 (Dreumel) and 2020 (Wamel) were too small for the coarse grid. This subsection explains how the nourishments were done.

First, a coarse sediment type was needed to make sure that the non-erodible inlet sills would not erode away. A new sediment type could not be added if the restart files wanted to be re-used, so it was decided to alter the grain size of one of the tracer sediments, ”Sediment12”, originally added for nourishment in upstream parts of the Rhine in Germany that is not used in this study as only the Waal is run.

Since the model already has dumping and dredging files for each discharge step that is re-used every time this discharge step comes back, a little trick had to be done to add an extra dumping and dredging manoeuvre. It was diced to add a discharge step for the dump moments with new Q-values 1 m^3/s off from the one matching the hydrograph that moment. The steps were made one minute long in hydraulical time and 0 days morphological time. As both moments are closest to a discharge step of 2020 in the used hydrograph, the following are used:

- for 15-04-2018: Q_{Lobith} 2019 m^3/s
- for 09-05-2019: Q_{Lobith} 2021 m^3/s

The next discharge step, that has a Q_{Lobith} of 2020 m^3/s, was shortened by one minute. The other boundary files for these new discharge steps were made simply by copying the one of 2020 m^3/s and renaming them with the new values.

In the `.mor` files for these new added discharges, the following settings are altered:

[Morphology]
MorFac = 1 [-] Morphological scale factor # used to be 720 for Q2020
MorStt = 0 [-] First time step relative to ITDATE for updating in Tunits # used to be 720
SedtransStt = 0 [-] Sediment transport computation starts after () # used to be 720

Polygons with the locations of the cells containing the parts of the inlets adjusted were added in a polygon file.

As the model automatically calls up an `RBK_ref_v5_2018_Q#CURRENTDISCHARGESTEP#.dad` file, the following two were added to the model: `RBK_ref_v5_2018_Q2019.dad` and `RBK_ref_v5_2018_Q2021.dad`. In these files, the coarse sediment is dumped with a volume calculated based on the bed level observed the model run just before the nourishment, the wanted new height and the grid cell square surface

D.5. Coarse model schematisation wall and inlet slope

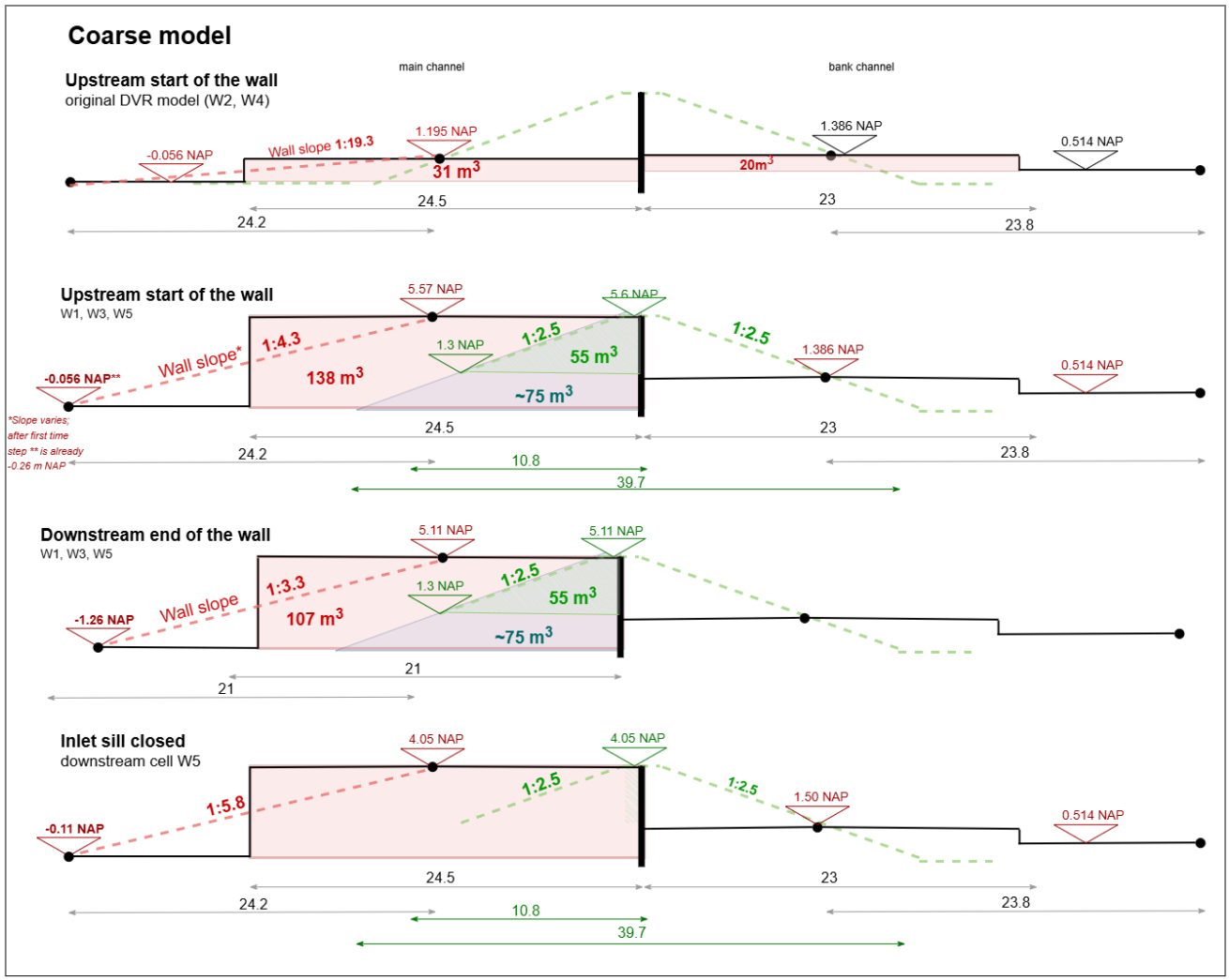


Figure D.6: Schematisation of wall and inlet sill in W5 model. Showing cross sectional area of wall at upstream end of LTW near Wamel for different schematisation (red) compared to as-built (green).

D.6. Refined model schematisation wall and inlet slope

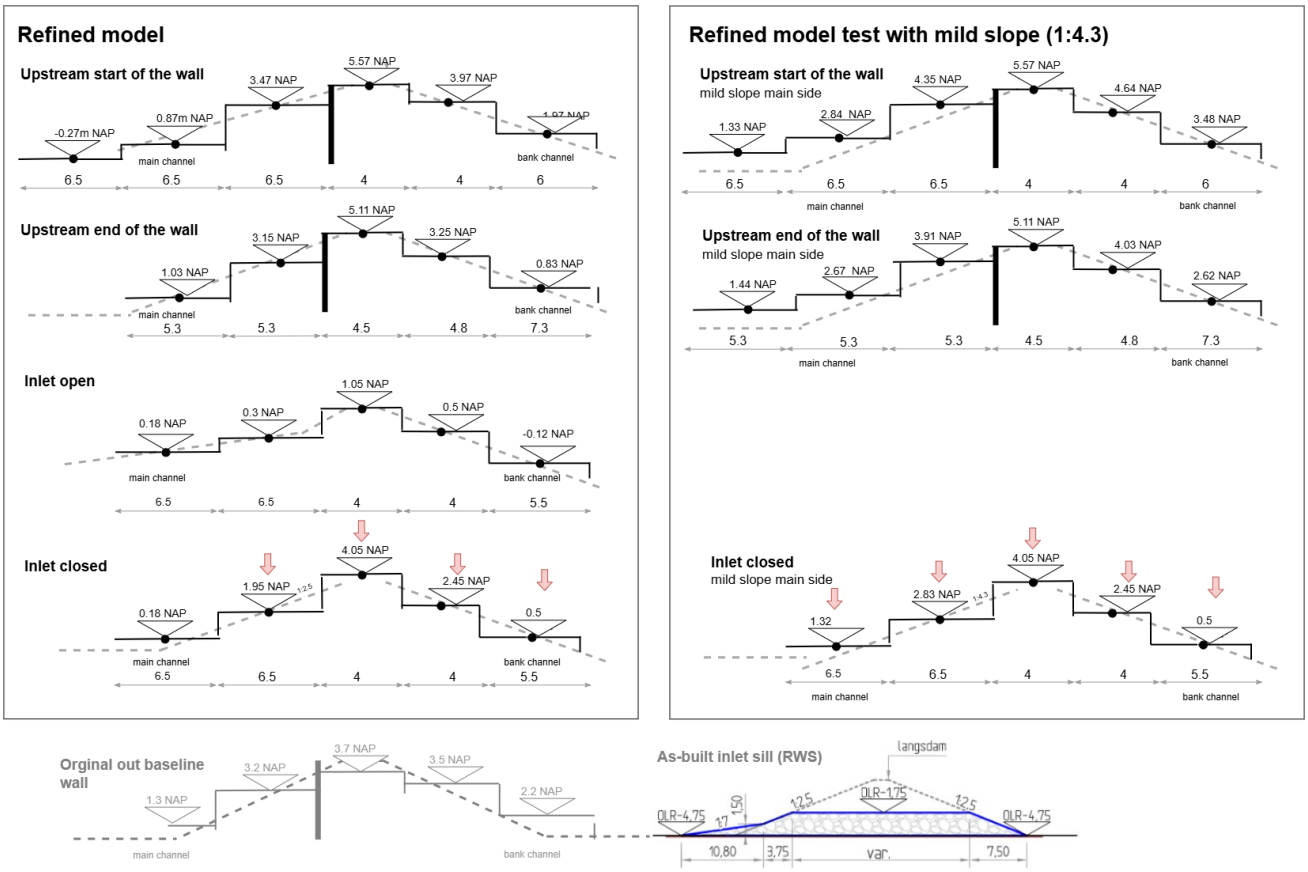


Figure D.7: Schematisation of wall and inlet sill in refined model.

D.7. Local adjusted A_{cal} in S2 test run

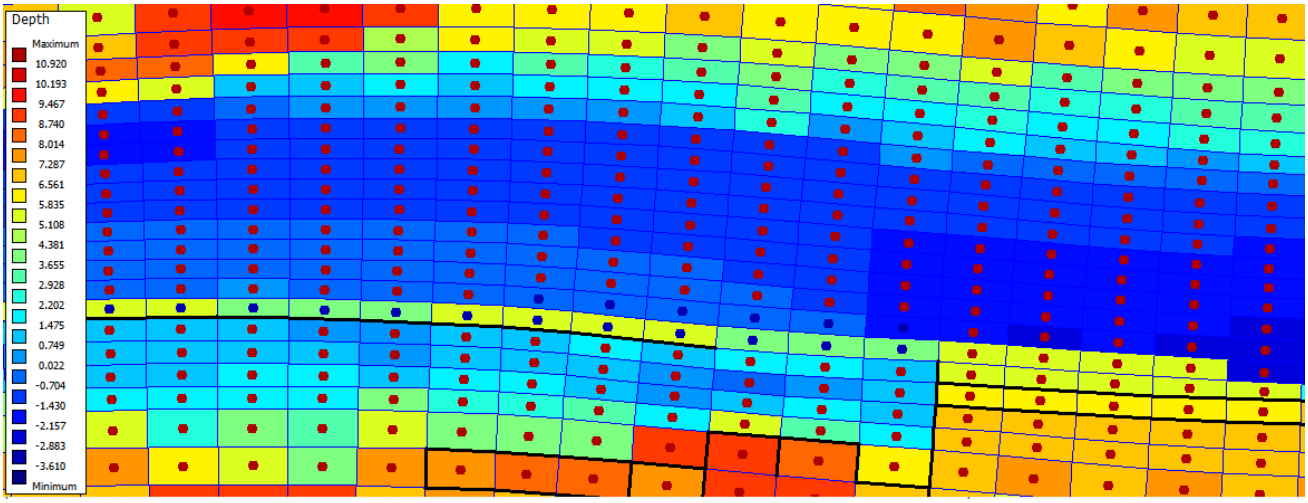


Figure D.8: Grid of S2 showing where the A_{cal} was locally reduced from 2.4 (red dots), to 0.5 (blue dots); in front of inlet sill and for the crest of the sill and wall (also for the rest of the wall to its downstream end, outside this frame).

E. Setting up the new refined model

The refined model was made using an existing fine grid from the case study of Omer et al. (2019b). The same set-up procedure as that used for the coarse Delft3D model (DVR grens regio project) was followed.

Input files
Baseline version 5.3.3.1808 (j18_5-v2) in ArcGIS 10.3.1.4959 provided several input files describing the river geometry, matching the refined grid (.aru, arv, .dep, .enc, .wr).

Some files containing spatially defined parameters were resampled onto the new grid with the Quickin software in the Delft3D-4 interface. This was the case for the initial bed composition defined by fractions and thickness files. After resampling, the thickness file was altered locally around the LTW. The higher resolution allowed the erodible river bed surrounding the structure to be represented with an extra row of cells that were given a limited thickness of 5 m to account for the hard structure extending into the river bed.

When resampling the fractions files, a ”Value of Closest Points”-interpolation was used, followed by pasting the distribution of the main channel to the floodplains and remaining empty extra cells with the ”Depth line sweep”-function. This created the same transverse uniform fraction distribution and longitudinal variations as the DVR model used on the coarse grid for the refined grid. The different fraction percentages comprising each layer thickness must add up to exactly 1.00 for the model to run. Fraction 11 is filled with the remaining percentage to comply with this requirement. With iterative small alterations to fraction 10, 9 and 8, all negative values were removed from fraction 11.

The ripple factor, which is defined by a depth file, was resampled and averaged onto the fine grid. Other sediment transport settings that were not spatially variable within the model domain, such as the MPM transport parameters and the bed roughness, were directly taken from the DVR model.

For the boundary conditions, the following was used:

- Hydrological condition upstream: for each discharge at Lobith, the same discharge applied around 868 rkm in the coarse model was used for the upstream end of the refined model at 888 rkm.
- Hydrological downstream: for each discharge at Lobith, a water level at the downstream end was specified based on observations at 935 rkm in model run W1.
- Sediment boundary condition: no sediment boundary conditions were given to the model. This was also the case for the coarse model of the Waal. The whole DVR model includes a fixed bed level at the upstream end of the Upper Rhine to prevent unrealistic local erosion. For this research, no boundary was imposed at the upstream ends. Perturbations tend to travel at a speed of 1 km/year in the Waal. Only 10 years are considered and the upstream end of the refined model is 23 rkm upstream of the area of interest (the LTW).

Hydrological spin-up
To limit spin-up time when a new discharge is prescribed at the upstream boundary, the model uses a local database to store water levels and flow velocities for every discharge value used. This information is copied onto the model when a new discharge step is prescribed. To create the initial hydrological database files, every discharge value was run as a separate stationary simulation of 5 days. From the resulting output files, the results were combined into two combining files for the database.

Morphological spin-up
To allow the initial observed bed levels and sediment compositions to adapt to model imperfections and geometry, a spin-up procedure was followed. This helps to ensure that rapid initial adjustments do not interfere with the analysis of actual morphological changes during the main simulation. The same procedure was followed as that used by Becker et al. (2023) for the coarse model. The procedure consists of two steps, in which the model was run for two wet years allowing the bed level and composition to change and giving the model 1440 minutes of spin-up time when a new discharge is prescribed. After the first two years, the new bed composition was used for a new 1 m thick top layer on the initial bed composition for the remaining thickness. Discarding the bed level changes, this new composition was used to simulate the two years a second time with the original initial bed level. Bed level change was only enabled during the first two years to allow the bed composition to adjust properly. After the second two years, the new bed level and

composition were used to generate new input files for the model together with new hydraulic restart files matching the new river bed. The procedure is shown in Figure E.1. The final resulting available sediment for the auxiliary bank channel for the start of the simulations is shown in.

A limitation of the morphological spin-up procedure, is that schematisation of the LTW inside the bathymetry was not jet done. During the spin-up was performed with a schematisation based on input files from Baseline, like variant W2.

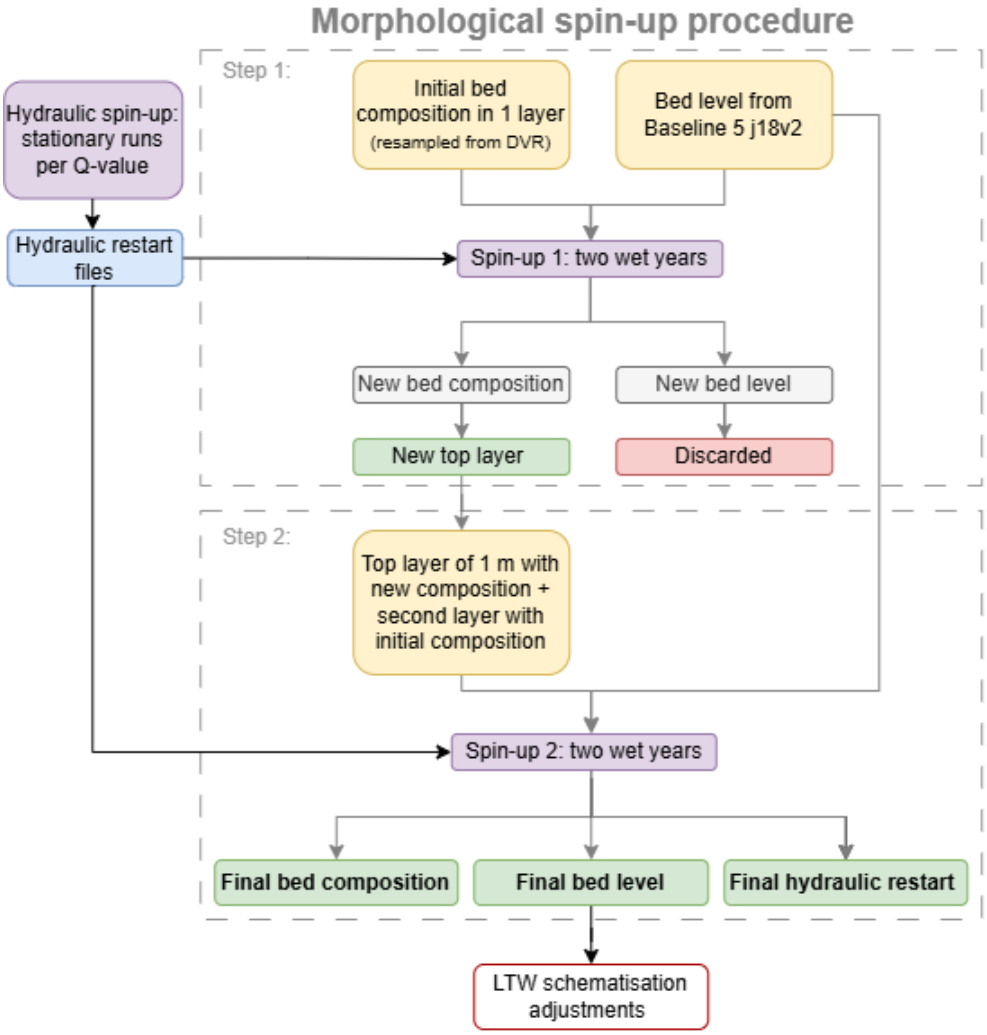


Figure E.1: Flowchart showing spin-up procedure followed for setting up the morphological models.

F. CFD project of inlet sill at Wamel results

This appendix shows some of the results from the CFD LTW project conducted by Deltares in April 2026 by Lynyrd de Wit and Amgad Omer (De Wit, 2026).

The research was conducted with a high-resolution particle model of the inlet sill at Wamel, based on bathymetry measurements of Q1 2025, but with the inlet sill as-built in April 2018 (the inlet sill was closed, without the lowered section added in May 2020). Figure F.1 shows the set-up of the model. It is important to note that the CFD model used a different formulation for the transverse bed slope correction than the DVR model; instead of Koch & Flokstra (1980), it worked with the Bagnold (1966) formulation. When calibrating the DVR model, Deltares was unable to recreate observation of main channel of the Waal with Bagnolds formulation.

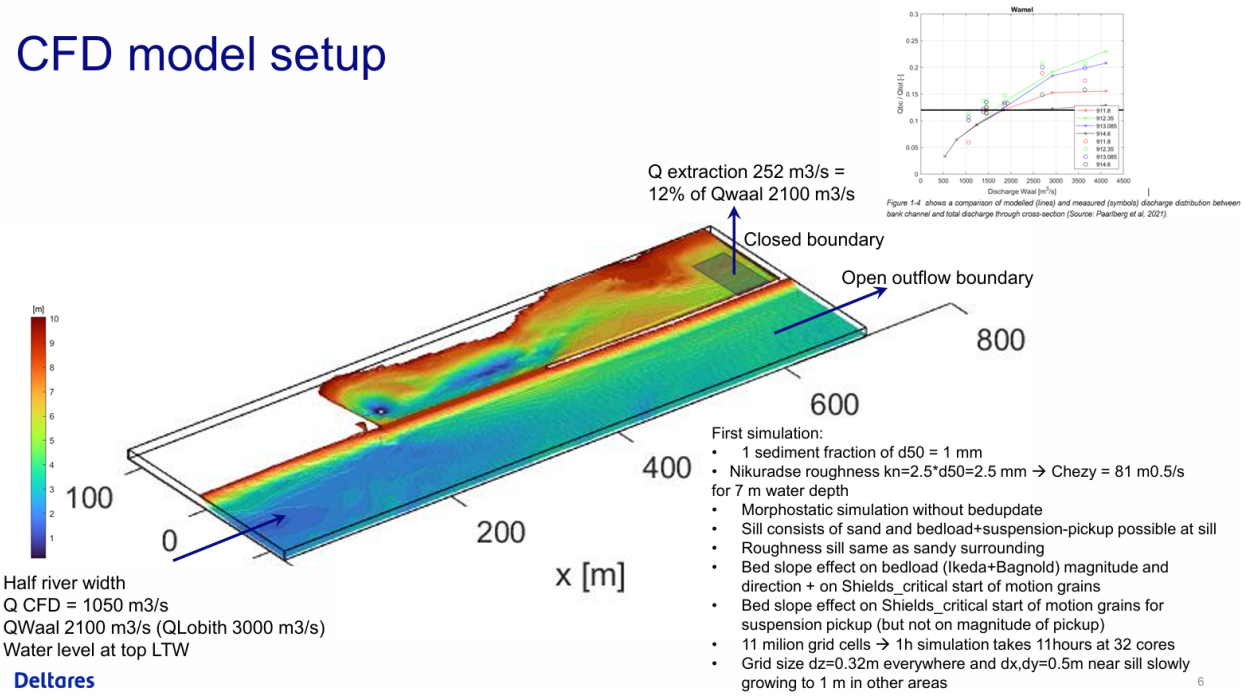


Figure F.1: CFD model set-up of Wamel inlet (De Wit, 2026)

Figure F.2 shows the flow velocity with the formation of a secondary (point 1) and primary gyres (point 2) against the upstream end of the auxiliary bank channel and a small eddy forming against the wall just downstream of the inlet sill (point 3). The flow velocities are highest over the downstream half of the inlet sill. The highest amount of sediment transport is located at the middle of the inlet sill, see Figure F.3. Although the velocities remain high, at the downstream end of the sill, sediment transport is reduced. The highest sediment transport is located more in the middle section of the inlet sill.

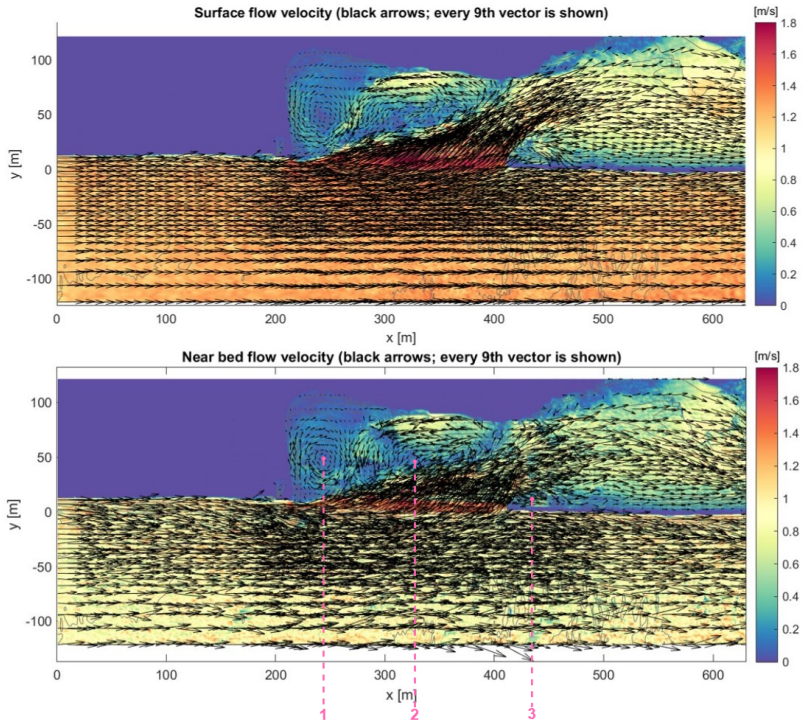


Figure F.2: CFD: top view of flow over inlet sill Wamel (De Wit, 2026).

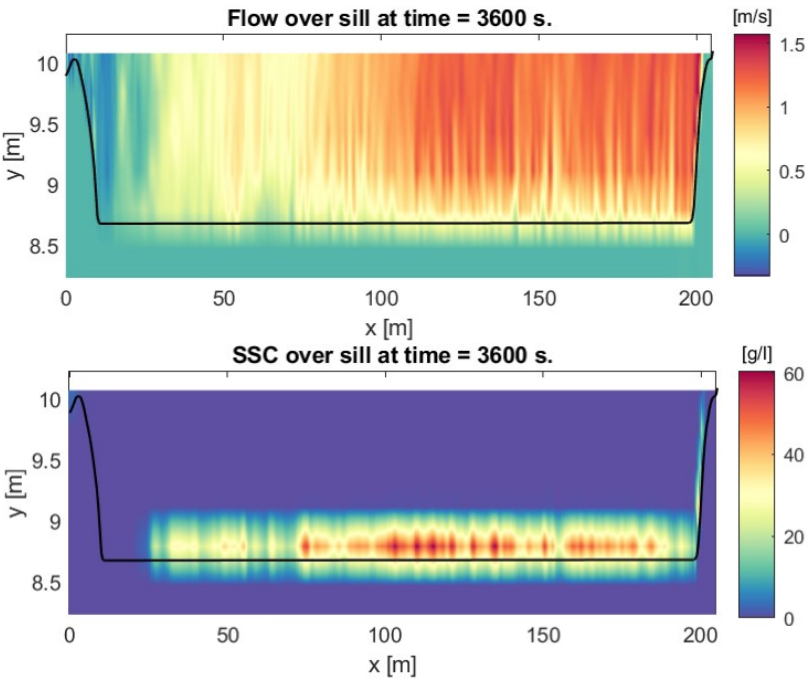


Figure F.3: CFD: cross section through inlet sill crest showing flow velocities and suspended sediment concentration (SSC) passing the inlet sill. x=0 is the upstream end of the inlet sill and x=200 the downstream end (De Wit, 2026).

G. Additional model results

G.1. Comparing W5, R5 and field data

This section further shows additional figures comparing the simulations with the LTW schematised inside the bathymetry (W5 and R5) with field data.

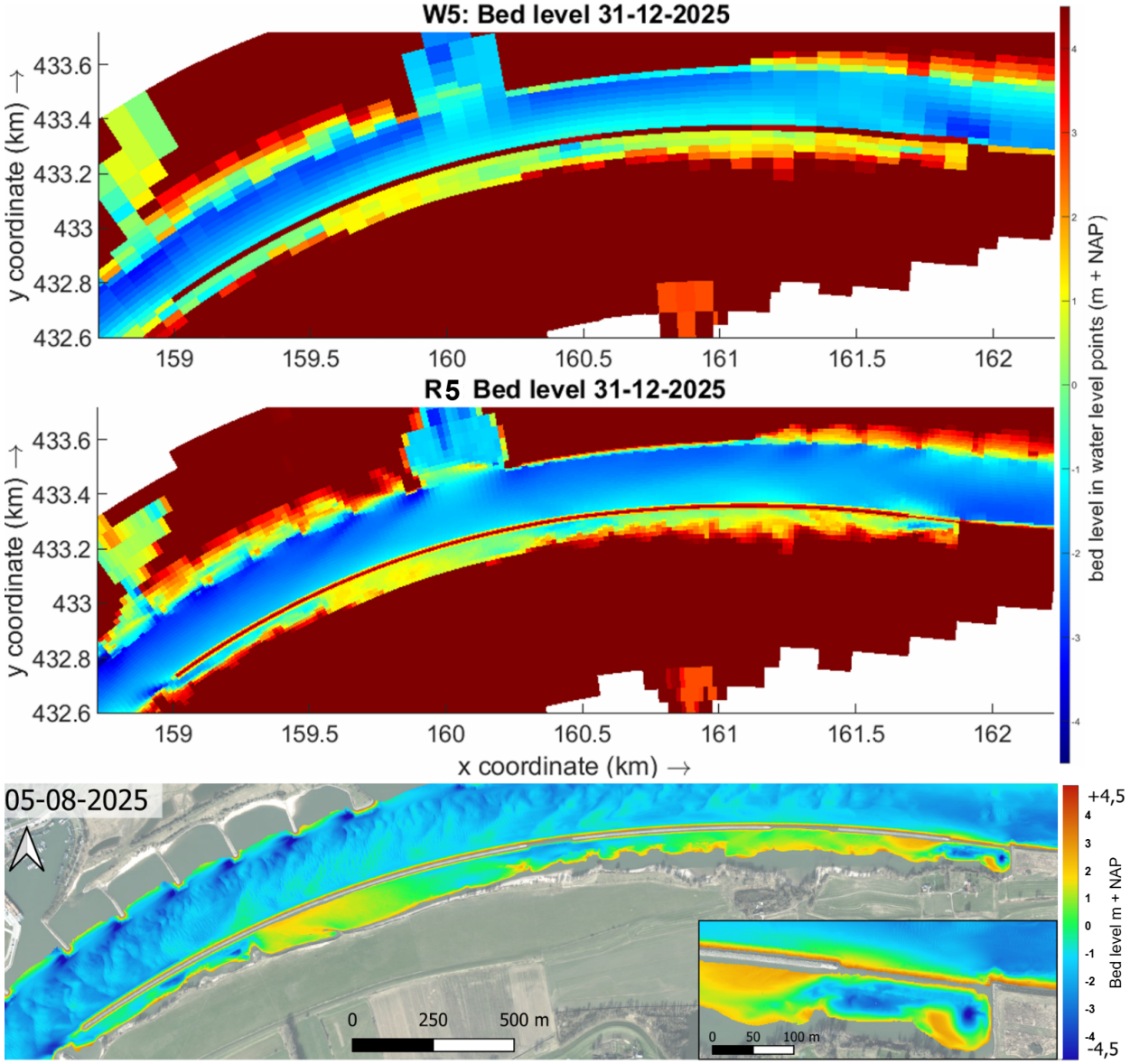


Figure G.1: Bed level height to NAP after 10 year simulations for variant W5 and R5

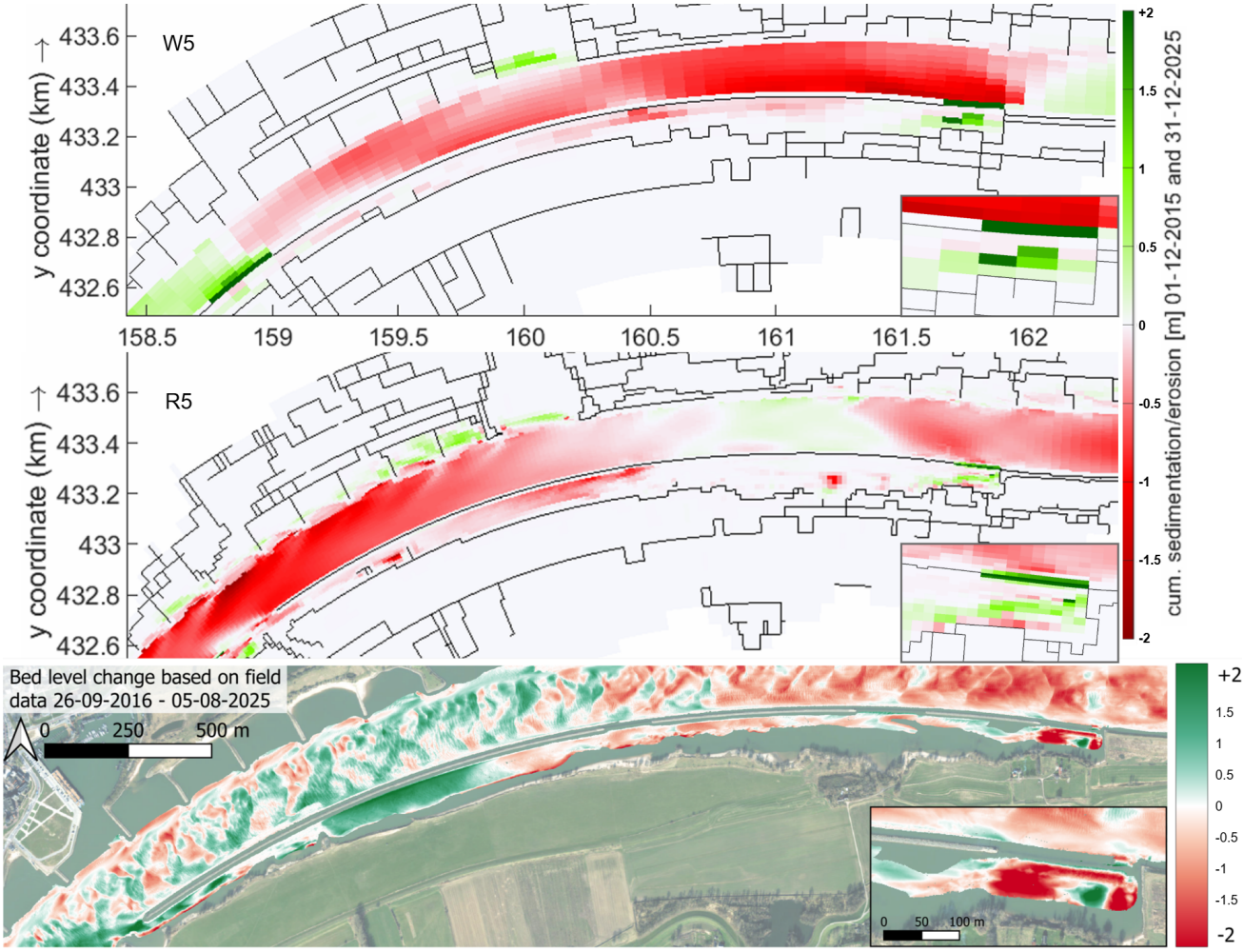


Figure G.2: Bed level change over 10 years for W5, R5 and from field data

G.2. Influence of wall schematisation method

Sediment overtopping the wall

Most of the sediment overtopping the wall does so at the upstream end of the wall. This is due to stronger transverse flow velocities from the widening that starts at the upstream end of the LTW. Table G.4 shows that most of the sediment passes at the first two cells at the upstream end, both when schematised in the bathymetry as with 2D weirs.

Table G.4: Combination of Wall_WA1a and Wall_WA1b for Runs W3 and W4 [m³]

	Wall_WA1a	Wall_WA1b	Wall_WA1 (a+b)
W3	35.61	2.82	38.43
W4	72.66	17.98	90.64

Bed level change in observations points

Figure G.3 shows that the bed level is systematically reduced when the wall is schematised in the bathymetry for the observation points in both the auxiliary bank channel (points P1-P5) and the main channel (point rkm 912)

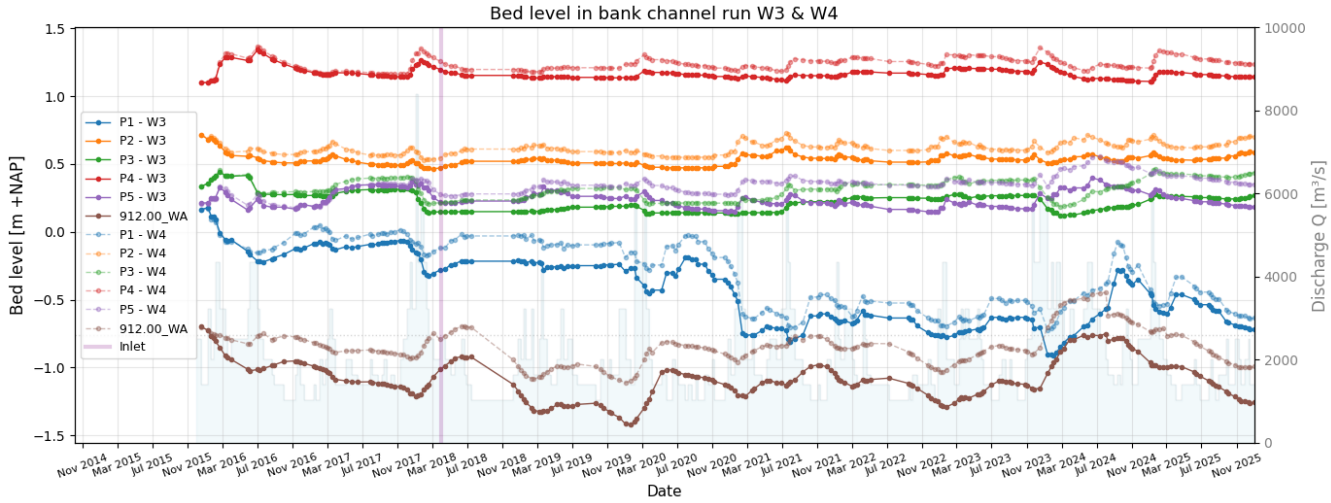


Figure G.3: Bed level change for observation points inside the auxiliary bank channel for variant W3 (in bathymetry) and W4 (2D weir). Locations of the observations points are shown in Figure D.5

G.3. Bedload transport through the inlet for W3a

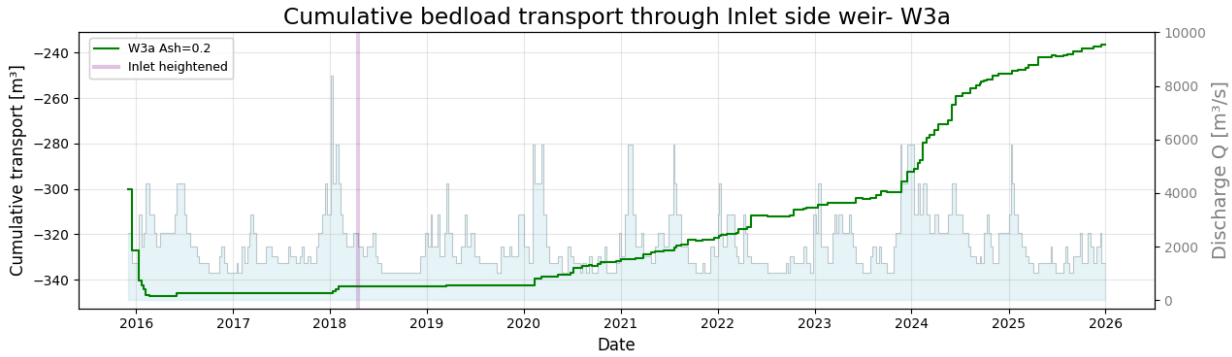


Figure G.4: Bedload transport into bank channel Wamel through inlet for W3a.

G.4. Total sedimentation/erosion of the auxiliary bank channel over time

The sediment balance over time for the refined model shows that during high discharge peaks the sediment balance goes up for R1, with more sediment entering than leaving, but after the heightening in R5 the balance goes down during peaks, indicating that the inlet sill blocks sediment from entering, resulting in erosion in the channel.

W1 and W5 show more similar behaviour, indicating that the heightened inlet sill had relatively less effect on the morphological development of the auxiliary bank channel due to the initially strong erosion. The erosion does increase more for W1 than for W5, although Figure 5.5 did show more sediment entering for W1. This suggests that the heightened inlet sill in the coarse model reduces the outflow, and when open, stronger flow velocities are dominant over the higher amount of sediment entering the system than leaving it.

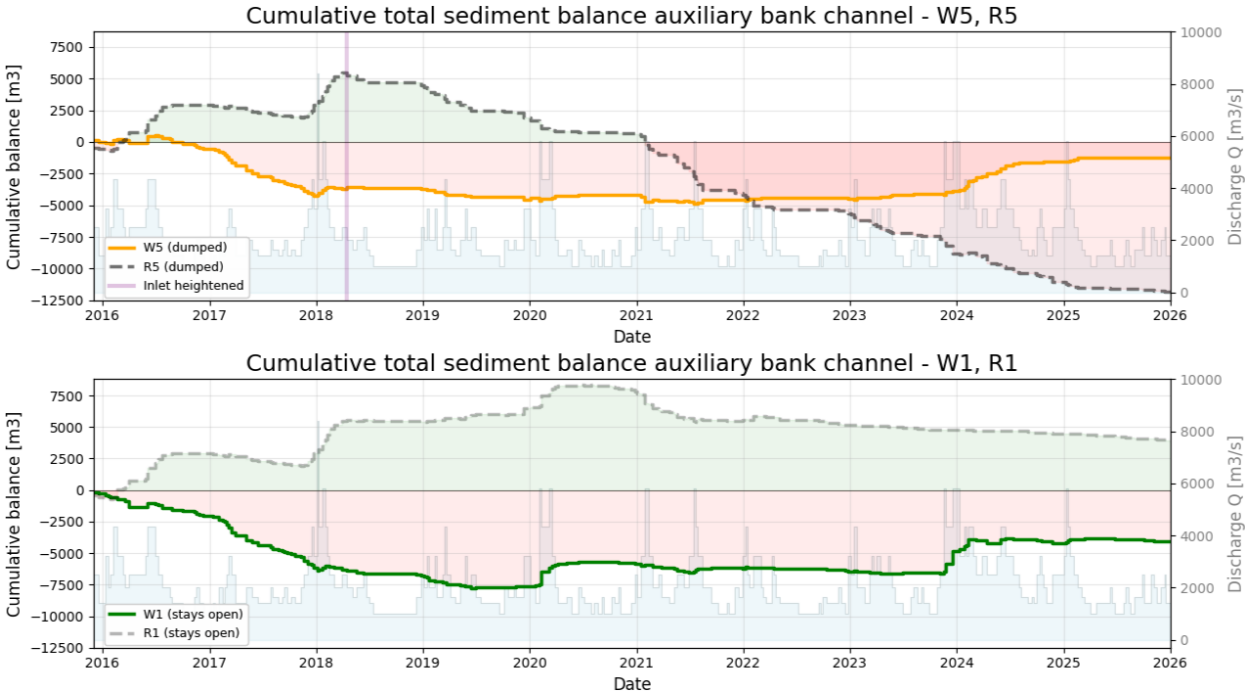


Figure G.5: Changing total amount of sediment in the auxiliary bank channel over time for schematisation variant 1 and 5 in the coarse and refined model.

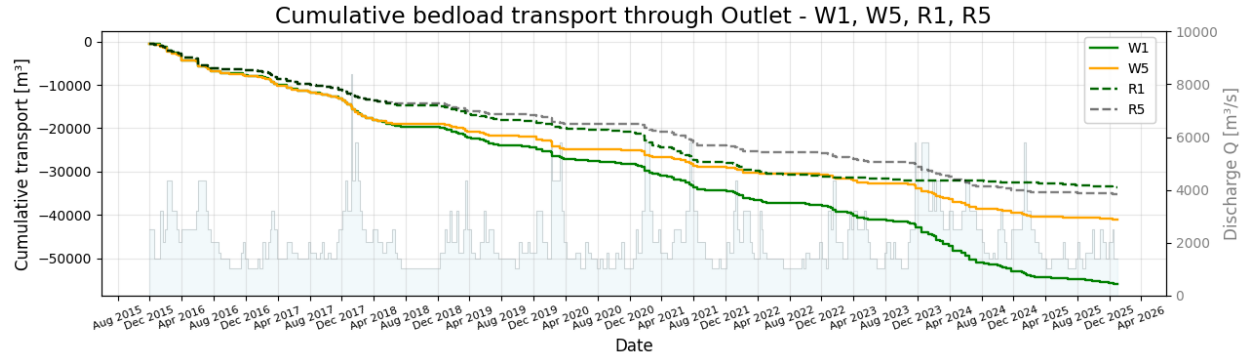


Figure G.6: Cumulative volume of sediment leaving the auxiliary bank channel through the outlet for schematisation variant 1 and 5 in the coarse and refined model.

G.5. Bed level change around outlet

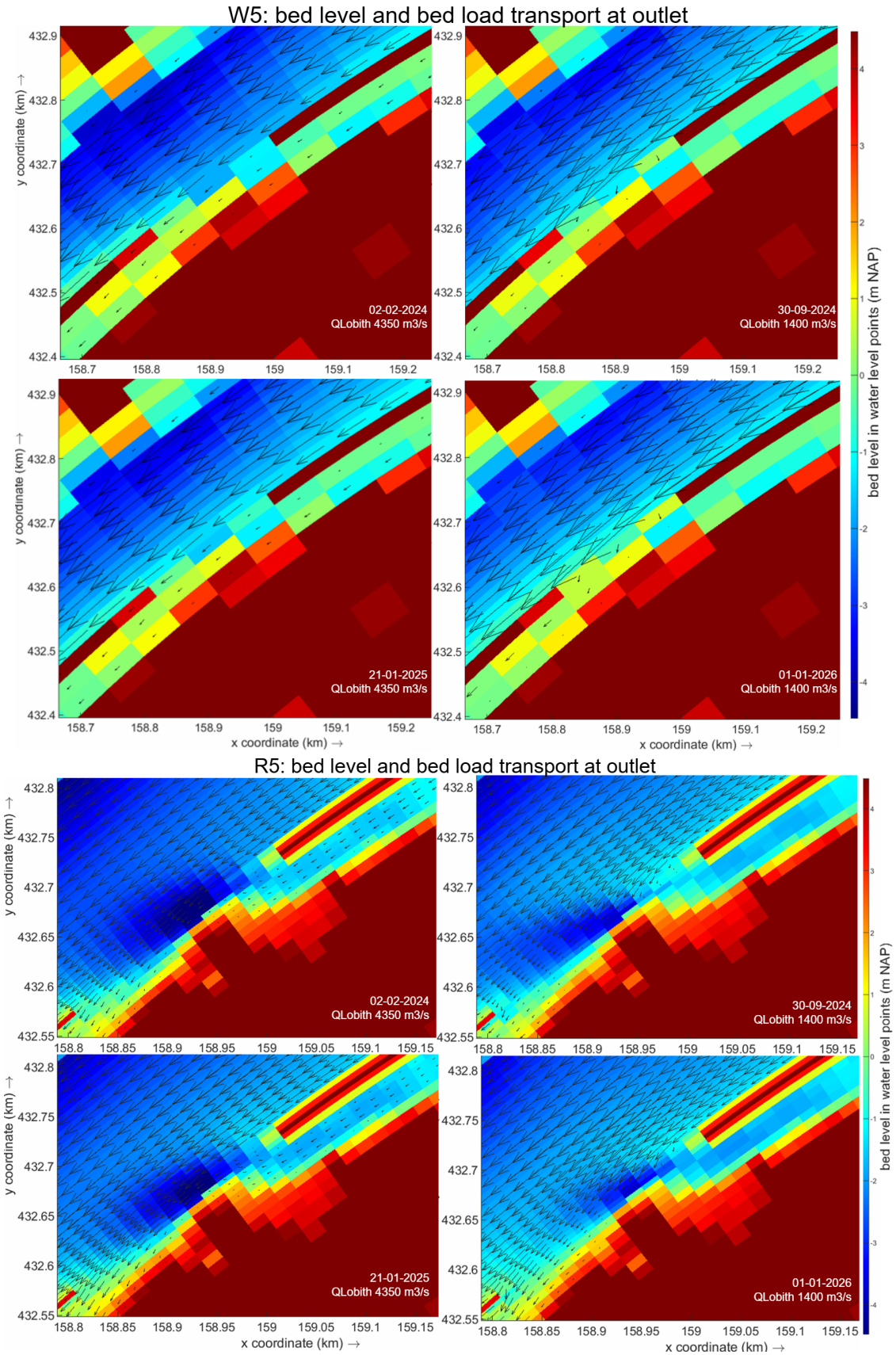


Figure G.7: Bed level and bed load transport (arrows) at outlet after period of high discharge and low discharge within the last two years for variant W5 and R5.

G.6. Sediment availability and outlet transport for W5 and R5

Figure 3.3 showed that the coarse and refined model had a different initial sediment availability in the auxiliary bank channel. This section examines how this initial difference evolves over the simulation, and how it relates to the difference in sediment transport leaving the channel through the outlet.

Figure G.8 shows that after the flood peak of January 2018, the amount of deposited sediment available in the auxiliary bank channel had become more similar between the two models, with less difference than at the start of the simulation. Two additional moments, in June 2021 and December 2025, show a similarly small difference (Figures G.10 and G.11). A difference does, however, appear to persist or re-emerge at the upstream reach of the wall, between x = 161 km and 161.5 km.

Figure G.12 shows the cumulative amount of sediment leaving the auxiliary bank channel through the outlet for W5 and R5. The two variants show different cumulative transport behaviour up to and during the January 2018 flood peak, after which the difference between them appears to stabilise, with both variants showing a similar rate of increase in cumulative outlet transport thereafter.

This pattern is consistent with the difference in initial sediment availability having influenced the outlet transport primarily during this initial period, with its effect diminishing once sediment availability in the two models converged after the flood peak. This would suggest that the morphological spin-up procedure, while sufficient to establish comparable long-term trends, was not long enough to fully equalise the initial sediment availability between the two models before the start of the simulated period.

This interpretation should, however, be treated with some caution. Only three additional moments are compared here, and the apparent convergence in sediment availability could partly reflect the specific hydrograph experienced rather than a general equalisation over time; a similar reduction in the outlet transport difference might, for instance, also be expected during any sufficiently long period of low discharge, followed by renewed divergence during a subsequent high-discharge event. Additionally, the possible role of the non-erodible bed constraint in shaping this apparent convergence cannot be ruled out based on the data considered here. Further work looking more systematically at how this difference develops through the full simulated period, and whether it depends on the hydrological sequence tested, would be needed to draw firmer conclusions.

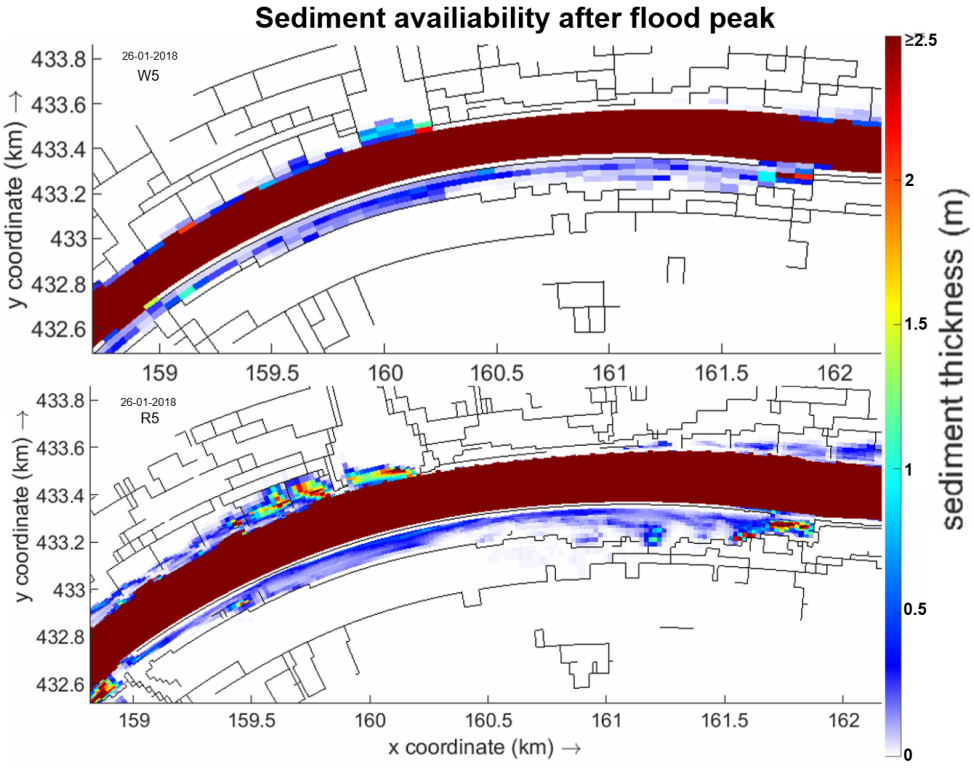


Figure G.8: Sediment availability in the auxiliary bank channel after flood peak in January 2018 with Q_Lobith of 8400 m^3/s for variant W5 and R5.

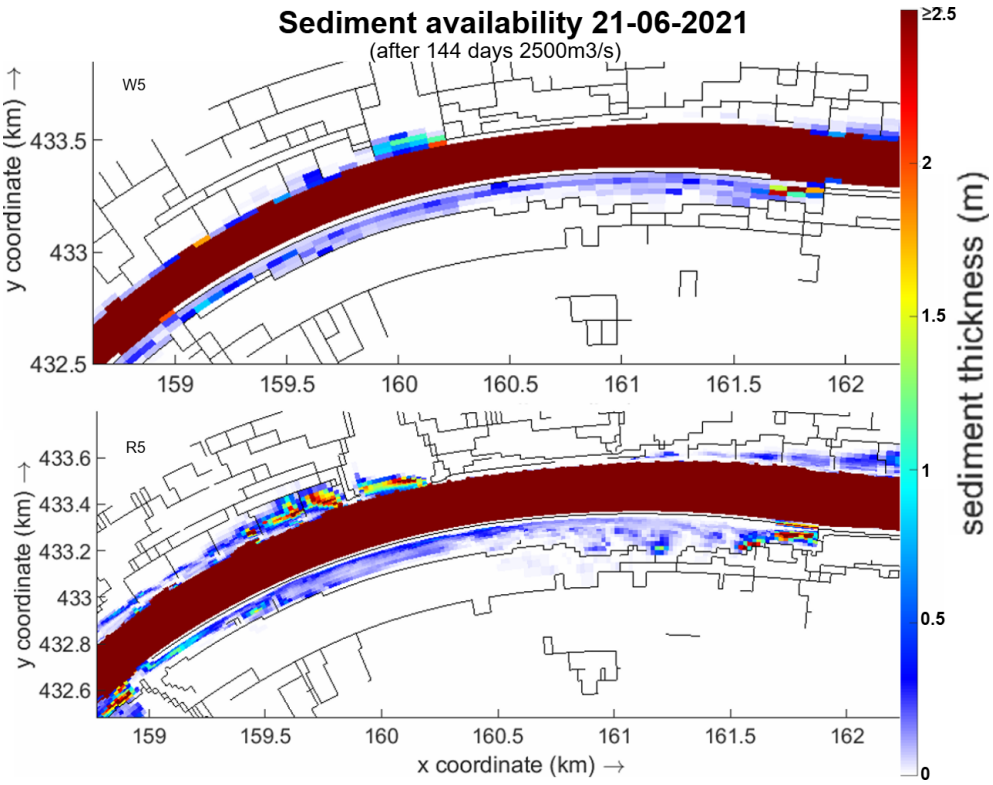


Figure G.9: Sediment availability in the auxiliary bank channel for 21-06-2021 after 144 days Q_Lobith of 2500 m^3/s for variant W5 and R5.

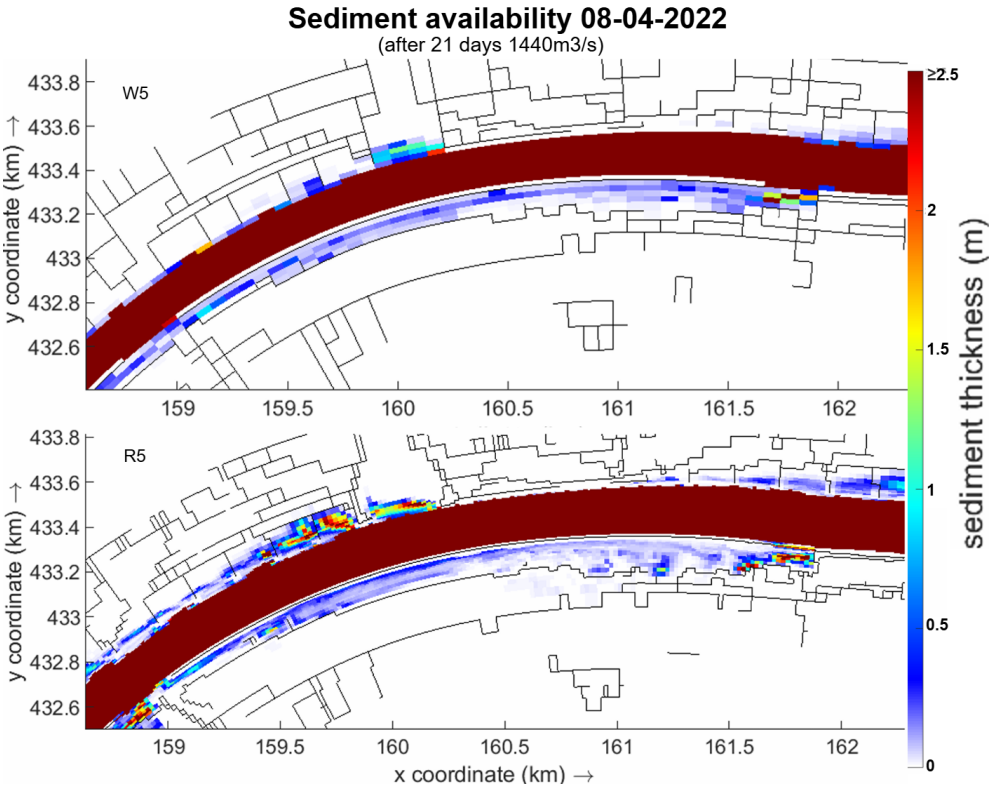


Figure G.10: Sediment availability in the auxiliary bank channel for 08-04-2022 after 21 days Q_Lobith of 1440 m^3/s for variant W5 and R5.

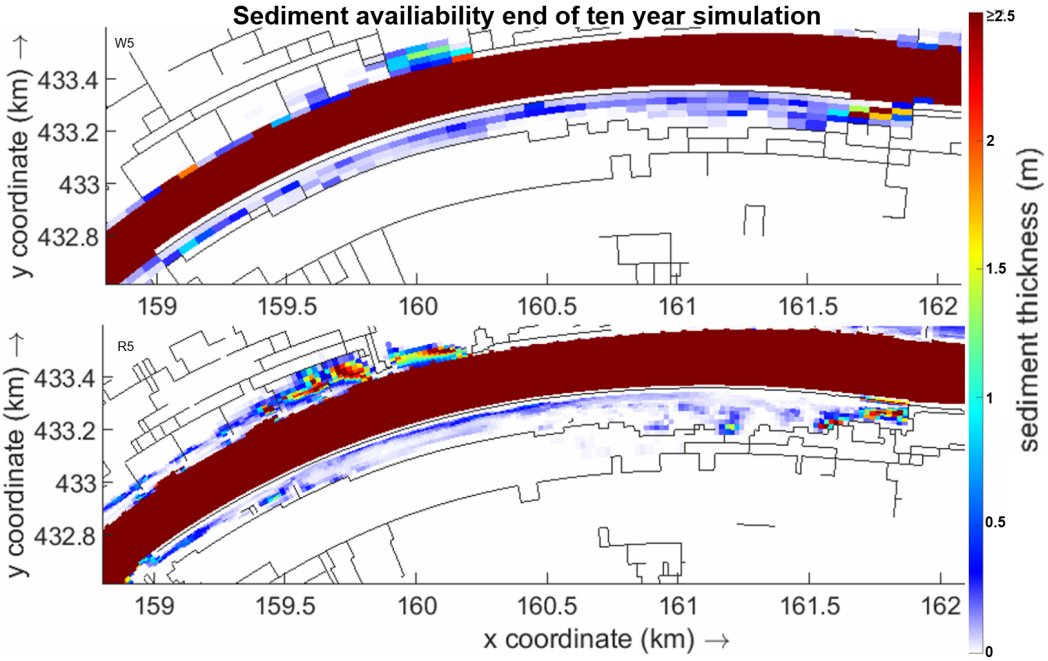


Figure G.11: Sediment availability in the auxiliary bank channel at the end of the ten-year simulations for variant W5 and R5, after 15 days of Q_Lobith of 1400 m^3/s.

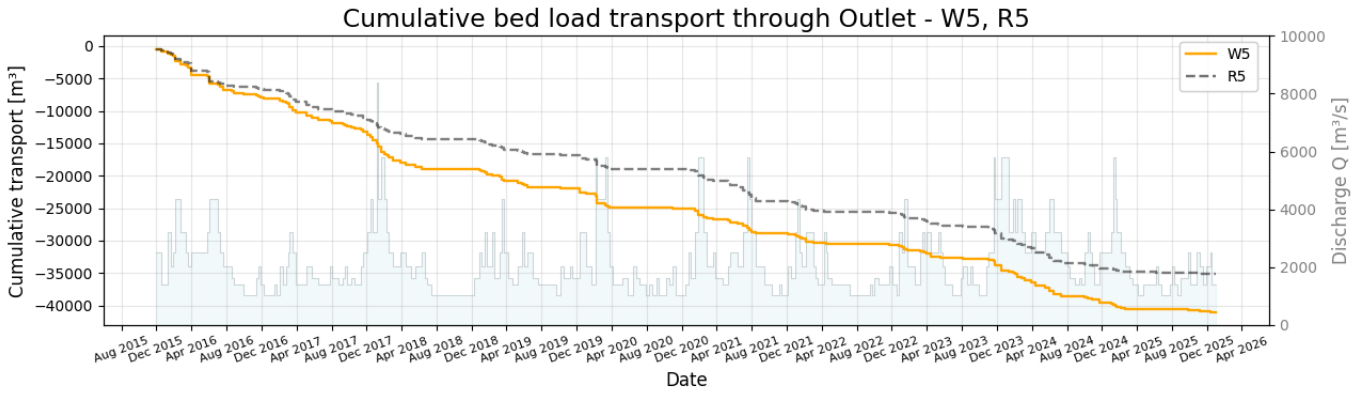


Figure G.12: Cumulative bedload transport through the outlet for variant W5 and R5.

G.7. Alluvial auxiliary bank channel in the refined model

This section provides additional figures with results of the refined test simulation with an alluvial river bed in the auxiliary bank channel discussed in section 5.2.6. Figure G.13 shows that when schematised without the fixed layer, erosion takes place during discharge peaks. Although the inlet sill was heightened, small increases in the sediment balance indicate deposition.

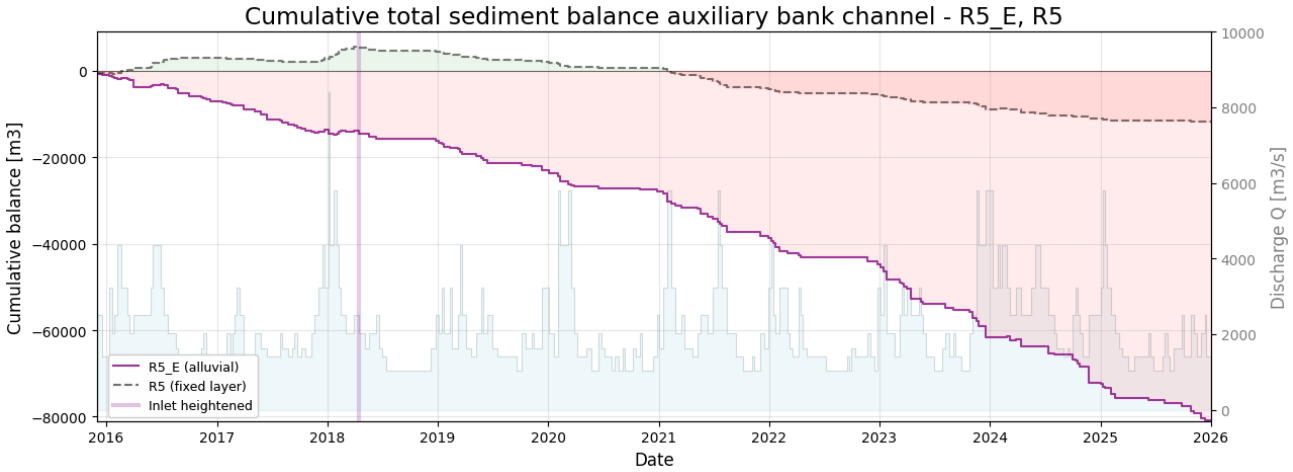


Figure G.13: Changing total amount of sediment in the auxiliary bank channel over time for the simulations with a fixed layer and alluvial river bed in the refined models.

The influence of heightening the inlet sill is less dominant on the overall development of the channel when the river bed is alluvial; this is also shown in the histogram in Figure G.14. However, sediment entering over the heightened inlet sill is strongly reduced compared to the open situation. The amount of sediment entering in the simulation with an erodible bed is higher than when a fixed layer is used. The erosion in the auxiliary bank channel increases the conveyance capacity and the discharge and sediment extraction from the main channel. This effect of the erosion in the upstream half of the auxiliary bank channel and the deposition in the downstream half is seen back in the discharge distribution along the LTW shown in Figure G.16.

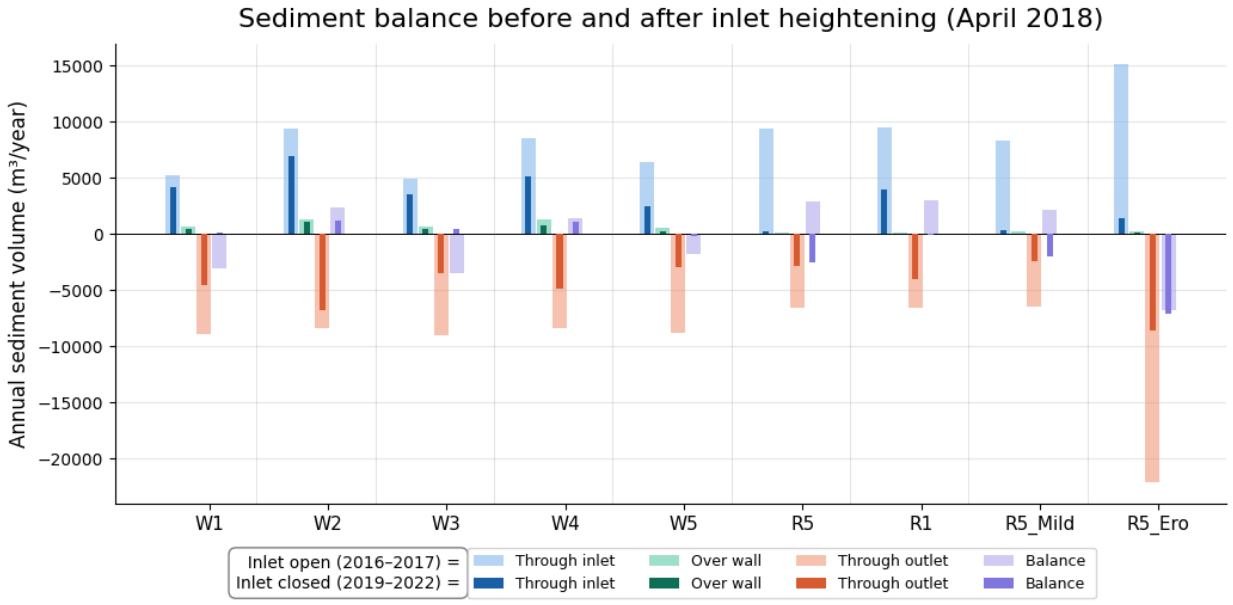


Figure G.14: Sediment transported in and out of the auxiliary bank channel through different cross sections and the resulting volume balance before and after the inlet was closed in April 2018 with a refined model simulation without the fixed layer in the auxiliary bank channel (R5_E).

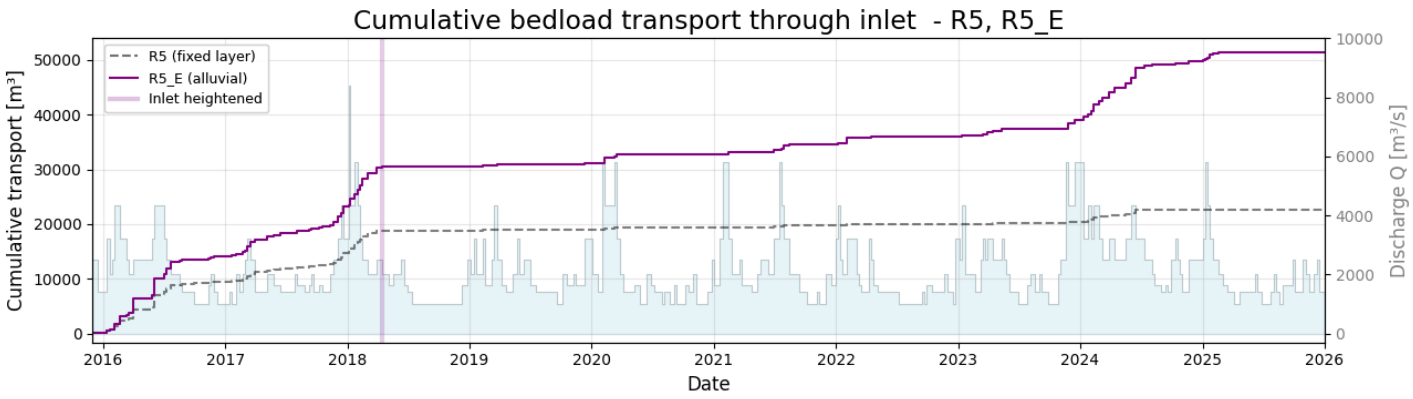


Figure G.15: Cumulative bedload transport over the inlet sill for variant R5 (with a fixed layer) and R5_E (with an alluvial bed).

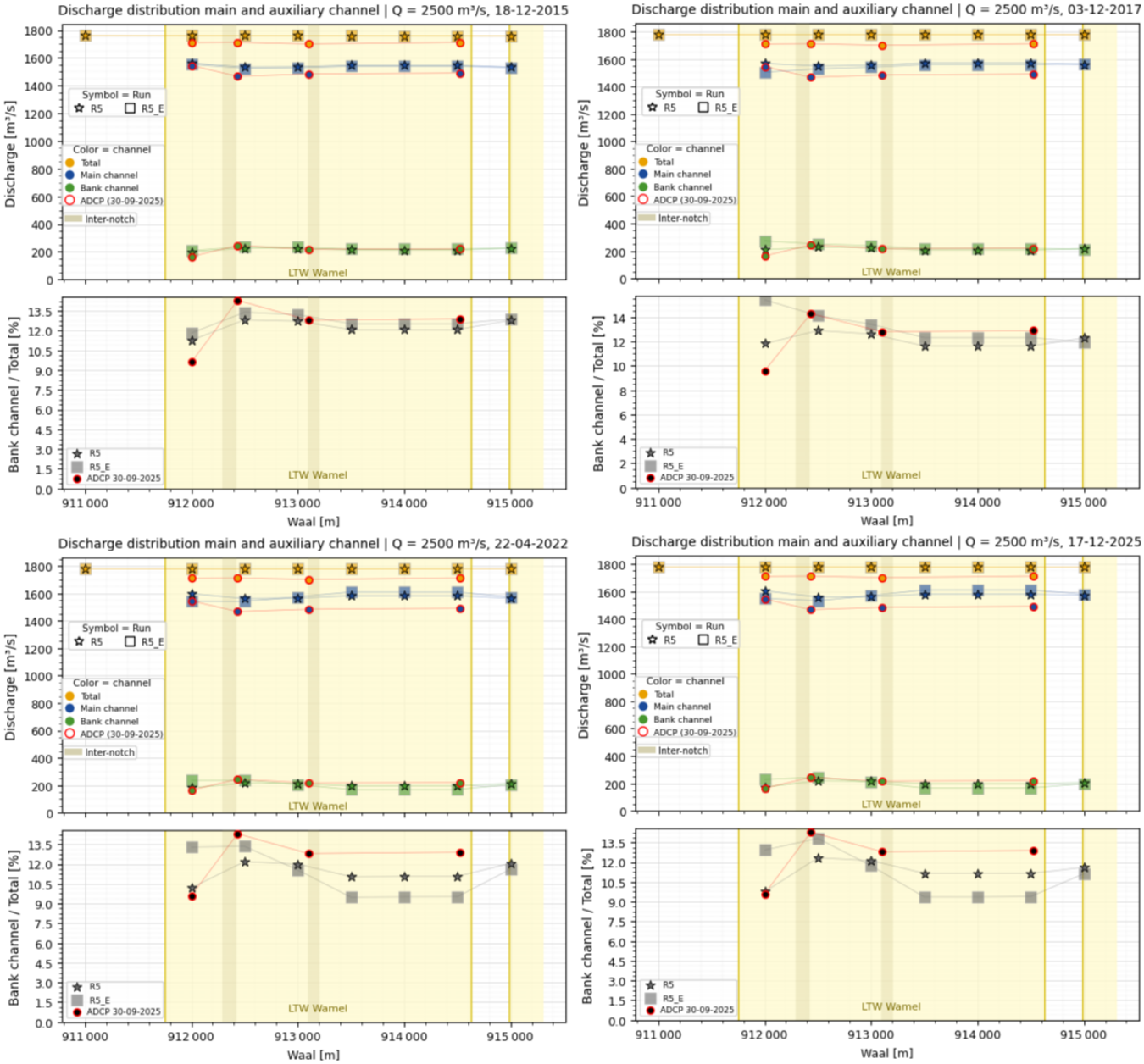


Figure G.16: Discharge distribution between the main and auxiliary bank channels for the refined model with a fixed layer (R5) and an alluvial riverbed in the auxiliary bank channel (R5_E.)

H. Discharge distribution short stationary model runs

This section shows that the discharge distribution did not change after adjustments to improve the side weir geometry in variant S2.

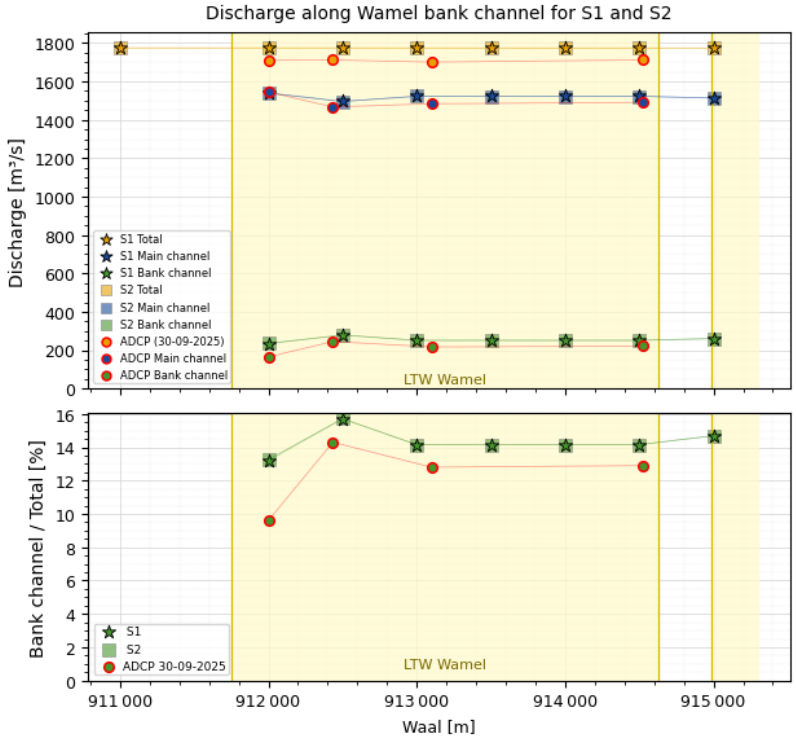


Figure H.1: Discharge distribution between the main and auxiliary bank channel for S1 and S2